MOLECULAR MECHANISMS UNDERLYING THE FAILURES OF TARGETED THERAPEUTICS IN THE TREATMENT OF MALIGNANT GLIOMA

A DISSERTATION
SUBMITTED TO THE FACULTY OF THE GRADUATE SCHOOL
OF THE UNIVERSITY OF MINNESOTA
BY

CHANI MARIE BECKER

IN PARTIAL FULFILLMENT OF THE REQUIREMENTS
FOR THE DEGREE OF
DOCTOR OF PHILOSOPHY

WILLIAM F. ELMQUIST
DAVID A. LARGAESPADA

MAY 2016

ACKNOWLEDGEMENTS

I have several groups of individuals to whom I am exceptionally grateful.

Firstly, I need to thank the people who brought me to the start of my graduate journey. For the endless support and encouragement, I have to thank Dr. Erik D'Aquino. Erik, you and your family provided me a home away from home in New York and I have always been grateful for your support and encouragement. I feel so lucky to have had an advisor in whom I could always count for both personal and professional advice and that sentiment has not changed over years or distance. You are intrinsically linked to my time and success at UB and I still miss you, your wife Kristin, and your sweet kids even after nine years. Thank you for preparing me so well not only for graduate school, but for life.

I never had any intention or desire to study cancer until my father was diagnosed with gastrointestinal stromal tumor (GIST). I knew then, at the age of 22, that I had met a formidable opponent in that disease. I remember feeling enraged, horrified, and fearful. Beyond these feelings, I also felt frustrated and helpless that four years of an undergraduate education in biomedical sciences wasn't enough to make sense of what was going on with my father. I needed to learn more about that stupid disease. In 2011, I joined a graduate program that would allow me to combine my hatred for cancer with my love of brains. It was the University of Minnesota that introduced me to neuro-oncology.

Mom and Dad, I am in your debt for your years of love and support. This dissertation pays homage to that debt in the hopes that I can repay you for all you've given and done for me. Ironically, while I used academia to facilitate my learning in the oncology space, you both became experts in your own rights on the subject. Ma, I am in awe of your own journey to become an expert in GIST and I am so proud of you. You've always demonstrated a fierce and voracious appetite for learning, so I wasn't really surprised, but Dad… you picked yourself up off the ground. You dusted yourself off, you dedicated your time to understanding cancer (at the age of 70!), and now, unbelievably, you are a mentor to others going through the same battle. I have no words to describe the swelling in my heart I feel when I think of such an incredible comeback.

To Mickey (Michelle), you may be my cousin by blood but you are my sister in every other sense of the word. I think of all the ways you've given to me, supported me, and guided me over the years and I'm so thankful and appreciative of you. To my Tall Man, Sean, I never wanted a brother until I met you. To you both, I think about staying over at your house on Friday nights when I was in high school and having our Finnegan Family breakfasts, I think about how you introduced me to Milwaukee and always gave me an outlet for fun. I'm so grateful for the two handsome young men you made whom I fondly refer to as my nephews, Ian and Evan. Thank you for raising them with such sweetness and affection that they drew me a sign that still, to this day, hangs on the only spare bedroom in your

house in Wisconsin and proclaims it “Chani’s room.” Thank you both for your unconditional love.

Secondly, I need to thank the people who led me through my graduate career. I need to start with Dr. Bill Elmquist because he was my introduction to the U of M… Do you remember, Dr. E, that you interviewed me during my first visit to the university? I really admired that you were such an expert on the blood-brain barrier and I was confused when you nudged me toward another faculty member who you said would be a better fit for my interests. You said Dr. John Ohlfest would focus on the biology on brain tumors, that you had an active collaboration with him, and that I should try to engage him as a mentor.

I worked so hard to set up a meeting with that man, but it took three or four e-mails before he finally responded to me. I later learned that he would occasionally throw roadblocks like these to test the motivation of an individual attempting to contact him. Eventually, though, I made it into his good graces and eventually, his lab. John was the first person to tell me that my time was valuable—something I had never heard before. The first couple years of grad school really dragged me down, the struggle of the studies and the persistence of the technical failures…but John always brought me back up. He was also the most passionate scientist I have ever met. His dedication was tireless, his excitement was tangible, and his energy was contagious. From a man who drove me to work hard and work fast, he also taught me to slow down and to take my time to plan and understand

science. I am so grateful for the time I had with him and for the man to whom he directed me for the remainder of my education.

Dr. David Largaespada, you are the man in whom John placed his trust for providing me the rest of my PhD studies. Thank you for taking me in. So many grad students throw themselves at your feet, they compete fiercely to win a spot under your direction, and you just let me slide into your lab without an audition. Thank you for hiring Zoe Zhang, Flavia Popescu, Rebecca LaRue, Tracy Marko, and others who have become close friends. Additionally, I am so grateful to you for letting me continue my work in glioblastoma, drug delivery, and the blood-brain barrier even though it wasn't the Sleeping Beauty model widely used in your own lab. Thank you for letting me stay my track and thank you for not only allowing me, but encouraging me to pursue my MBA. I know not all PIs would be as supportive, and I feel lucky and grateful to have been given the green light with such genuine enthusiasm. Thank you for encouraging the development of my leadership and for more or less forcing me into taking on a couple of undergraduates to help me with my work. They were more helpful than I could have anticipated. Joey McFarren and Olivia Wicker, thank you for working with me and becoming such close friends.

Even after joining David's lab, I realized I still needed the guidance of an expert in chemotherapeutic brain penetrance. It would take two people to replace the one man I lost. Dr. E, you may have turned me down once, but thank you for not turning me down a second time. Thank you for creating such a phenomenal lab with immensely talented people like Rajendar Mittapalli, Rajneet Oberoi,

Shruthi Vaidhyanathan, and Karen Parrish. Thank you for being my advisor and for providing a level of support that I will never forget.

Before I graduate, I have one story I need to recount for you. On a very busy, very frustrating day, when I had too much going on, I made a mistake of my own efforts that was going to cost me $25. At the time, I was struggling to make ends meet financially, and so I decided to charge that $25 to one of your accounts. I didn't ask you, I just e-mailed you and said, rather unapologetically in retrospect, that the cost of my mental sanity that day was $25. I told you that I charged it to your account and that I'd make it up to you later. I wasn't sure what your reaction would be at the time and in my anger and frustration, I didn't really care. Your response, however, blew me away. "Make it $50," you said. "You're worth it." I'm not sure I ever told you how much I appreciated you in that moment and how much you endeared yourself to me afterward. Thank you for your vote of confidence.

Thank you, also, for your unhesitating and unwavering support in my pursuit of a business education. Your encouragement drove me to my final mentor in the course of my graduate studies, Matthew Fox, CEO. I learned science and problem solving from David and Bill, but from you, Matt, I learned strategy and organization. Thank you for taking me on as a protégé even though I came to you with no business experience. You've given me new ways to analyze and communicate with the world, and I've found that I've become a more efficient and productive person. Your focus and ambition remind me so strongly of the mentor I lost along the way, and I'm grateful to have found a teacher in you. I was always told it's a

gift and a privilege to find a job where you love going to work every day and I have affirmed this philosophy through my experiences with you.

Lastly, I need to thank the individual who has made this entire graduate journey worthwhile: my husband, Michael Maher. You know, love, I can actually trace every step of my graduate career through the course of our relationship. We met during my first year of graduate school, we became friends and started dating during my second year. We moved in together during my third year, we got engaged during my fourth year, and we got married at the start of my fifth year. Doof, my failures would not have been so tolerable and my victories not so sweet without you by my side. Thank you for your kindness, your generosity, your sense of humor, and your smart, sharp wit. Thank you for bringing me so much joy. I love you so much.

DEDICATION

This thesis is dedicated to Dr. Nicholas Lydon and Dr. Brian Druker, the men who created and pioneered the use of a drug that saved my father's life.

Thank you for imatinib.

ABSTRACT

Glioblastoma multiforme (GBM) is a lethal cancer. Without treatment, patients diagnosed with this disease survive nine months. With the best therapeutics science has to offer, including surgical resection, radiation therapy, and temozolomide, patients survive only five more months. Despite numerous clinical trials, the vast majority of tested drugs fail to provide therapeutic benefit to patients. It was the intent of this thesis to characterize the molecular mechanisms that prevent or limit the efficacy of targeted agents against malignant glioma. This work specifically explores how the internal characteristics of the tumor including its invasiveness and genetic heterogeneity as well as external attributes of therapeutic agents including brain penetrance contributes to the chemotherapeutic failure in GBM. By clarifying the biological processes that constrain treatment of this disease, scientists can strategize the development of better therapeutics with greater likelihoods for clinical success.

We compared the brain distribution, molecular targeting efficiency, and survival benefit of GDC-0980 and GNE-317, two PI3K/mTOR inhibitor analogues. We showed that GDC-0980 is liable for efflux by P-glycoprotein (Pgp) and Breast Cancer Resistance Protein (BCRP) at the blood-brain barrier (BBB) while GNE-317 remains relatively resistant to efflux. Because GNE-317 is more brain penetrant than GDC-0980, it showed greater accumulation in the brain and stronger ability to impede the activation of PI3K/mTOR pathways in the GL261 mouse glioma model. Unexpectedly, neither drug affected survival, an effect that underscores the challenges presented by the genetic heterogeneity associated with cancer and the consequences of inadequate target selection.

We also sought to determine the influence of anti-angiogenic therapy (AAT) on the delivery and efficacy of concurrently administered targeted agents. Again, we used GDC-0980 and GNE-317 to determine whether susceptibility to efflux impacted these parameters. We demonstrated that the vascular endothelial growth factor (VEGF) monoclonal antibody, bevacizumab (Avastin) could decrease the brain distribution of GDC-0980, although not significantly, but had no effect on the brain accumulation of GNE-317. We further showed that while bevacizumab alone provided a survival benefit in patient-derived glioma xenograft models, this therapeutic benefit could only be enhanced with co-treatment of a brain-penetrant drug like GNE-317. Collectively, these data suggest that AAT-induced BBB normalization is more likely to limit the delivery of targeted agents that are subject to active efflux.

Finally, we examined the therapeutic potential of targeting cancer stem cells (CSCs) through experiments with parthenolide and LC-1 in the GL261 mouse glioma model. Effectively killing CSCs is an important goal in brain tumor research because this cell population is thought to responsible for tumor growth and recurrence, and is known to be particularly resistant to chemotherapies. *In vitro* studies of parthenolide and LC-1 in multiple glioma cell lines demonstrated that both drugs exhibited similar cytotoxicity profiles and were able to induce total cell death. LC-1 was also shown to be brain penetrant and non-toxic after prolonged exposure, and produced a demonstrable delay in tumor growth and a significant survival benefit. For these reasons, glioma stem cells remain a compelling therapeutic target for future clinical therapies.

(494 words)

TABLE OF CONTENTS

ACKNOWLEDGEMENTS i

DEDICATION vi

ABSTRACT vii

TABLE OF CONTENTS ix

LIST OF TABLES xiv

LIST OF FIGURES xv

ABBREVIATIONS xviii

FORWARD xxi

CHAPTER 1: Introduction 1

1.1 Hallmarks of Cancer 2

1.2 Glioma Classification & Staging 3

1.3 Gliomagenesis 5

1.4 Glioma Stem Cells 8

1.5 Genetic Contributions & Clonal Evolution in Glioblastoma Multiforme 9

1.6 Clinical Presentation & Treatment of Glioblastoma Multiforme 12

1.7 Glioblastoma Multiforme as a Disease of the Whole Brain 16

1.8 Clinical Imaging in the Evaluation of Glioma 17

1.9 Glioma Modeling 20

1.10 Blood-Brain Barrier Biology 23

1.11 GBM Therapeutics in the Clinical Pipeline 24

1.12 Statement of Problem & Research Plan 24

CHAPTER 2: The Influence of Active Efflux at the BBB on the PK/PD Properties of Dual PI3K/mTOR Inhibitors in the Treatment of Malignant Glioma 69

2.1 Introduction 72

2.2 Materials and Methods 74

2.2.1 Animal Care 74

2.2.2 Chemicals and Reagents 75

2.2.3 Tissue Culture 75

2.2.4 Intracranial Tumor Implantation 76

2.2.5 Blood-Brain Barrier Imaging 77

2.2.6 Steady-State Pharmacokinetics 77

2.2.7 Quantification of GNE-317 and GDC-0980 in Brain and Plasma by LC-MS/MS 78

2.2.8 Regional Distribution of GDC-0980 and GNE-317 in GL261 Tumor-Bearing Mice 79

2.2.9 Immunohistochemistry 80

2.2.10 Statistical Analysis 81

2.3 Results 81

2.3.1 The GL261 Glioma Model is Characterized by Heterogeneous Blood-Brain Barrier Disruption 81

2.3.2 GNE-317 Exhibits Similar Cytotoxic Activity and Greater Brain Penetrance than GDC-0980 82

2.3.3 GNE-317 Penetrates Regions with Invasive Cells More Effectively Than GDC-0980 83

2.3.4 GNE-317 Inhibits PI3K/mTOR Pathways More Effectively than GDC-0980 85

2.3.5 *In Vivo* Efficacy of GDC-0980 and GNE-317 86

2.4 Discussion 86

CHAPTER 3: The Influence of Antiangiogenic Therapy on the Distribution and Efficacy of Concurrently Administered Targeted Agents in Malignant Glioma 93

3.1 Introduction 96

3.2 Materials & Methods 99

3.2.1 Animal Care 99

3.2.2 Chemicals and Reagents 99

3.2.3 Cell Viability Studies 100

3.2.4 Xenograft Tumor Implantation 100

3.2.5 Blood-Brain Barrier Imaging 101

3.2.6 Plasma and Brain Distributions of GDC-0980 and GNE-317 in FVB Non-Tumor-Bearing Mice 102

3.2.7 Regional Distribution of GDC-0980 and GNE-317 in GBM10 Tumor-Bearing Mice 103

3.2.8 Quantification of GDC-0980 and GNE-317 in Brain and Plasma by LC-MS/MS 104

3.2.9 Immunohistochemistry 105

3.2.10 Survival Studies in Glioma Models 107

3.2.11 Statistical Analysis 107

3.3 Results 108

3.3.1 The GBM10 Model is Characterized by Heterogeneous Blood-Brain Barrier Disruption and is Similarly Susceptible to GDC-0980 and GNE-317 108

3.3.2 Time Profiles of GDC-0980 and GNE-317 Distributions in Brain and Plasma 109

111

3.3.3 GNE-317 Exhibits Greater Brain Penetrance than GDC-0980 in an Orthotopic Xenograft Glioma Model
3.3.4 Pharmacodynamic Effects of GNE-317 and GDC-0980 in Brain Tumors 113

3.3.5 Bevacizumab Modulates Survival in Brain Tumor-Bearing Animals Treated with Concurrent Therapeutics 114

3.4 Discussion 115

CHAPTER 4: The Therapeutic Potential of Targeting Glioma Stem Cell Populations 145

4.1 Introduction 148

4.2 Materials & Methods 150

4.2.1 LC-1 Preparation and PTL Purification 150

4.2.2 Preparation of PTL and LC-1 Stock Solutions 150

4.2.3 Cell Culture 150

4.2.4 Alamar Blue Cytotoxicity Assays 151

4.2.5 Animal Care 152

4.2.6 Pharmacokinetic Studies 152

4.2.7 LC-1 Toxicity Study in Healthy Mice 153

4.2.8 Intracranial Tumor Implantation 154

4.2.9 LC-1 Survival Study in Tumor-Bearing Mice 155

4.3 Results 155

4.3.1 LC-1 Demonstrates a Similar Cytotoxicity Profile to Parthenolide 155

4.3.2 LC-1 Brain Penetrance 156

4.3.3 LC-1 is Well-Tolerated in Animal Toxicity Studies 157

4.3.4 *In Vivo* Efficacy of LC-1 158

4.4 Discussion 159

CHAPTER 5: Recapitulation and Future Directions 173

5.1 Molecular mechanisms underlying the failures of targeted agents in the treatment of malignant glioma 174

5.2 Strategies to enhance the efficacy of targeted agents 177

5.3 Alternative treatments with therapeutic potential for malignant glioma 180

BIBLIOGRAPHY 182

LIST OF TABLES

CHAPTER 3

Table 3.1: Plasma and brain pharmacokinetics of GNE3-17 and GDC-0980 126

CHAPTER 4

Table 4.1: Cytotoxicity of parthenolide and LC-1 against glioma cell lines 164

Table 4.2: Pharmacokinetic data for LC-1 in non-tumor-bearing mice 166

LIST OF FIGURES

CHAPTER 1

Figure 1.1: World Health Organization classification of glioma by histological presentation 50

Figure 1.2: Generation of primary and secondary GBMs 52

Figure 1.3: Developmental theories of gliomagenesis 54

Figure 1.4: CD133+ cells give rise to a tumor with varied populations of cells 56

Figure 1.5: TCGA provided data implicating three highly active pathways in glioblastoma 58

Figure 1.6: Heat map of molecular signatures giving rise to four distinct cohorts of glioblastoma 60

Figure 1.7: Clonal evolution of glioblastoma 62

Figure 1.8: RANO criteria determine the classification of response to treatment in malignant glioma 64

Figure 1.9: The blood-brain barrier is composed of both physical and biochemical components 66

Figure 1.10: Invasive glioma cells lie behind an intact blood-brain barrier 68

CHAPTER 2

Figure 2.1: Different imaging modalities visualize tumors residing behind an intact BBB 91

Figure 2.2: Quantified signal volumes 93

Figure 2.3: Characterization of the GL261 murine model 95

Figure 2.4: Cytotoxic and pharmacokinetic comparison of GDC-0980 and GNE-317 97

Figure 2.5: Comparison of steady-state kinetics in GDC-0980 and GNE-317 between wild-type FVBn and *Mdr1a/b-/- Bcrp-/-* triple knockout (TKO) mice. 99

Figure 2.6: Brain-to-plasma ratios of GDC-0980 in wild-type and efflux transporter knockout mice 101

Figure 2.7: Regional distribution of GDC-0980 and GNE-317 in a GL261-GFP-Luc tumor-bearing brain 103

Figure 2.8: Immunohistochemistry of phospho-proteins one hour after drug treatment 105

Figure 2.9: Immunohistochemistry of phospho-proteins six hours after drug treatment 107

Figure 2.10: Immunohistochemistry of unphosphorylated proteins 1 hour after drug treatment 109

Figure 2.11: Immunohistochemistry of unphosphorylated proteins 6 hour after drug treatment 111

Figure 2.12: *In vivo* efficacy studies 113

Figure 2.13: Summary of comparison between GDC-0980 and GNE-317 115

CHAPTER 3

Figure 3.1: Characterization of the BBB properties associated with the GBM10 orthotopic xenograft model 120

Figure 3.2: Comparison of the cytotoxic effects of GDC-0980 and GNE-317 independent of the brain's influence on drug delivery 122

Figure 3.3: Time profiles of GDC-0980 and GNE-317 distributions in brain and plasma 124

Figure 3.4: Dosing of bevacizumab and its effects on TRD accumulation 128

Figure 3.5: Dosing of bevacizumab seals the BBB to restrict dye permeation 130

Figure 3.6: Influence of bevacizumab on tumor and brain distribution of GNE-317 132

Figure 3.7: Influence of bevacizumab on tumor and brain concentrations of GNE-317 134

Figure 3.9: Influence of bevacizumab on tumor and brain concentrations of GDC-0980 138

Figure 3.10: Immunohistochemistry one hour after treatment with Bevacizumab, GDC-0980 or GNE-317 or in combination 140

Figure 3.11: *In vivo* efficacy studies in the GBM10 orthotopic xenograft glioma model 142

Figure 3.12: *In vivo* efficacy studies in the GBM59 orthotopic xenograft glioma model 144

CHAPTER 4

Figure 4.1: Molecular structures of parthenolide (PTL) and LC-1 162

Figure 4.2: Dose-response cytotoxic profiles with PTL and LC-1 in glioma cell lines 168

Figure 4.3: CBC data from non-tumor bearing mice treated with LC-1 mouse 170

Figure 4.4: *In vivo* survival data 172

ABBREVIATIONS

ABC, ATP-binding cassette;

ATP, adenosine triphosphate;

AUC, area under the plasma concentration time curve;

BBB, blood-brain barrier;

BBBD, Blood-brain barrier disruption;

BCRP, Breast Cancer Resistance Protein;

BKO, BCRP knockout *(Bcrp-/-)*;

BSA, bovine serum albumin;

CBC, Complete blood counts;

CED, Convention-enhanced delivery;

CE-MR, contrast-enhanced magnetic resonance;

CNS, Central Nervous System;

CR, complete response;

CSC, cancer stem cell;

CT, computed tomography;

DMAMCL, dimethylamino-micheliolide;

DMSO, dimethylsulfoxide;

DNA, deoxyribonucleic acid;

^{18}F-FDOPA, 6-[^{18}F]fluoro-dihydroxy-L-phenylalanine;

GBM, glioblastoma multiforme;

GEM, genetically engineered mouse;

GFP, Green Fluorescent Protein;

HP-β-CD, 2-hydroxypropyl-β-cyclodextrin;

HPLC, high performance liquid chromatography;

HPLC-MS/MS, HPLC-tandem mass spectrometry;

Luc, Luciferase;

MR, magnetic resonance;

mTOR, mechanistic target of rapamycin;

PBS, phosphate-buffered saline;

PET, positron emission tomography;

PD, progressive disease;

PD, pharmacodynamic;

PI3K, phosphoinositide 3-kinase;

PK, pharmacokinetic;

PKO, P-gp knockout (*Mdr1a/b*$^{-/-}$);

PR, partial response;

PTL, parthenolide;

P-gp, P-glycoprotein;

RANO, Response Assessment in Neuro-Oncology;

RBC, red blood cells;

RT, radiation therapy;

SD, stable disease;

SVZ, subventricular zone;

TCGA, the Cancer Genome Atlas;

TICs, tumor-initiating cells;

TKO, triple knockout (*Mdr1a/b*$^{-/-}$ *Bcrp*$^{-/-}$);

TRD, Texas red-dextran;

T1-MR, T1-weighted magnetic resonance;

T2-FLAIR, T2-weighted fluid-attenuated inversion recovery;

WBC, white blood cells

FORWARD

In 2000, Drs. Douglas Hanahan and Robert Weinberg, pioneers in the field of cancer biology, forecasted the course of oncology research:

> *"Some would argue that the search for the origin and treatment of this disease will continue over the next quarter century in much the same manner as it has in the recent past, by adding further layers of complexity to a scientific literature that is already complex almost beyond measure. But we anticipate otherwise: those researching the cancer problem will be practicing a dramatically different type of science than we have experienced over the past 25 years. Surely much of this change will be apparent at the technical level. But ultimately, the more fundamental change will be conceptual" (Hanahan & Weinberg, 2000).*

In this thesis fifteen years later, it is my endeavor to support their prediction; in the field of neuro-oncology research, the most pressing concern is not the degree of detail that could further define the disease, but rather the broader observation that despite our best efforts, brain tumor therapies continue to fail in clinical trials. It is the goal of this thesis to understand and learn from such failures.

CHAPTER 1

Introduction

1.1 Hallmarks of Cancer

Cancer is a disease first described by Egyptian physician Imhotep in 2500 BC (Mukherjee, 2011). He described a bulging mass protruding from the breast of one of his female patients and despite an anthology of remedies for various ailments, he could not conceive of a treatment for this woman with breast cancer. Today, approximately 4,600 years later, while our understanding of the biological mechanisms contributing to cancer grows by leaps and bounds, we are still stuck at the same hurdle of how to combat the disease. To fight cancer, institutes have been created, wars have been waged, and an entire medical discipline has been formed, all with the purpose of finding a cure.

Scientists have generated tomes of literature to provide the understanding of cancer we have today. Drs. Douglas Hanahan's and Robert Weinberg's seminal review of cancer biology describes the disease's progression as a manifestation of Darwinian evolution (Hanahan & Weinberg, 2000): genetic alterations confer selective advantages for growth. Such alterations can include small changes to the DNA sequence, larger changes like chromosomal rearrangements and copy number aberrations, as well as epigenetic modifications that affect expression (McLendon et al., 2008a). The accumulation of five to seven specific alterations over time is thought to be required to cause the transformation of a normal cell to a cancer (Huether & McCance, 2013).

Notably, the majority of cancers are caused by environmental factors as only 5-10% of cancers are inherited (Nagy, Sweet, & Eng, 2004). The disease is characterized by multiple acquired capabilities impacting molecular, biochemical,

and cellular functioning. These traits are the hallmarks of cancer and include the following: a self-sufficiency in growth signals, insensitivity to antigrowth signals, evasion of apoptosis, limitless replicative potential, sustained angiogenesis, and tissue invasion and metastasis (Hanahan & Weinberg, 2000). More recent work has identified two emerging hallmarks: alteration of metabolic processes and immune evasion (Hanahan & Weinberg, 2011). Through such efforts, scientists now have a concrete understanding of the general mechanisms underlying carcinogenesis.

1.2 Glioma Classification & Staging

Gliomas are cancers of the glial or glial precursor cells that normally provide supportive functions to neurons in the brain. Glioma make up 80% of all primary brain tumor diagnoses with approximately 15,000 new cases diagnosed in the United States every year (Schwartzbaum, Fisher, Aldape, & Wrensch, 2006). Based on the World Health Organization's classification system of brain tumors, glioma are classified histologically as ependymomas, astrocytomas, oligodendrogliomas or mixed oligoastrocytomas on the basis of cell-type specific markers (Hulleman & Helin, 2005).

Astrocytomas account for approximately half of all gliomas and comprise four distinct subtypes: pilocytic astrocytoma (grade I), infiltrating astrocytoma (grade II), anaplastic astrocytoma (grade III), and glioblastoma multiforme (GBM, grade IV) (Hulleman & Helin, 2005). Grading of tumors corresponds to the stage of growth, with grade I being the least severe and grade IV being the most

aggressive form of growth (**Figure 1.1**) (Eckley & Wargo, 2010). As expected, staging also correlates with survival outcomes. Pilocytic astrocytomas are typically considered a benign form of growth because of their slow rate of growth and high cure rates associated with substantial long-term survival (Hulleman & Helin, 2005). In contrast, infiltrative astrocytomas have a prognosis of 10-15 years, anaplastic astrocytomas beget 2-3 years, and glioblastomas multiforme have a dismal 14-month survival estimate (Hulleman & Helin, 2005). This poor prognosis, coupled with the knowledge that GBMs account for 80% of all malignant glioma (Omuro & DeAngelis, 2013), explains why the majority of glioma research is focused on this specific subtype of disease.

The decreasing survival outcomes associated with the increase in staging can be likened to a clock counting down: as low grade glioma develop new genetic mutations, they typically progress into to higher grade glioma until reaching the lethal grade IV tumor (Holland, 2001). Through this developmental process, the resulting glioma is considered a secondary GBM (**Figure 1.2**) (Gonçalves, Xavier-Magalhães, Costa, Pojo, & Lourenço, 2013; Ohgaki & Kleihues, 2013). Despite the logical progression associated with this form of development, secondary GBMs account for only 10% of total diagnoses. Primary GBMs considered *de novo* for their diagnoses with no prior clinical history, make up the majority of cases (Ohgaki & Kleihues, 2013). As will be discussed later in this chapter, primary and secondary GBMs are likely two distinct pathological entities. Regardless of its developmental course, research efforts have largely focused on grade IV astrocytomas because they are so universally fatal.

The naming of these tumors also provides information regarding their molecular features, with characteristics accumulating at each grade of growth. Pilocytic astrocytomas, for example, are named for their long hair-like processes (Stüer et al., 2007). Infiltrating astrocytoma demonstrate invasive cells migrating away from a tumor core. Anaplastic astrocytoma, beyond an invasive character, also maintain cells with notable de-dedifferentiated qualities. Grade IV glioma, glioblastoma multiforme, is a histological melting pot of molecular pathology including a high degree of pleomorphism, an elevated rate of mitotic activity, intratumoral hemorrhaging, and a unique morphologic feature known as pseudopalisading necrosis (Vigneswaran, Neill, & Hadjipanayis, 2015). Not found in any other cancer, pseudopalisading necrosis is observed as an area of dead or dying tissue surrounded immediately by a configuration of densely populated live cells (Rong, Durden, Van Meir, & Brat, 2006). Recent research suggests this particular feature may arise as a result of tumor cells frantically migrating away from hypoxia arising after vascular insult (Rong et al., 2006). The heterogeneous presentation of glioblastoma multiforme closely mirrors its widely variable genetic makeup, also to be discussed later in this chapter.

1.3 Gliomagenesis

The exact mechanism detailing the formation of a glioma is not known. The development of malignant gliomas is largely considered random, but radiation exposure and a few rare, hereditary syndromes are known to increase the risk of the disease (Omuro & DeAngelis, 2013; P. Y. Wen & Kesari, 2008). Glioma risk is

not increased from exposure to cell phones, head injury, processed foods, pesticides, or season of birth (Omuro & DeAngelis, 2013). There are three major theories describing the gliomagenesis developmental process, although they are not necessarily exclusive of one another (**Figure 1.3**) (Gonçalves et al., 2013; Hulleman & Helin, 2005). All three theories discuss a potential “cell of origin” that acquires genetic mutations and ultimately gives rise to the tumor.

One of the most widely accepted hypotheses of cancer development is the acquisition of mutations in stem cells associated with a particular organ (Lobo, Shimono, Qian, & Clarke, 2007). Notably, the adult human brain has two sources of stem cell neurogenesis: the hippocampus and the subventricular zones (SVZ) (Bergmann, Spalding, & Frisen, 2015). Three important pieces of research support this hypothesis in glioblastoma multiforme: (1) the observation that GBM contains a population of cells expressing traditional stem cell markers including Nestin and Sox2 (Gonçalves et al., 2013; Singh et al., 2004) and this population demonstrates multiple stem cell properties including the growth of neurospheres in culture and a pluripotent capacity with the ability to give rise to multiple differentiated cell types (Singh et al., 2004); (2) stem cells have the long lifespan necessary for the accumulation of many genetic alterations (Adams, Jasper, & Rudolph, 2015); (3) the presence of oligoastrocytomas of mixed astrocyte and oligodendrocyte lineage can be explained by a neural stem cell capable of developing into either cell type (Hulleman & Helin, 2005). For these reasons, the neural stem cell theory of gliomagenesis has gained significant traction in recent years.

A second theory of gliomagenesis postulates that a glial progenitor cell, rather than a non-committed stem cell, gives rise to gliomas (**Figure 1.3**). Glial progenitor cells are abundant in the adult brain, typically serving a role to expand and mature cells (Goldman & Sim, 2005). The support for this theory of gliomagenesis closely mirrors many of the features discussed above: (1) glial progenitor cells are pluripotent (Gonçalves et al., 2013); (2) they have extensive mitotic competence necessary for the generation of multiple genetic mutations (Goldman & Sim, 2005); (3) the presence of olilgoastrocytomas can well be explained by the pluripotent nature of such cells acquiring mutations eventually producing a cancer phenotype. Comparatively, the shared immature phenotype between the neural and glial progenitor cells provides the foundation for characteristic and functional similarities.

Alternatively, rather than immature cells acquiring mutations that give rise to gliomas, a third hypothesis proposes that differentiated, mature glial cells acquire mutations capable of causing a de-differentiated cancer phenotype (**Figure 1.3**) (Hulleman & Helin, 2005). This convention is more in line with the classical hypothesis of cancer formation. In support of this idea, glial cells are the only known cell type in the adult brain to be replication-competent other than neural stem cells and glial progenitor cells (Gonçalves et al., 2013). Unfortunately, such a theory does not well explain the presence of oligoastrocytomas, gliomas containing cancer cells of multiple lineages including both astrocytes and oligodendrocytes (Hulleman & Helin, 2005). For this theory to be true, both an astrocyte and an oligodendrocyte would have to independently acquire the exact

mutations necessary to produce a cancer phenotype at the same time; although possible, this situation is highly unlikely. In the case of oligoastrocytomas, an immature precursor becoming malignant seems a much more reasonable theory for cancer development.

Despite the disparate natures of the presented theories, one of the most compelling proposals for gliomagenesis unites disparate molecular mechanisms in a single, elegant framework. The slow, progressive accumulation of mutations in a mature glial cell may contribute to the development of a secondary GBM, during which a patient's initial tumor escalates from a stage II to III to IV glioma (Maher et al., 2001). In contrast, a diagnosis of a primary GBM without any prior clinical evidence of disease may be due to the acquisition of genetic mutations in primitive neural stem or glial progenitor cells (Hulleman & Helin, 2005). The suggestion that different courses of development give rise to primary and secondary glioblastoma is also supported by the distinct genetic signatures of each clinical diagnosis (Ohgaki & Kleihues, 2007). While it remains difficult to provide definitive evidence for one theory over another, strong support of this dual-development framework in gliomagenesis is beginning to shape clinical trial design for potential therapeutics.

1.4 Glioma Stem Cells

There is a growing body of literature supporting the idea that some cancers, like glioma, are initiated and maintained by a population of tumor cells that closely mirror normal adult stem cells (J. Chen, McKay, & Parada, 2012; Tan, Park, Ailles,

& Weissman, 2006). This idea is the cancer stem cell theory. Just as normal stem cells are frequently capable of self-renewal and pluripotency, so too are cancer stem cells (CSCs), sometimes called tumor-initiating cells (TICs) (Kreso & Dick, 2014). Although a great deal of controversy remains concerning which tumors definitively contain or derive from CSCs and how best to define them, the cancer stem cell model has generated significant attention because CSCs may possess therapeutically relevant properties (Kreso & Dick, 2014; Llaguno, Chen, McKay, & Parada, 2011). Indeed, CSCs have been shown to propagate glioblastoma growth following chemotherapy, ultimately leading to recurrence (J. Chen et al., 2012). Targeting such populations may help to prevent these aggressive patterns of growth.

The first evidence for brain tumor stem cells came in the form of a *Nature* paper published in 2004 (Singh et al., 2004). The authors utilized what is considered the "gold standard measure" of experiments to determine stemness (Kreso & Dick, 2014) by demonstrating the recapitulation of clonal growth in functional *in vivo* repopulation assays. Briefly, stem cells defined by the cell surface protein CD133 were isolated from a human glioma, FACS sorted and then orthotopically implanted into an immunodeficient mouse (Singh et al., 2004). Not only did a full tumor develop with almost identical histological pathology to the original patient tumor, but as few as 100 cells were able to accomplish the job. Importantly, the CD133+ cells gave rise to a varied population of cells within the tumor and CD133- cells were unable to form a tumor, even at numbers as high as 100,000 cells (**Figure 1.4**) (Singh et al., 2004). Although the consistency of CD133

positivity as a marker for glioma stem cells remains debatable, and the frequency of glioma stem cells ranges from 2-30% (E. S. Molina, Pillat, Moura-Neto, Lah, & Ulrich, 2014), their presence is accepted in the field and they have become a frequent target for novel chemotherapeutics.

1.5 Genetic Contributions & Clonal Evolution in Glioblastoma

Not only is every cancer a distinct disease unto itself, but every tumor, even within the same diagnosis, is also considered unique. There is no “one size fits all” approach that can be used to evaluate or treat every tumor. Each tumor is a heterogeneous composite of cells containing a variety of genetic mutations (Kreso & Dick, 2014). Despite the challenges in characterizing such a heterogeneous type of disease, large-scale sequencing efforts reveal that certain mutations are often shared within a particular type of cancer. One such project, sponsored by the National Institute of Health through a program known as The Cancer Genome Atlas (TCGA), provided the most detailed analysis on glioblastoma to date—and made the data publicly available (McLendon et al., 2008a). This monumental study reported the most prevalent genetic alterations in 206 individual patient tumor samples. To summarize, 88% of samples had a functional signal alteration in the RTK/Ras/PI3K pathway, 87% exhibited alterations in p53 signaling, and 78% demonstrated alterations in RB signaling (**Figure 1.5**) (McLendon et al., 2008a). These data, published in 2008, provided the most promising targets for novel chemotherapeutic development in the history of glioma therapy.

Data provided by TCGA led to the stratification of glioblastoma into four individual subclasses: proneural, classical, mesenchymal, and neural. Originally, these subgroups were defined solely by their gene expression profiling. Each subtype embodies a distinct pattern of genetic aberrations: proneural maintains alterations of *PDGFRA* and point mutations in *IDH1;* classical demonstrates a focused predilection for *EGFR* amplification, *CDKN2A* deletion and a notable lack of *TP53 alterations*; mesenchymal is characterized by partial deletions of *NF1* and frequent *PTEN* mutations; neural present with more diverse genotypes (Verhaak et al., 2010). Beyond these alterations, each subtype expresses a particular set of markers characteristic to a specific cell type and recognition of these profiles has influenced the pathological nomenclature. For example, the proneural subtype is enriched with an oligodendrocytic signature, classical is strongly associated with astrocytic markers, mesenchymal maintains a cultured astroglial profile, and neural demonstrates a mixed panel of oligodendrocytic, astrocytic, and neural differentiation markers which is anticipated based on its more heterogeneous genetic composition (Verhaak et al., 2010). This form of classification has proved consistent outside of the TCGA dataset in a secondary validation cohort of tumor samples as well as in xenografted patient tumors in mice (**Figure 1.6**) (Verhaak et al., 2010). Two potential limitation of this classification scheme, however, are the presence of multiple subclasses within a tumor due to extensive genetic heterogeneity or tumor evolution, and the development of one subtype to another due to continued genomic evolution (Sottoriva et al., 2013). Despite these difficulties in interpreting an analyzing the genetic profiles of GBM, recognition of

its disparate genetic makeup has contributed to a greater molecular understanding of the disease.

The four subtypes of GBM are also associated with distinct clinical presentations, although a single tumor can present with multiple subtypes due to the heterogeneity of disease. The proneural subclass makes up 13% of GBM diagnoses, neural account for 12%, classical for 26%, and mesenchymal for 94% (N. Lin et al., 2014). Of note, the proneural subclass and its characteristic IDH mutations almost exclusive correlate with a secondary rather than primary GBM diagnosis (Nobusawa, Watanabe, Kleihues, & Ohgaki, 2009), which is in line with 10% secondary prevalence historically reported in the literature (Ohgaki & Kleihues, 2013). Secondary GBMs are thought to arise from sequential mutations in a mature glial cell (Maher et al., 2001), and it is therefore no surprise that the proneural subtype is associated with the least aggressive, best clinical prognosis (N. Lin et al., 2014). In contrast, the molecular subtypes associated with a greater propensity of primary GBM diagnoses are associated with poorer survival outcomes. Neural and mesenchymal subclasses have an intermediate outcome compared to proneural, and classical has the worst outcome (numerical quantifications not reported) (N. Lin et al., 2014). Collectively, these subtypes provide both a greater understanding of the disease and an opportunity to provide a more customized course of treatment.

While the molecular manifestations of glioblastoma have been well defined, they are not consistent over time, even within the same patient. A process known as clonal evolution drives the ebb and flow development of varying populations of

cells within an individual tumor (Greaves & Maley, 2012). While the coexistence of multiple clones within a single tumor is assumed to be due to random mutation in individual cells, the maintenance and growth of specific populations is under selective pressure and can be favored or disfavored by the tumor's microenvironment (**Figure 1.7**) (Inda, Bonavia, & Seoane, 2014). Treating a tumor that continuously evolves in response to multiple cues can be likened to an attempt at hitting a moving target. A particularly strong example of this phenomenon comes from a comparison of the genetic signatures of gliomas collected from patients before treatment with chemotherapy and recurrent tumors after chemotherapy has become ineffective. In 43% of the cases examined, approximately half of mutations identified in the original tumor were no longer present in the recurrent tumor (Johnson et al., 2014). Another similar study suggests as little as 11% of genetic events are shared between therapeutically naïve and post-treatment recurrent tumors (Ramaswamy & Taylor, 2015). Such data suggest chemotherapy induces a selective pressure in glioma whereby cells unaffected by treatment regenerate a new tumor with disparate molecular features and novel therapeutic targets. Therapeutics with the greatest clinical potential will therefore possess a wide range of molecular targets capable of inducing cytotoxic effects in all cancer cells.

1.6 Clinical Presentation & Treatment of Glioblastoma Multiforme

The diagnosis of a glioblastoma has become standardized and the care for affected individuals is highly consistent. The vast majority (90%) of glioblastoma diagnoses occur in adults over the age of 40, with 50% occurring over the age of

60 (Chang et al., 2005). There is a slight bias towards men being affected (60%) and the vast majority (86%) of affected individuals are of Caucasian descent (Chang et al., 2005). The initial clinical presentation of such individuals most frequently involves headache (56%), memory loss (35.5%), cognitive changes (34%), motor deficits (33%), language deficits (33%), and seizures (32%)(Chang et al., 2005). The most commonly performed diagnostic test is a magnetic resonance imaging (MRI) scan with contrast to reveal the presence of a brain tumor (Chang et al., 2005). Malignant gliomas typically enhance with gadolinium contrast, demonstrate central areas of necrosis, and are surrounded by white matter edema (Chang et al., 2005). They are usually unifocal but can, on occasion, present with multiple masses. The most common tumor location is the frontal lobe (41%), followed by the temporal lobe (33%), parietal lobe (23%) and less frequently, the occipital lobe (3%) (Keles, Anderson, & Berger, 1999). Although MRI can give clinicians a clue as to the type of tumor present in a patient, only histological staining or genetic sampling (Shirahata et al., 2007) of a biopsy sample can definitively confirm the specific type of cancer.

The first treatments for glioblastoma are intended to provide relief for some of the initial symptoms patients experience at diagnosis. 84% of patients are administered corticosteroids both to reduce pain-causing swelling and to stimulate an increase in appetite (Chang et al., 2005). 71% of patients are administered antiepileptics to try and mitigate the seizures that are often induced by the tumor (Chang et al., 2005). After addressing the comfort of the patient, clinical attention turns to the tumor itself. Most individuals diagnosed with GBM receive some form

of debulking surgery, but patients over 65 years of age are less likely to receive such invasive forms of treatment (Iwamoto, Reiner, Panageas, Elkin, & Abrey, 2008) due to increased risks for morbidity and toxicity as well as recognition that current therapies are highly aggressive and only considered palliative in nature (Iwamoto et al., 2008). Regardless of the election to submit to surgical resection, the procedure is considered part of the traditional standard of care afforded patients with GBM.

Following surgical debulking, patients usually receive some form of radiation therapy (RT) and chemotherapy. RT is a common clinical tool in cancer because it induces genomic instability through double-strand breaks in DNA (Sancar, Lindsey-Boltz, Ünsal-Kaçmaz, & Linn, 2004). Endogenous damage sensors detect these breaks and, in many cases, induce cell death to eliminate damaged cells (Sancar et al., 2004). The benefit of RT specifically in the treatment of GBM was first published in 1979 and demonstrated prolonged survival with increased applications of RT up to 6000 rad (Walker, Strike, & Sheline, 1979). With this dosing, patient survival increases from five months to eleven-to-twelve months (Walker et al., 1979). Whole brain RT was originally utilized in patients first due to technical limitation preventing more focal application and then later due to attempts at targeting not only the core of the tumor, but also the invasive cells that are not seen in gross imaging efforts. Currently, however, partial brain/focal RT is accepted as the current standard of care because it has been shown to provide equivalent therapeutic benefit with fewer side effects (Fiveash & Spencer, 2003). Additional research in novel applications of RT remain ongoing.

Temozolomide (TMZ), a DNA alkylating agent, is considered first-line therapy for newly-diagnosed glioblastoma and is dosed concurrent to and following RT. Treatment of GBM patients with TMZ marginally improves survival from twelve months to fourteen-to-fifteen months (Stupp et al., 2005). This therapeutic benefit is most effective in the 80% of patients whose tumors display methylation of the promoter region of MGMT, the gene encoding the O^6-methylguanine DNA methyltransferase DNA repair enzyme (Hegi et al., 2005; McLendon et al., 2008b; Paz et al., 2004). In doses ranging from 75-150 mg per square body meter, the orally-administered drug functions to methylate DNA preferentially at the O^6 position of guanine (Friedman, Kerby, & Calvert, 2000; Stupp et al., 2005). This methylation inhibits partnering to a nucleotide, resulting in long-lived nicks to the DNA (Friedman et al., 2000). The accumulation of such nicks eventually limits replication and cell death usually follows (Friedman et al., 2000). Because the effects of this mechanism are not targeted to any particular genes or any specific population of cells, TMZ is considered a generally cytotoxic therapy. The lack of specificity in targeting can have deleterious effects on optimal functioning. For instance, GBMs treated with TMZ can occasionally give rise to a hypermutated phenotype (Johnson et al., 2014; Ramaswamy & Taylor, 2015) brought on by drug-induced inactivation of the *MSH6* mismatch repair gene (Yip et al., 2009). Inactivation of this gene has consequently shown to cause resistance to TMZ and a recurrence of the tumor (Yip et al., 2009). More targeted therapies with less of a predisposition to resistance are therefore urgently needed.

In May of 2009, the FDA granted accelerated approval for the first antiangiogenic therapy (AAT) in GBM: Genentech's Avastin (bevacizumab). Bevacizumab is a monoclonal antibody targeted against the pro-angiogenic molecule, vascular endothelial growth factor (VEGF) that is produced in excess amounts by tumors like GBM (Plate, Breier, Weich, Mennel, & Risau, 1994). The drug binds VEGF to prevent the molecule from docking to and activating the tyrosine kinase VEGF receptor (VEGFR) that would initiate downstream signal cascades to promote angiogenesis and vascular permeability (Gil-Gil, Mesia, Rey, & Bruna, 2013). Although initial data from clinical trials were very promising, the use of the drug in GBM remains contested. Reviews of previous efforts utilizing bevacizumab cite both the difficulties in measuring tumor response as well as the lack of appropriate control arms in phase II clinical trials as rationale for an inability to accurately assess treatment response (de Groot & Mandel, 2014). More recent trials show no benefit to overall survival compared to therapy without bevacizumab (de Groot & Mandel, 2014). For these reasons, the European Medicines Agency has rejected the drug for use in glioblastoma (de Groot & Mandel, 2014) and there has been considerable discussion about revoking the existing approval for bevacizumab in the United States, as well.

1.7 Glioblastoma Multiforme as a Disease of the Whole Brain

GBM remains a difficult disease to treat because of its invasive quality. Glioma cells are known to migrate along myelinated fiber tracts and vascular basement membranes as much as four centimeters away from contrast-enhancing

tumors (Giese, Bjerkvig, Berens, & Westphal, 2003; Silbergeld & Chicoine, 1997). Because they are physically removed from the bulk tumor, invasive cells escape surgical resection only to later cause tumor recurrence and death (Berens & Giese, 1999). Even extensive surgical measures like hemispherectomies do not eradicate the disease (Giese et al., 2003). The inability to target invasive cells therefore means that tumor recurrence is an inevitable characteristic of the disease (Fazeny-Dörner et al., 2003; P. Y. Wen & Kesari, 2008). Almost all (96%) patients experience recurrent tumor growth within two centimeters of the resection cavity (Berens & Giese, 1999). In recognition of this inevitability, surgical debulking efforts are limited to the bulk tumor to prevent adverse events associated with removal of normal brain tissue (Giese et al., 2003). RT is limited to the bulk tumor with the same reasoning, that adverse events associated with whole-brain treatment should be limited (Fiveash & Spencer, 2003). In avoiding some of the adverse events associated with whole-brain treatment, invasive cells are not sufficiently targeted and inevitably lead to tumor recurrence.

Considerable effort has been expended to better understand the invasive cells that are so problematic in GBM. In comparing gene expression profiles between invading and noninvading cells, genes implicated in cell motility such as *ATX*, *PYK2*, and *P311* and genes associated with anti-apoptotic pathways such as *BCLW* and *DAP3* are more highly expressed in the invasive cells (Hoelzinger et al., 2005; Mariani et al., 2001). Akt pathways are activated in this population while Erk pathways are down-modulated (J. R. Molina, Hayashi, Stephens, & Georgescu, 2010). These data provide a detailed characterization of invasive cells,

describing them as more motile, less prone to cell death and less proliferative than their bulk tumor counterparts. This composition of traits makes invasive cells more resistant to cytotoxic insult (Lefranc, Brotchi, & Kiss, 2005) and the dichotomy of these differential expression patterns contributes to the heterogeneity of the disease and the challenge in finding effective therapies capable of targeting all tumor cells.

1.8 Clinical Imaging in the Evaluation of Glioma

A wide range of imaging modalities are used to evaluate the anatomic qualities of brain tumors. T1-weighted magnetic resonance (T1-MR) with gadolinium contrast and computed tomography (CT) are the most commonly used imaging techniques for the diagnosis and evaluation of brain tumors (Fink, Muzi, Peck, & Krohn, 2015). Although CT is more readily available in the clinical setting, contrast-enhanced MR (CE-MR) is considered better because of the greater degree of detail the imaging provides (Fink et al., 2015). In this imaging modality, a GBM will usually present as a heterogeneous area of contrast enhancement (Pafundi et al., 2013). This pattern manifests as a result of the intermittent blood-brain barrier disruption characteristic of GBM that allows for the leakage of contrast (Karunanithi et al., 2013). T2-weighted fluid-attenuated inversion recovery (T2-FLAIR) is a second MR imaging sequence that provides a very different image of a brain tumor. T2-FLAIR delineates increased water within brain and therefore visualizes edema; because even a small number of invasive glioma cells are thought to induce edema, this imaging technique is hypothesized to provide an

indirect indication of invasive cells (Ellingson et al., 2012). T2-FLAIR is therefore a more sensitive imaging tool than either CT or T1-MR in the evaluation of brain tumors.

Beyond anatomic analyses, other imaging modalities can provide a degree of functional characterization of brain tumors. Functional MR (fMR) and forms of positron emission tomography (PET) scans with varying contrast agents are examples of such techniques and are beneficial tools in identifying brain tumors because cancerous tissues are more metabolically active than normal tissues(Fink et al., 2015). For this reason, these tools are more sensitive at detecting tumor than CT or conventional MR. fMR can aid in surgical planning by helping to differentiate tumor from non-neoplastic masses and critical areas of normal parenchyma (Bogomolny et al., 2004). While PET has similar capabilities, the standard ^{18}F-fluorodeoxyglucose (^{18}F-FDG) radiotracer normally utilized in a clinical setting is not appropriate for the brain (Bell et al., 2015). The brain utilizes more glucose than any other organ in the body, so there is significant background using the conventional tracer (Bell et al., 2015). Imaging brain tumors is therefore more frequently utilized with a 6-[^{18}F] fluoro-dihydroxy-L-phenylalanine (^{18}F-FDOPA) radiotracer (Bell et al., 2015). Although it is arguably the most sensitive imaging tool to date, ^{18}F-DOPA-based PET lacks resolution and its use has therefore been relatively limited. The discussion regarding the capabilities of imaging techniques becomes especially salient in the context of evaluating the growth of brain tumors and the efficacy of therapeutics.

The criteria for therapeutic response designated by the Response Assessment in Neuro-Oncology (RANO) Working Group defines disease progression and response to treatment on the basis of standardized imaging analyses (**Figure 1.8**) (Fink et al., 2015). In reference to the T1 framework, complete response (CR) is defined as the absence of tumor, partial response (PR) is >50% reduction in tumor size, stable disease (SD) is <50% reduction and/or <25% increase in tumor size, and progressive disease (PD) is >25% increase in tumor size (Fink et al., 2015). Despite the clarity of these parameters, there are still challenges with the analyses and interpretations of clinical imaging. In one such instance, pseudoprogression occurs as a false enhancement of MR imaging due to the transiently increased permeability of tumor vasculature following irradiation and temozolomide (P. Y. Wen et al., 2010). In another example, pseudoresponse manifests as a decrease in MR signal after anti-angiogenic therapy seals the blood-brain barrier and prevents the leakage of contrast agents (P. Y. Wen et al., 2010). Both cases demonstrate the fallibility of clinical imaging in interpreting glioma growth and response to chemotherapy. Research in functional imaging techniques remains a popular but contentious topic in neuro-oncology and considerable effort has been expended to improving the technology and increasing its clinical feasibility and accuracy.

1.9 Glioma Modeling

Testing novel chemotherapies targeting GBMs requires an appropriate animal model. Ideally, an animal model of GBM should recapitulate the same

histopathological, genetic, and imaging properties observed in the human condition (Jacobs, Valdes, Hickey, & De Leo, 2011). It should also share the same invasive and angiogenic qualities and should imitate the therapeutic responses of human glioma (Stylli, Luwor, Ware, Tan, & Kaye, 2015). A perfect model would further mimic the more subtle features of human brain tumors including stromal interactions and immune system influences (Kegelman et al., 2014). There are two fundamentally different approaches that have been utilized to model GBM: the first technique aims to generate tumors *de novo*, arising from the host brain by various methods and the second model uses an animal as a vehicle for propagating transplanted glioma cells into a full tumor (Brandner, 2013). Every approach comes with its distinct mixture of benefits and disadvantages and all models continue to be utilized in current research efforts.

The *de novo* or "spontaneous" generation of glioma can be generated through chemical induction or genetically engineered mouse (GEM) models. Some of the earliest work in brain tumor models came through the local introduction of carcinogenic methylcholanthrene (coal tar) pellets (Seligman, Shear, & Alexander, 1939; Stylli et al., 2015). More modern efforts at genetic manipulation occur through either germline modification or gene transfer to somatic cells (L. Chen, Zhang, Yang, Hagan, & Li, 2013). With both of these approaches, genes of interest that are thought to drive cancer formation are introduced to an animal at early phases of development. For germline modification, genetic constructs are microinjected into gametes such as an oocyte, egg or early embryos or embryonic stem cells (L. Chen et al., 2013). The gene(s) then randomly integrate into the host

genome (L. Chen et al., 2013). In somatic gene transfer, a viral or transposon vector containing the genes of interest is introduced to the brain of neonatal mice at P0-P1 (Wiesner et al., 2009). Both techniques are relatively unpredictable in their abilities to produce a tumor, but if a mass should develop, it would occur over a period of months, a time course considered fairly slow in cancer research (Newcomb & Zagzag, 2009). The phenotype of any such tumor would also be limited by the specific genes introduced to the system, so the similarity to human GBMs is variable. Despite these limitations, the advantages of GEM models include the establishment in immunocompetent animals, customization of the genetic constructs, and an organic pattern of growth with stromal and tumor interactions (L. Chen et al., 2013). Spontaneous models remain a valuable tool in cancer biology, particularly because of their strengths during investigations into the carcinogenesis of particular genetic mutations or chemicals.

Transplant models of gliomagenesis provide an alternative method of brain tumor induction. Unlike spontaneous models of brain tumor generation, transplant models have a predictable and reproducible rate of growth and cells are injected into a known location (Newcomb & Zagzag, 2009). For these reasons, this type of model is most frequently utilized in preclinical trials of chemotherapeutics (C. Dai & Holland, 2001). The possible modes of transplantation revolve around two central variables: location and genetics of origin. Glioma cells can be either transplanted orthotopically in the brain or heterotypically, via subcutaneous injection in the flank (Stylli et al., 2015). Transplanted glioma cells can come from an animal of the same strain (syngeneic), an animal of the same species but

dissimilar strain (allograft), or an organism of a different species (xenograft). All models can be used for preclinical evaluation of therapeutics, but syngeneic models are considered particularly advantageous because tumors can be cultured in immunocompetent animals that facilitate immunotherapy studies (Candolfi et al., 2007). Although a researcher has great flexibility and control over the application of transplant models, genetic drift is a known consequence of cell culture maintenance (Yost et al., 2013). Because the cell culture environment is quite different from the primary tumor physiological conditions, the line can undergo clonal selection and effectively transform its mutational profile (Yost et al., 2013). Dramatic changes in the mutational profile of the original tumor can limit the ability to accurately model the human condition. To help mitigate this complication, tumor cell lines can be grown and incubated in the flanks of immunodeficient mice rather than in a traditional cell culture environment (Carlson, Pokorny, Schroeder, & Sarkaria, 2011). Regardless of the limitations of the transplant model, its use persists primarily because of the technical ease of the procedure and ability to monitor for changes in genetic expression due to culture conditions.

Animal models provide the most promising opportunity to identify therapeutic targets and to test novel chemotherapies (C. Dai & Holland, 2001). Based on the wide range and flexibility in inducing a model of GBM, researchers can match a specific drug to a model that embodies the exact subtype or gene the compound was created to target. They can also purposely choose a less translationally relevant model to bias their results and increase the odds of obtaining significantly positive data. Preclinical data obtained through animal

models must therefore be heavily scrutinized and conclusions should be conservatively limited to the scope of the testing parameters.

1.10 Blood-Brain Barrier Biology

The blood-brain barrier (BBB) is an essential instrument in maintaining homeostasis within the brain. Composed of both physical and biochemical barrier elements, the BBB is made of a specialized network of proteins that provide a number of functions to regulate the neural microenvironment (Abbott, Rönnbäck, & Hansson, 2006). Small gaseous molecules and lipophilic agents diffuse freely through the lipid membranes composing endothelial cell membranes, but most molecular traffic is controlled by the BBB (Abbott et al., 2006). In particular, the physical barrier buffers the brain interstitial fluid from fluctuations in composition that normally occur in plasma due to changes in respiration, digestion, and exercise, while the biochemical barrier, through multiple transport systems, regulates molecular traffic to supply nutrients to and remove waste products from the brain (Abbott, 2005). Through these processes, the BBB helps not only to regulate the microenvironment of the brain, but also to protect its most important cells, the neurons and glia.

The physical components of the blood-brain barrier are provided in the form of endothelial cells and their specialized network of tight junction proteins. These tight junctions occlude the intercellular space normally present between endothelial cells, and provide a structural hindrance to paracellular diffusion of molecules into the brain interstitial fluid (**Figure 1.9**) (Abbott et al., 2006). Tight

junctions are so limiting that even the movement of small ions like sodium and chloride is restricted (Abbott et al., 2006). The family of claudin proteins that make up these tight junctions further restrict permeability of larger molecules that might otherwise be able to penetrate the brain (Noell, Mack, Wolburg, Wolburg-Buchholz, & Fallier-Becker, 2011). Astrocyte-based secretion of Sonic hedgehog signal to endothelial cells expressing Hedgehog receptors is known to be responsible for the promotion and sustainability of BBB functional integrity (Alvarez et al., 2011). The functional consequences of BBB physicality were first visualized more than 100 years ago, when scientists observed that certain dyes, upon injection in the vascular system, stained all organs but the brain and spinal cord (Ehrlich, 1904). Complementary follow-up studies demonstrated that the same dyes, injected into cerebrospinal fluid, stained only CNS tissue (Goldmann, 1913). These experiments established a physical barrier that would one day become attributed to endothelial cell tight junctions of the blood-brain barrier.

As a consequence of the physical attributes of the BBB that largely prevent paracellular trafficking between cells, most molecules move transcellularly from the blood into the brain. This trafficking is accomplished by a series of transporter proteins located on both the luminal and abluminal membranes of the vasculature (Deeken & Loscher, 2007). These transporters bind substrates selectively and function not only to limit the penetrance of molecules into the brain, but also to efflux molecules to the bloodstream that have already accessed the brain. The brain endothelial transporters providing nutrients include glucose carriers, amino acid carriers, ion transporters, and transporters for nucleosides, nucleobases, and

many other substances (Begley & Brightman, 2003). In cases where compounds need to be ferried against a concentration gradient, transporters powered by adenosine triphosphate (ATP) frequently help to facilitate this movement (Abbott et al., 2006). This family of transporters, known as the ATP-binding cassette (ABC) transporters, include 48 human members and encompass a wide variety of functions (Robey, Massey, Amiri-Kordestani, & Bates, 2010). Of these 48 members, many have well-established roles in drug resistance; the two best studied ABC transporters are P-glycoprotein (P-gp) and Breast Cancer Resistance Protein (BCRP) for their prominent roles in drug efflux (Agarwal et al., 2011b). Both transporters have broad and partly overlapping substrate specificities that include a wide variety of drugs in almost every therapeutic class (Agarwal, Hartz, Elmquist, & Bauer, 2011a). The presence of these transporters at the BBB is thought to provide a major impediment to drug delivery in the treatment of malignant glioma (Agarwal et al., 2011a).

The BBB is disrupted in many different neuropathologies. In brain tumors, downregulation of tight junction proteins like claudin 1/3 cause the breakdown of tight junctions and the subsequent development of leaky vasculature (Abbott et al., 2006; Noell et al., 2011). Leaky blood vessels allow the permeation of large molecules into the brain tumor, which explains why even unresectable brain tumors respond to chemotherapy to some extent (Fazeny-Dörner et al., 2003). Unlike the bulk tumor, invasive cells reside behind an intact BBB and therefore remain largely inaccessible by chemotherapeutics (**Figure 1.10**) (Agarwal, Sane, Oberoi, Ohlfest, & Elmquist, 2011). Antiangiogenic therapy that restores the BBB

provides a similar effect to the bulk tumor and limits the delivery of concurrently administered chemotherapeutics (Claes et al., 2008). The same protection the BBB affords to the brain to prevent toxic insult also limits the delivery of helpful drugs capable of targeting a tumor.

1.11 GBM Therapeutics in the Clinical Pipeline

The development of novel therapeutics for GBM remains a significant challenge. The heterogeneous nature of the disease makes appropriate targeting a formidable task; even if a list of appropriate targets could be generated, very few of them would be considered “druggable” or “ligandable” by conventional medicinal chemistry approaches (Patel, Halling-Brown, Tym, Workman, & Al-Lazikani, 2013). Although sometimes used interchangeably, “druggability” refers to the likelihood of finding a bioavailable small molecule to binds a particular target with the capability of modifying its function, while “ligandability” refers to the ability of a molecule to bind its target with high affinity (Edfeldt, Folmer, & Breeze, 2011). Druggability is often deemed the more difficult parameter to address in cancer therapeutics for two reasons: (1) many of the genes mutated in cancer are tumor suppressor genes, and it is strategically more challenging to appropriately restore appropriate levels of function to a hypoactive or absent protein than it is to inhibit hyperactive function; and (2) targets must be selected relatively downstream within a molecular pathway because a common mechanism of drug resistance is the mutation of a gene located downstream in the same molecular pathway that restores pathological functioning (Wang, Han, Mousses, & Von Hoff, 2006). For

these reasons, investigation into inhibitors of PI3K, MDM2/4, and CDK4/6 are highly valued against GBM; two dual PI3K/mTOR inhibitors will be discussed at length in subsequent chapters of this dissertation.

In the event a therapeutic is able to engage its intended target effectively and with high affinity, the BBB may further present an obstacle to that therapy's potential efficacy by limiting its delivery in the brain. Determining brain penetrance prior to clinical trials is therefore of paramount importance. It is well established that a brain penetrant compound must be small in size (<400 Daltons) and relatively lipophilic (<8 hydrogen bonds) (Pardridge, 2007), but it must also exhibit minimal liability for efflux, a concept to be addressed further in Chapter 2 and again in Chapter 3 in the context of anti-angiogenic therapy.

As the search continues for new products to combat GBM, two important therapeutic classes are beginning to gain considerable attention in clinical trials: immunotherapies and agents targeting glioma stem cell populations. As of June 2015, the clinical pipeline of GBM therapeutics included four Phase III products, forty-eight products in Phase II, and twenty-one products in Phase I (Hedden, 2014). The only four therapies to reach Phase III clinical trial status were immunotherapies, while anti-stem cell therapies as a class are not yet mature enough to have reached Phase III trials (Hedden, 2014). Both modes of therapy hold significant therapeutic potential. Toward this understanding, Chapter 4 of this dissertation describes preclinical testing of one particular drug known to target cancer stem cell populations in the context of malignant glioma.

1.12 Statement of Problem & Research Plan

At the end of 2015, the world's preeminent website for tracking and organization of clinical trials, clinicaltrials.gov, has logged over 1,000 clinical studies under the search phrase, "glioblastoma multiforme." This website has been active since the year 2000, which means that clinicians the world over have conducted approximately 68 trials per year on average. In that time, a span of 15 years, only one study has successfully produced a new treatment that has influenced the standard of care in GBM (Stupp et al., 2005). Over that same time period, the National Institute of Health initiated a new program to sequence and characterize the genetic mutations giving rise to the disease: the Cancer Genome Atlas (McLendon et al., 2008a). These efforts provided concrete targets for novel therapeutic applications and still, only minimal progress has been made. The best treatments known to science afford only five additional months' survival benefit over untreated patients (Stupp et al., 2005; Walker et al., 1979). Collectively, however, survival for patients diagnosed with GBM is a dismal fourteen months (Stupp et al., 2005). Fourteen months is not enough time.

One productive trial in 1,000 is a success rate of 0.01%. It is also a failure rate of 99.9%. In recognition of this bleak statistic, scientists need not only focus on determining newer, better therapies, but also on understanding why so many previous efforts have failed. These failures underlie not only the complexities of the disease, but also the intricacies of the brain, itself. It is my hypothesis that targeted therapeutics have failed in the treatment of malignant glioma due to the

invasiveness of disease, its genetic heterogeneity, and insufficient delivery of drugs.

In the following chapters, I will describe the importance of chemotherapeutic brain penetrance in treating GBM (Chapter 2). I will also denote the negative impact of anti-angiogenic therapy on concurrent chemotherapeutic delivery and efficacy in the disease (Chapter 3). Finally, I will demonstrate the importance of appropriate target selection in development and application of chemotherapeutics treating GBM (Chapter 4).

Figure 1.1

World Health Organization classification of glioma by histological presentation. Grade I tumors are often considered benign and Grade IV are thought to be the most malignant and most lethal form of disease. Figure from (Eckley & Wargo, 2010).

Figure 1.1

Grade	Comments
Grade I tumor (juvenile pilocytic astrocytoma)	Benign, slow-growing tumor; usually associated with long-term survival; least likely to recur
Grade II tumor (astrocytoma)	Increased hypercellularity; no mitosis; no vascular proliferation; no necrosis; can recur as a higher-grade tumor
Grade III tumor (anaplastic astrocytoma)	High rate of hypercellularity; high rate of mitosis; no vascular proliferation; no necrosis; high rate of tumor recurrence
Grade IV tumor (glioblastoma)	Very high rate of hypercellularity; very high rate of mitosis; presence of vascular proliferation; presence of necrosis

Figure 1.2

Generation of primary and secondary GBMs. Generation of primary and secondary GBMs are thought to arise through different mechanisms. Primary GBMs are thought to occur through the acquisition of numerous genetic mutations with the initial clinical phenotype presenting as a glioblastoma. Secondary GBMs, in contrast, are thought to occur through the gradual acquisition of mutations over time that give rise to different phases of glioma over time. Figure from (Ohgaki & Kleihues, 2013).

Figure 1.2

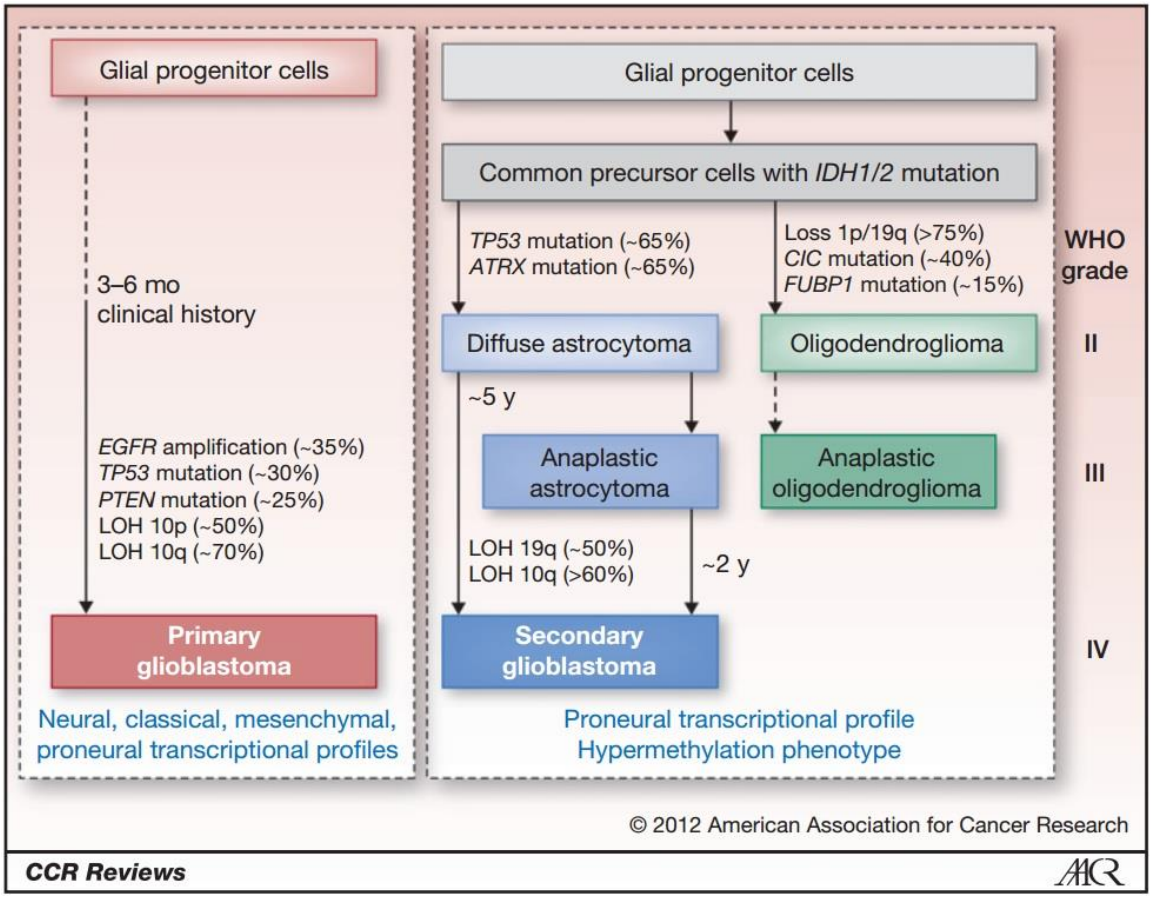
Glial progenitor cells
3–6 mo
clinical history
EGFR amplification (~35%)
TP53 mutation (~30%)
PTEN mutation (~25%)
LOH 10p (~50%)
LOH 10q (~70%)
Primary glioblastoma
Neural, classical, mesenchymal, proneural transcriptional profiles
Glial progenitor cells
Common precursor cells with IDH1/2 mutation
TP53 mutation (~65%)
ATRX mutation (~65%)
Loss 1p/19q (>75%)
CIC mutation (~40%)
FUBP1 mutation (~15%)
Diffuse astrocytoma
Oligodendroglioma
~5 y
Anaplastic astrocytoma
Anaplastic oligodendroglioma
LOH 19q (~50%)
LOH 10q (>60%)
~2 y
Secondary glioblastoma
Proneural transcriptional profile
Hypermethylation phenotype
WHO grade
II
III
IV
© 2012 American Association for Cancer Research
CCR Reviews
AACR

Figure 1.3

Developmental theories of gliomagenesis. Developmental theories of gliomagenesis encompass two main tracts, although they are not mutually exclusive of each other. Glioma are thought to arise either from (1) immature neural stem or glial precursor cells or (2) from mature and differentiated glial cells. Figure from (Gonçalves et al., 2013).

Figure 1.3

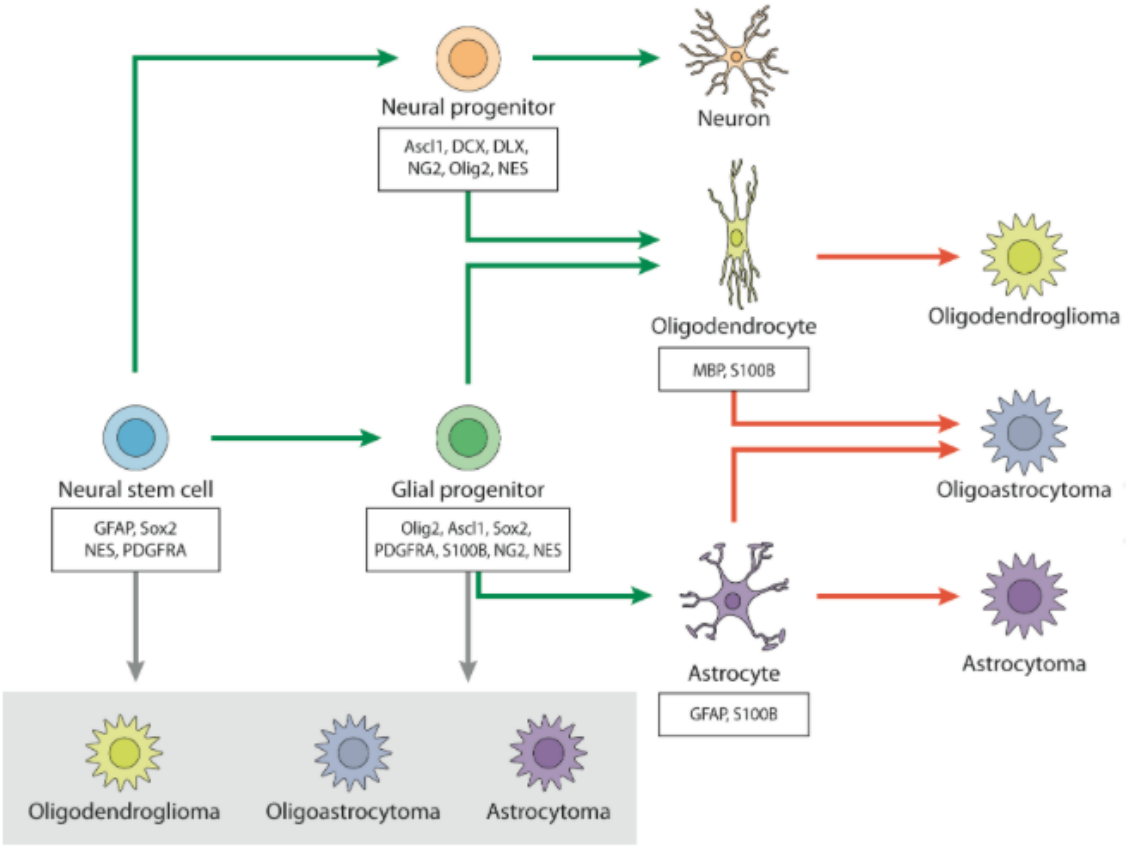
Neural progenitor
Ascl1, DCX, DLX,
NG2, Olig2, NES
Neuron
Oligodendrocyte
MBP, S100B
Oligodendroglioma
Neural stem cell
GFAP, Sox2
NES, PDGFRA
Glial progenitor
Olig2, Ascl1, Sox2,
PDGFRA, S100B, NG2, NES
Oligoastrocytoma
Astrocyte
GFAP, S100B
Astrocytoma
Oligodendroglioma
Oligoastrocytoma
Astrocytoma

Figure 1.4

CD133+ cells give rise to a tumor with varied populations of cells. (A) Staining for CD133+ is inconsistent within a tumor, suggesting that only subpopulations are express this marker. (B) Undifferentiated CD133+ populations (black arrow) coexist with differentiated GFAP+ cells (red arrow). (C) An initial population of cells selected for CD133 positivity can be specifically implanted into an animal and the tumor resulting from the animal has cells shown in (D) that are largely CD133-, thereby confirming the multipotency of the original CD133+ population. (E) Limiting dilution studies and proliferation assays (F) demonstrate that CD133+ populations exhibit growth characteristics typical of stem cells including growth in neurospheres and a high proliferative capacity. Figure from (Singh et al., 2004).

Figure 1.4

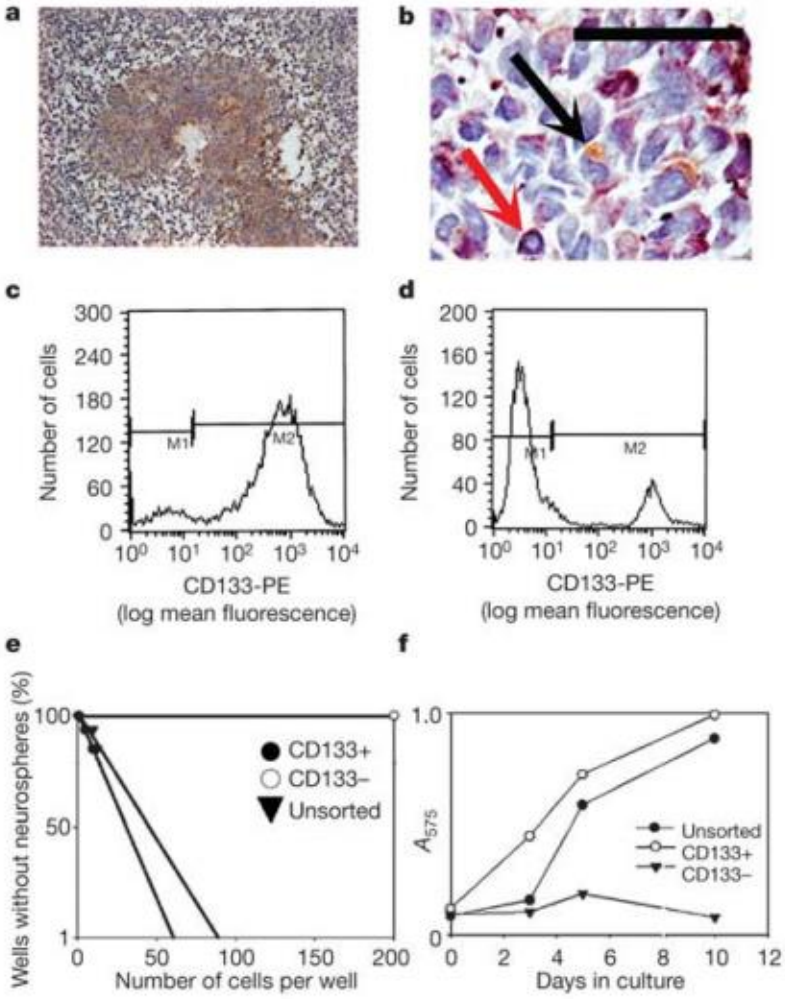
a
b
c
d
Number of cells
M1
M2
CD133-PE
(log mean fluorescence)
e
f
Wells without neurospheres (%)
CD133+
CD133–
Unsorted
Number of cells per well
A_{575}
Days in culture

Figure 1.5

TCGA provided data implicating three highly active pathways in glioblastoma: RTK/Ras/PI3K, p53, and RB. Variable components are mutated within each of the pathways but provide with similar functional outputs that favor growth and proliferation and disfavor apoptosis and senescence. Figure from (McLendon et al., 2008a).

Figure 1.5

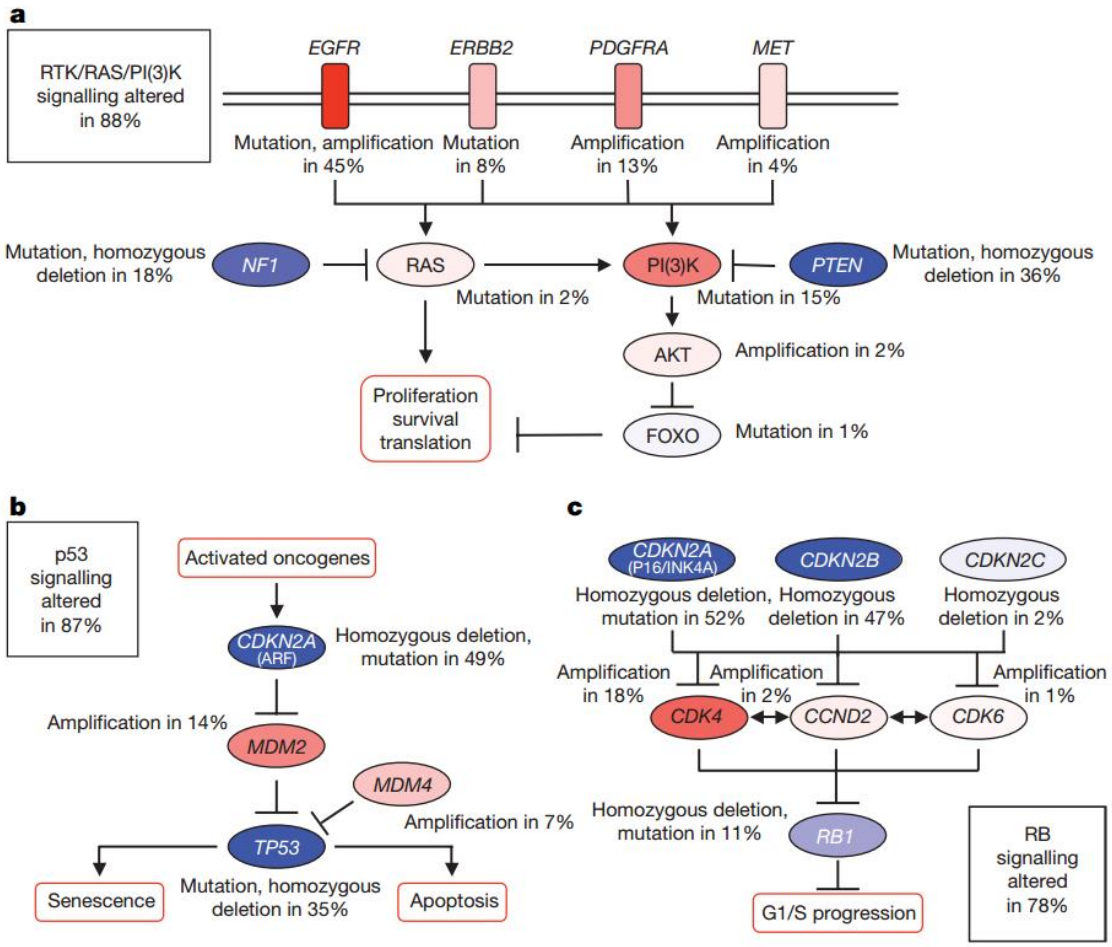
a
RTK/RAS/PI(3)K signalling altered in 88%
EGFR
ERBB2
PDGFRA
MET
Mutation, amplification in 45%
Mutation in 8%
Amplification in 13%
Amplification in 4%
Mutation, homozygous deletion in 18%
NF1
RAS
Mutation in 2%
PI(3)K
PTEN
Mutation, homozygous deletion in 36%
Mutation in 15%
AKT
Amplification in 2%
Proliferation survival translation
FOXO
Mutation in 1%
b
p53 signalling altered in 87%
Activated oncogenes
CDKN2A (ARF)
Homozygous deletion, mutation in 49%
Amplification in 14%
MDM2
MDM4
Amplification in 7%
TP53
Senescence
Mutation, homozygous deletion in 35%
Apoptosis
c
CDKN2A (P16/INK4A)
CDKN2B
CDKN2C
Homozygous deletion, mutation in 52%
Homozygous deletion in 47%
Homozygous deletion in 2%
Amplification in 18%
Amplification in 2%
Amplification in 1%
CDK4
CCND2
CDK6
Homozygous deletion, mutation in 11%
RB1
G1/S progression
RB signalling altered in 78%

Figure 1.6

Heat map of molecular signatures giving rise to four distinct cohorts of glioblastoma. Each subtype expresses a particular set of markers characteristic to a specific cell type, which has influenced the pathological nomenclatures. These patterns have been observed in (A) TCGA core samples and (B) validated in a separate set of samples as well as in (C) xenografts. Figure from (Verhaak et al., 2010).

Figure 1.6

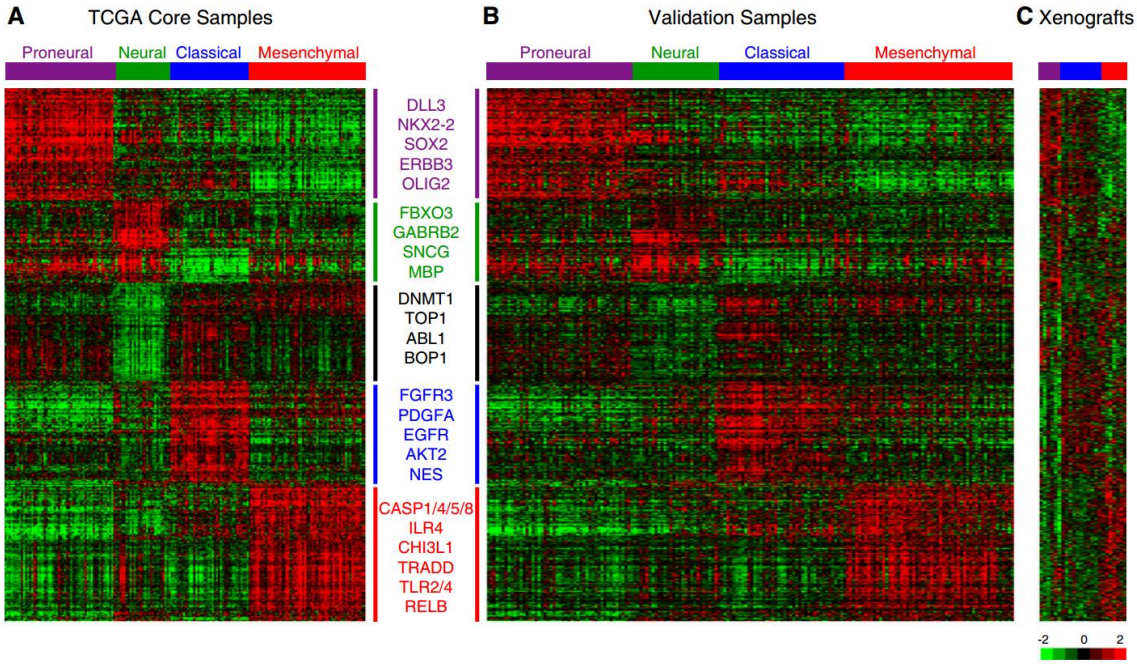
A
TCGA Core Samples
Proneural
Neural
Classical
Mesenchymal
B
Validation Samples
Proneural
Neural
Classical
Mesenchymal
C Xenografts
DLL3
NKX2-2
SOX2
ERBB3
OLIG2
FBXO3
GABRB2
SNCG
MBP
DNMT1
TOP1
ABL1
BOP1
FGFR3
PDGFA
EGFR
AKT2
NES
CASP1/4/5/8
ILR4
CHI3L1
TRADD
TLR2/4
RELB
-2
0
2

Figure 1.7

Clonal evolution of glioblastoma. Maintenance and growth of specific populations is under selective pressure and can be favored or disfavored by the tumor's microenvironment. This process can be visualized via a heterogeneous population of cells that is (A) devoid of stem cells or (B) inclusive of stem cells. Figure adapted from (Inda et al., 2014).

Figure 1.7

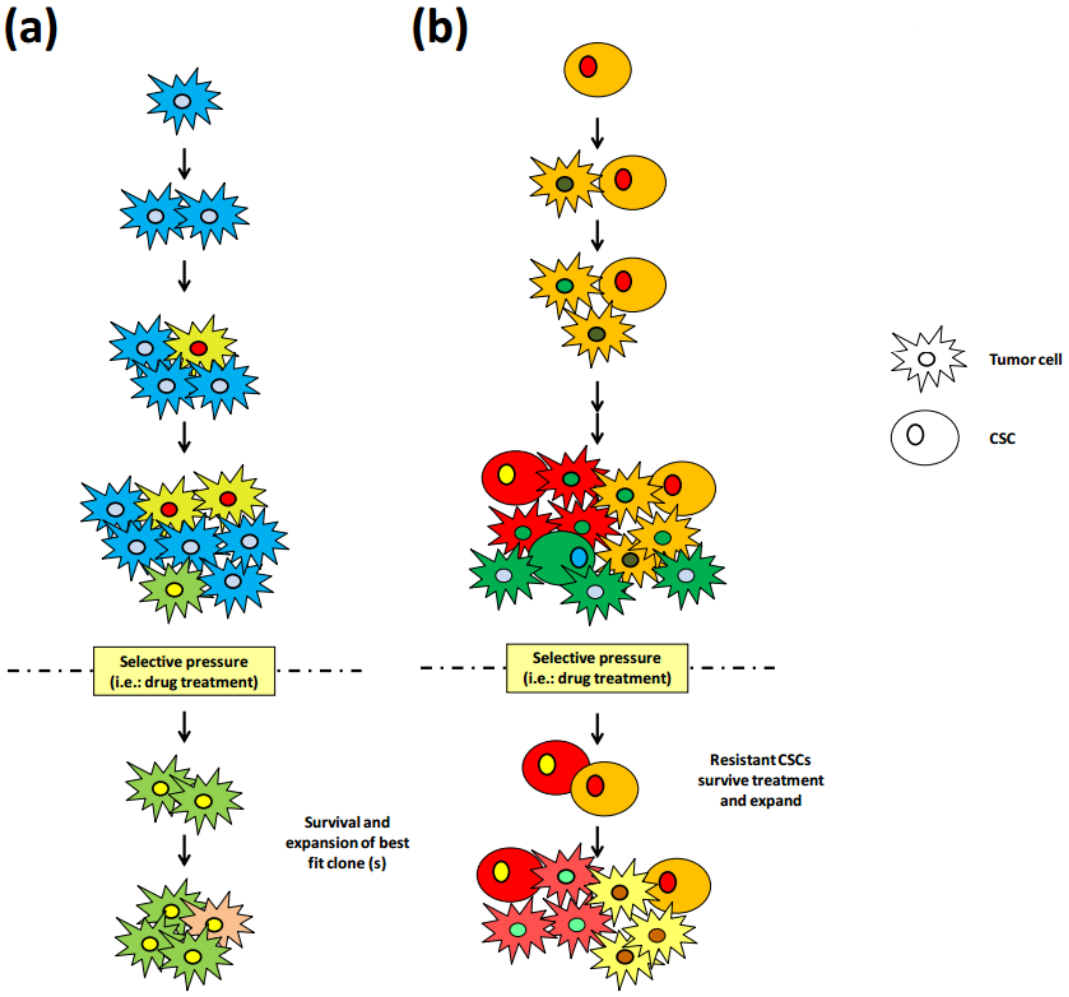
(a)
(b)
Selective pressure
(i.e.: drug treatment)
Survival and
expansion of best
fit clone (s)
Selective pressure
(i.e.: drug treatment)
Resistant CSCs
survive treatment
and expand
Tumor cell
CSC

Figure 1.8

RANO criteria determine the classification of response to treatment in malignant glioma. Complete response (CR), partial response (PR), stable disease (SD), and progressive disease (PD) are defined in the context of image enhancement, corticosteroids, and clinical status. Figure from (Fink et al., 2015).

Figure 1.8

Summary of RANO Response Criteria for High-Grade Gliomas

Criterion	CR	PR	SD	PD
T1-weighted gadolinium-enhancing disease	None	≥50% decrease	<50% decrease and <25% increase	≥25% increase*
T2/FLAIR	Stable or decreased	Stable or decreased	Stable or decreased	Increased*
New lesion	None	None	None	Present*
Corticosteroids	None	Stable or decreased	Stable or decreased	NA†
Clinical status	Stable or improved	Stable or improved	Stable or improved	Worsened*
Requirement for response	All of above	All of above	All of above	Any of above

*Progression occurs when this criterion is present.
†Increase in corticosteroids alone will not be considered in determining progression in absence of persistent clinical deterioration.
CR = complete response; PR = partial response; SD = stable disease; PD = progressive disease; FLAIR = fluid-attenuated inversion recovery; NA = not applicable

Figure 1.9

The blood-brain barrier is composed of both physical and biochemical components. The physical component is best represented by tight junctions present in endothelial cells (A) and (B) while the biochemical component is illustrated in part by a variety of transporter proteins (A). Figure from (Abbott et al., 2006).

Figure 1.9

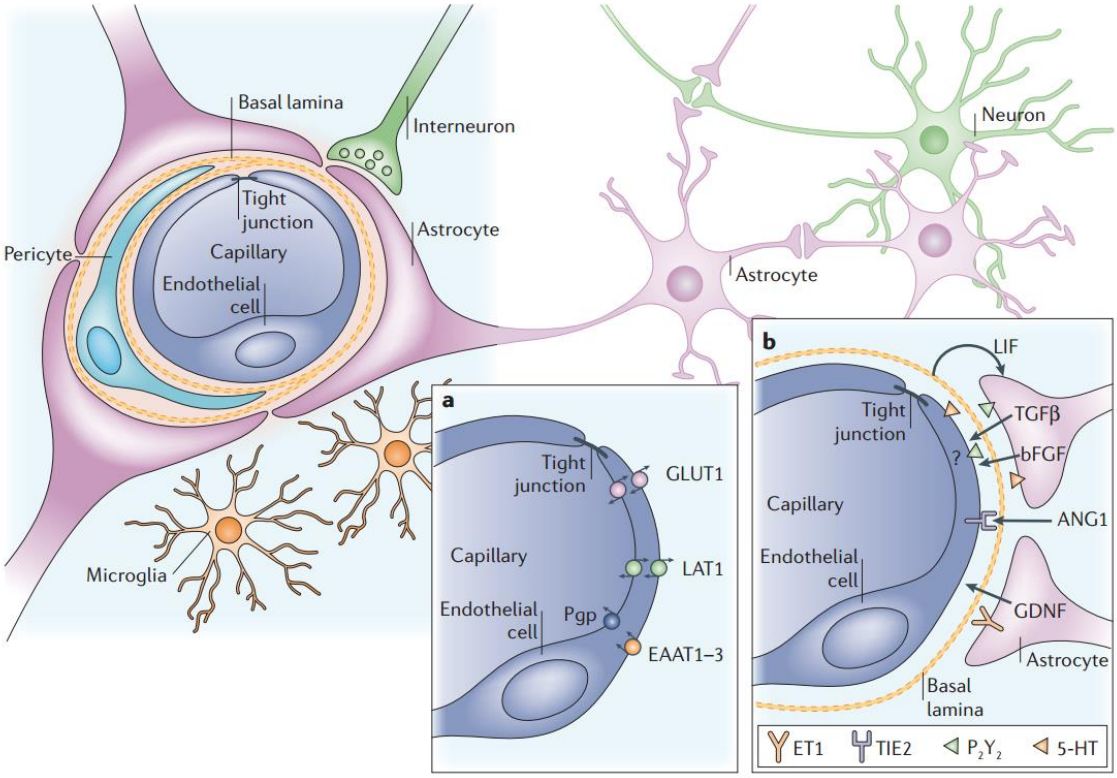
Basal lamina
Interneuron
Tight junction
Capillary
Endothelial cell
Pericyte
Astrocyte
Neuron
Astrocyte
Microglia
a
Tight junction
GLUT1
Capillary
LAT1
Endothelial cell
Pgp
EAAT1–3
b
LIF
Tight junction
TGFβ
?
bFGF
Capillary
ANG1
Endothelial cell
GDNF
Astrocyte
Basal lamina
ET1
TIE2
P2Y2
5-HT

Figure 1.10

Invasive glioma cells lie behind an intact blood-brain barrier. Behind an intact BBB, these cells are relatively inaccessible by therapeutics. This figure illustrates drug delivery in (A) a normal tumor environment, (B) a state following surgical resection of the bulk tumor identified during imaging and (C) an ideal scenario where high levels of drug permeate the brain in its entirety. Figure from (Agarwal et al., 2011).

Figure 1.10

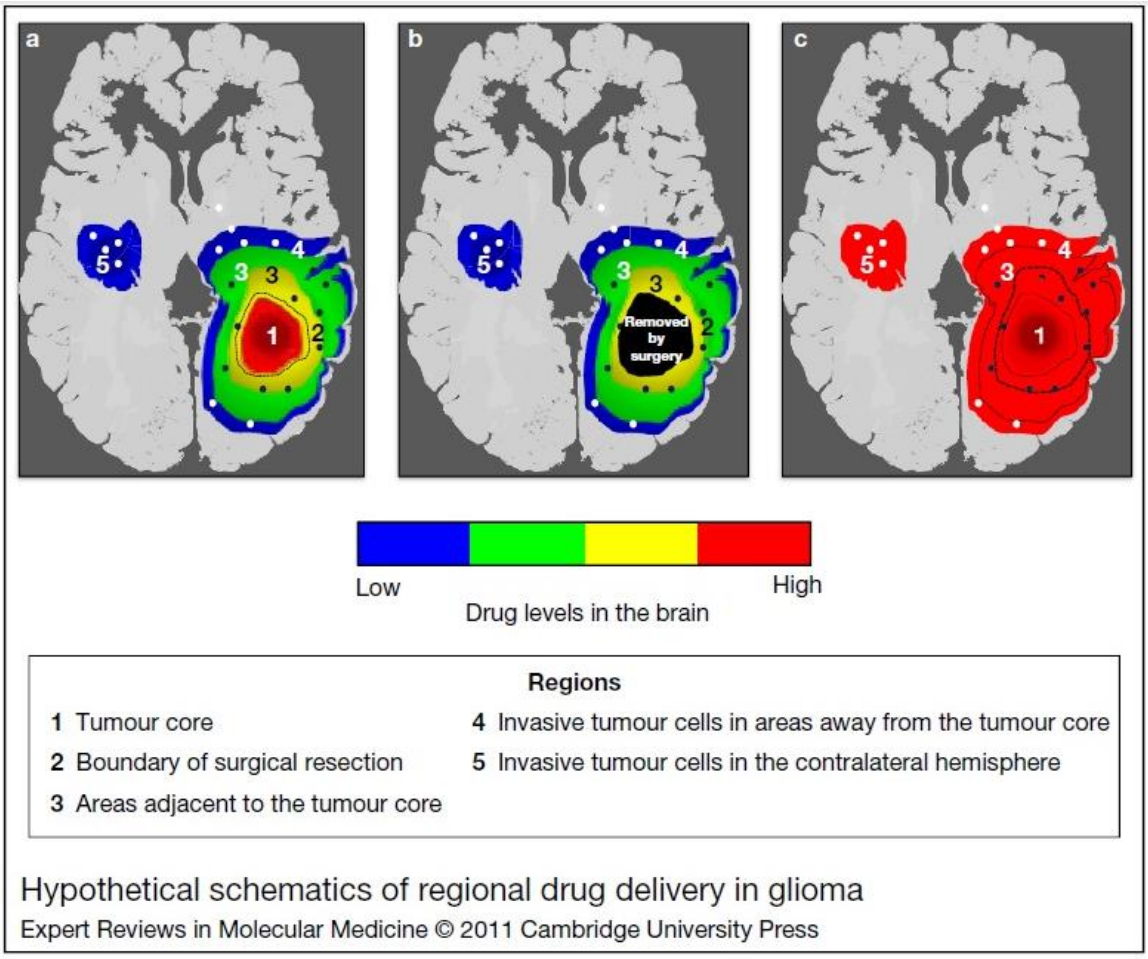

Hypothetical schematics of regional drug delivery in glioma

CHAPTER 2

The Influence of Active Efflux at the BBB on the PK/PD Properties of Dual PI3K/mTOR Inhibitors in the Treatment of Malignant Glioma

Chani M. Becker[1,2,6], Rajneet K. Oberoi[2,3,6], Stephan J. McFarren[1,2], Daniel M. Muldoon[1,2], Deanna H. Pafundi[5], Jenny L. Pokorny[5], Debra H. Brinkmann[5], John R. Ohlfest[1,2,4,6], Jann N. Sarkaria[5,6], David A. Largaespada[2,4,6], William F. Elmquist[1,2,3,6]

Adapted by permission from Duke University Press/Society for Neuro-Oncology

Chani M. Becker et al., Decreased affinity for efflux transporters increases brain penetrance and molecular targeting of a PI3K/mTOR inhibitor in a mouse model of glioblastoma multiforme, Neuro-Oncology (2015) 17 (9): 1210-1219.

Affiliations:

1. Department of Neuroscience, University of Minnesota, 6-145 Jackson Hall, 321 Church St SE, Minneapolis, MN 55455

2. Brain Tumor Program, University of Minnesota, 3-115 Cancer & Cardiovascular Research Building, 2231 6th St SE, Minneapolis, MN 55455

3. Department of Pharmaceutics, University of Minnesota, 9-177 Weaver-Densford Hall, 308 Harvard St SE, Minneapolis, MN 55455

4. Department of Pediatrics, University of Minnesota, 6th Floor East Building, 2450 Riverside Ave, Minneapolis, MN 55454

5. Department of Radiation Oncology, Mayo Clinic, 200 First St SW, Rochester, MN 55905

6. Brain Barriers Research Center, University of Minnesota, 9-177 Weaver-Densford Hall, 308 Harvard St SE, Minneapolis, MN 55455

Running title: BBB transport and delivery of PI3K/mTOR inhibitors to GBM

Funding:

National Institute of Neurological Disease and Stroke (NS077921 to WF Elmquist and JN Sarkaria)

National Cancer Institute (CA138437 to WF Elmquist and JR Ohlfest)

Children's Cancer Research Foundation (DA Largaespada)

Keywords: Blood-brain barrier, efflux transport, molecularly-targeted agents, p-glycoprotein, brain tumors

Conflicts of Interest:

JN Sarkaria: research funding from Genentech, Inc.

DA Largaespada: co-founder and part owner of two biotechnology companies, Discovery Genomics, Inc and NeoClone Biotechnology; Genentech, Inc. grant recipient.

WF Elmquist: consulting relationship with Genentech, Inc.

Author Contributions:

Conception and design: RK Oberoi, JR Ohlfest, JN Sarkaria, WF Elmquist

Development of methodology: CM Becker, RK Oberoi, JN Sarkaria

Acquisition of data (provided animals, acquired and managed patients, provided facilities, etc.): CM Becker, RK Oberoi, DH Pafundi, DH Brinkmann, JL Pokorny, JN Sarkaria

Analysis and interpretation of data (e.g., statistical analysis, biostatistics, computational analysis): CM Becker, RK Oberoi, JN Sarkaria, DA Largaespada, WF Elmquist

Writing, review, and/or revision of the manuscript: CM Becker, RK Oberoi, JN Sarkaria, DA Largaespada, WF Elmquist

Administrative, technical, or material support (i.e., reporting or organizing data, constructing databases): SJ McFarren, DM Muldoon

Study supervision: JN Sarkaria, DA Largaespada, WF Elmquist

2.1 Introduction

Glioblastoma multiforme (GBM) is the most commonly diagnosed primary tumor of the central nervous system, with 15,000 new cases diagnosed annually in the United States (Schwartzbaum et al., 2006). Median survival for patients diagnosed with GBM is only 14 months, and has not improved in recent years despite major advances in molecularly-targeted therapeutics (Stupp et al., 2005). Knowledge of the genetic and molecular mechanisms driving GBM and other types of cancers has led to the creation of targeted kinase inhibitors; despite such specific targeting, such drugs have not been clinically successful. These failures in clinical trials are often attributed to ineffective drugs, poor target selection, or various molecular mechanisms of resistance (Haar et al., 2012; Wilson, Karajannis, & Harter, 2014). Unfortunately, there has been limited consideration of drug delivery in the treatment of GBM and the inability of these drugs to effectively reach their targets.

Delivery of chemotherapeutics to the brain remains a significant challenge in the treatment of GBMs because of the tumor's invasive nature. Advanced imaging techniques demonstrate the presence of invasive cells that protected by an intact BBB and therefore remain largely inaccessible to chemotherapeutics (**Figure 2.1**). These imaging modalities that show changes in the BBB and extent of tumor invasiveness have been previously described (Pafundi et al., 2013). T1-gadolinium contrast enhanced (T1-CE) MR is limited in detecting only the core tumor mass where the BBB is disrupted (Karunanithi et al., 2013) and cannot detect invasive glioma cells in surrounding areas, where the BBB remains intact

(middle panels, **Figure 2.1A and 2.1B**). Alternatively, ^{18}F-DOPA PET (right panels, **Figure 2.1A and 2.1B**) and T2-weighted fluid-attenuated inversion recovery (T2-FLAIR) MR scans (left panels, **Figure 2.1A and 2.1B**) delineate a larger volume of tumor than T1-CE in the same patients (quantified signal volumes in **Figure 2.2**). Because glioma detection and the extent of malignant regions for surgical resection are primarily determined through contrast enhancement on T1-CE (Pafundi et al., 2013), some portion of the tumor is invariably left behind during surgery (**Figure 2.1B**). These images from glioma patients clearly demonstrate the need for chemotherapeutics capable of accessing invasive glioma cell populations that lie behind the protection of an intact BBB.

The design of brain penetrant drugs has traditionally addressed several key molecular characteristics including size, charge, lipophilicity, polarity, and molecular flexibility (Gabathuler, 2010; Pardridge, 2007). However, the affinity for drug efflux transporters is rarely considered despite recent advances in computational modeling that predict with 90% accuracy a molecule's efflux pump substrate affinity from its molecular structure (Levatic et al., 2013). This recent work has led to the identification of pharmacophores specific to substrates and non-substrates. Examples include amines and aromatic rings for "effluxophores" and aliphatic rings or saturated aliphatic chains for "anti-effluxophores" (Levatic et al., 2013). The designation and nomenclature associated with these pharmacophores should serve as a guiding tool in the development of brain-penetrant pharmaceutics.

The purposes of this study were to compare two dual PI3K/mTOR inhibitors with different affinities for P-gp and BCRP with respect to their BBB penetration to specific regions of tumor and to determine how these tumor delivery differences translate to molecular targeting efficacy and survival. An understanding of this mechanism in different regions of the brain tumor will allow us to develop compounds and novel therapeutics that can be more effective against invasive GBM, i.e., those tumor cells that are left behind following resection (Berens & Giese, 1999). We hypothesized that the strategic re-design of GDC-0980, a compound with high affinity for the described BBB efflux pumps, into a low-affinity oxetane derivative, GNE-317 (Heffron et al., 2012), would mediate not only increased brain penetrance, but also a greater ability to inhibit PI3K/mTOR pathways and improve survival in the GL261 model. Inhibition of these targets in particular is an important clinical goal since these pathways drive GBM growth and development (McLendon et al., 2008a; Sami & Karsy, 2013). In our work, we characterized the differential pharmacokinetic and pharmacodynamic properties of these compounds *in vivo*. Our data show that decreasing the substrate affinity for P-gp and BCRP increases brain penetrance and improves inhibition of the targeted signaling pathways. Collectively, these data suggest that brain-penetrant molecularly-targeted anticancer agents may be more efficacious in glioma if they demonstrate minimal substrate affinity for BBB efflux transporters, and the targeted agents are appropriate for the genetic drivers of tumor growth. Furthermore, the advent of such drugs may be derived from existing compounds rather than being synthesized *de novo*.

2.2 Materials and Methods

2.2.1 Animal Care

All procedures were carried out in accordance with the guidelines set by the Principles of Laboratory Animal Care (NIH, Bethesda, MD) and were approved by the Institutional Animal Care and Use Committee (IACUC) of the University of Minnesota (Minneapolis, MN). Animals were allowed food and water ad libitum. Female C57BL/6J mice were purchased from Jackson Laboratory. FVB/n wild-type (WT), *Mdr1a/b-/-* (P-gp knockout (PKO) mice), *Bcrp-/-* (BCRP knockout (BKO) mice), and *Mdr1a/b*$^{-/-}$*Bcrp*$^{-/-}$ mice (triple knockout (TKO) mice) were all purchased from Taconic Farms Inc.

2.2.2 Chemicals and Reagents

GDC-0980 and GNE-317 were provided by Genentech Inc. Drugs were suspended in dimethylsulfoxide (DMSO) for *in vitro* studies and in a vehicle of 0.5% methyl cellulose with 0.2% Tween 80 for *in vivo* work. Ammonium formate and acetonitrile were high performance liquid chromatography (HPLC) grade and were procured from Sigma-Aldrich (St. Louis, MO). Texas Red Dextran 3000 MW (TRD) was purchased from Molecular Probes (Invitrogen).

2.2.3 Tissue Culture

GL261 is an aggressive C57BL/6J-derived glioma line (Newcomb & Zagzag, 2009). This cell line was a kind gift from Dr. John Ohlfest (University of

Minnesota, Minneapolis, MN) and was transfected with both green fluorescent protein (GFP) and luciferase (Luc) from separate plasmids using methods described previously (Wu, Oh, Ericson et al., 2007). The resultant monoclonal GL261-GFP-Luc cells were maintained in DMEM supplemented with 10% FBS and penicillin/streptomycin (100 U/mL) and were cultured at 5% oxygen. Cell selection used 4 mg/ml puromycin (Invivogen) and 4 mg/ml G418 (Invivogen). Cellular viability assays were set up in a 96-well format with 2000 cells plated per well in the culture conditions described above. Cells were incubated in the presence of drug or vehicle for 48 hours and viability was assessed by MTS assay (Promega) according to the manufacturer's instructions. Absorbance at 490 nm was used to determine viability and at 650 nm to account for background using a Synergy Mx automated plate reader (BioTek). Numerical values from drug-treated wells were normalized to the values of vehicle-treated wells to yield percent survival.

2.2.4 Intracranial Tumor Implantation

Gliomas were established by intracranial inoculation of 30,000 GL261-GFP-Luc cells in 1 µL volume to 7-week-old C57BL/6J mice as previously described (Wu, Oh, Gharagozlou et al., 2007). Cells were prepared for inoculation by culturing to subconfluence and washing with phosphate-buffered saline (PBS), followed by trypsinization and filtration through a 40 um mesh, and resuspended in sterile PBS. Animals were anesthetized with an intraperitoneal (i.p.) injection of a ketamine/xylazine cocktail (53.7 mg/mL and 9.26 mg/mL xylazine delivered 1 mL/kg) before surgery. Cells were injected into the right ventral striatum at

coordinates 2.5 mm lateral and 0.5 mm anterior from the bregma at a ventral depth of 3 mm from the surface of the brain (Wu et al., 2007). Cells were injected at a continuous rate of 0.2 µL/min over 5 minutes. The progression of tumor growth was determined through bioluminescence imaging using the IVIS50 system (Caliper Life Sciences) after an i.p. injection of 100 µl of 28.5 mg/ml d-luciferin (substrate for luciferase enzyme, Gold Biotechnology) 10 minutes before imaging (Ohlfest et al., 2005). Animals were sedated using 2-5% isoflurane provided by nose cones within the imager. In survival studies, mice that became moribund were euthanized with carbon dioxide.

2.2.5 Blood-brain Barrier Imaging

When tumors reached a signal of 5e8 p/sec/cm^2/sr, C57BL/6J mice bearing GL261-GFP-Luc tumors were given an intravenous (i.v.) injection of 1.5 mg/ml Texas Red-dextran (TRD) (3000 MW, Life Technologies) (Agarwal et al., 2012). After 10 minutes, animals were euthanized with carbon dioxide and perfused with 10 ml PBS over one minute. Brains were harvested and flash frozen in isopentane (-80°C). Brains were sliced on a cryostat into 20 µm sections and mounted on charged glass slides. Sections were imaged using the GFP and Texas Red filters of a Leica DMI 6000B microscope. Images were acquired in grayscale using an associated Retiga 2000R camera (QImaging) at a variety of exposure times; the different exposure times were necessary to increase visualization in the smaller tumor-bearing slices and to prevent signal saturation in the larger tumor-bearing slices. The individual images were acquired using QImaging QCapture Pro v 6.0

software, compiled (Microsoft Image Composite Editor), and synthetically colored (Adobe Photoshop).

2.2.6 Steady-state Pharmacokinetics

The steady-state brain-to-plasma ratios for both GDC-0980 and GNE-317 were determined using Alzet osmotic minipumps (model 1003D, Durect Corporation) in FVB/n mice. The minipumps were filled with 100 µl of either a 5 mg/ml solution in DMSO of GNE-317 or a 10 mg/ml solution in DMSO of GDC-0980. On the day of the experiment, mice were anesthetized using 5% isoflurane and maintained under anesthesia with 2% isoflurane during surgery. The pumps were surgically implanted in the peritoneal cavity of the mice, after which the mice were allowed to recover on a heated pad. The pumps yielded a constant intraperitoneal infusion of 5 µg GNE-317/hr or 10 µg GDC-0980/hr. For GDC-0980, additional steady-state analyses were carried out in PKO, BKO, and TKO mice. After 48 hours (greater than 5 half-lives for either drug), animals were euthanized and both blood and brain were harvested and processed as described previously (Oberoi, Mittapalli, & Elmquist, 2013). Briefly, whole brains were rapidly removed, rinsed with ice-cold saline, blotted dry and transferred to pre-weighed tubes. Plasma was obtained by centrifuging the blood at 3500 rpm for 15 minutes at 4°C. Plasma and brain specimens were stored in -80°C until analysis by HPLC-tandem mass spectrometry (HPLC-MS/MS).

2.2.7 Quantification of GNE-317 and GDC-0980 in Brain and Plasma by LC-MS/MS

The plasma and brain concentrations of GNE-317 and GDC-0980 were determined using HPLC-MS/MS. On the day of the analysis, frozen brain samples were thawed at room temperature and brain weights were determined. Samples were homogenized using 3 volumes of 5% ice-cold bovine serum albumin prepared in phosphate-buffer saline (PBS) (pH = 7.4). Brain concentrations were corrected for the residual drug in brain vascular space (H. Dai, Marbach, Lemaire, Hayes, & Elmquist, 2003). Drug concentrations in GNE-317 alone or GDC-0980 alone treated groups were analyzed as follows: 100 μL of plasma or 200 μL of brain homogenate samples were placed in microcentrifuge tubes containing 10 μL of 2 μg/mL of internal standard (GNE-317: AG1478 (4-[3-chloroanilino]-6,7-dimethoxyquinazoline) or GDC-0980: dasatinib, free base) and extracted via vigorous vortexing with 500 μL of ice-cold ethyl acetate. Following centrifugation at 7500 rpm for 15 minutes at 4°C, 400 μL of the supernatant was transferred to microcentrifuge tubes and dried under nitrogen. Dried samples were re-constituted with 100 μL of mobile phase for GNE-317 (60:40:0.1, v/v%, 20 mM ammonium formate, pH 3.5: acetonitrile: formic acid) or GDC-0980 (72:28:0.1, v/v/v%, 20 mM ammonium formate, pH 3.5: acetonitrile: formic acid) and transferred to glass autosampler vials. The chromatographic system consisted of Agilent Technologies model 1200 HPLC system (Santa Clara, CA). Separation of the analyte was achieved using Agilent ZORBAX XDB Eclipse C_{18} column (4.6 x 50 mm, 1.8 um). The LC-system was linked to TSQ Quantum triple quadrupole mass spectrometer

(Thermo Finnigan) and data analysis was performed using Xcalibur software. The instrument was equipped with selected reaction monitoring (SRM) mode with an electrospray ionization source operated in positive ion mode at a spray voltage of 5000 V for both GNE-317 and GDC-0980. The mobile phase flow rate was 0.25 mL/min. The mass-to-charge transitions were programmed for: GNE-317 (415.11 → 385.13) and internal standard AG1478, (317.03 → 300.98) and GDC-0980 (499.24 → 340.98) and internal standard dasatinib (499→ 401). The assays were both linear over a range of 1.9 ng/ml to 1000 ng/ml with a coefficient of variation lower that 20% for all samples throughout both assays.

2.2.8 Regional Distribution of GDC-0980 and GNE-317 in GL261 Tumor-Bearing Mice

GL261-GFP-Luc cells were implanted in 7-week-old C57BL/6J mice. When tumors reached 5e7 photons/sec/cm^2/sr (radiance), animals were orally administered the maximum tolerated dose of GDC-0980 (7.5 mg/kg), GNE-317 (30 mg/kg) or vehicle once a day for three days. The maximum tolerated doses were defined as the greatest dose that could be administered to mice with <10% drop in bodyweight. Even at these different doses, both doses provide similar plasma concentrations, and thus, the same overall systemic exposure. At 1 or 6 hours after the third dose, mice were euthanized with carbon dioxide and perfused with 30 ml PBS. With the aid of GFP goggles (Biological Laboratory Equipment), brains were dissected into tumor core, tumor rim, and normal brain tissue (Agarwal et al., 2012). Tissue samples and blood were processed as described above and tissue

specimens from each group were analyzed for drug concentrations using LC-MS/MS.

2.2.9 Immunohistochemistry

GL261-GFP-Luc cells were implanted in 7-week-old C57BL/6J mice. When tumors reached bioluminescence radiance of 5e7 p/sec/cm^2/sr, mice were randomized into three groups (n=5-6 animals/group): (a) control (vehicle treated, p.o.), (b) GDC-0980 (7.5 mg/kg, p.o.), and (c) GNE-317 (30 mg/kg, p.o.). Drug solutions were prepared and administered once per day for three days as described above. All mice were anesthetized with carbon dioxide 1 or 6 hours after the third dose and perfused with 30 ml PBS. Brains were harvested and stored in 10% buffered formalin for 48 hours and then switched to 70% ethanol until processing. Formalin-fixed, paraffin-embedded brains were sectioned at 5 μm thickness and then heat-fixed onto charged glass slides for staining. Following deparaffinization and rehydration, antigen epitopes on tissue sections were exposed using an unmasking solution (Vector Laboratories). Tissue section slides were then exposed to 3% hydrogen peroxide to remove endogenous peroxidases. Blocking was conducted with 3% bovine serum albumin (BSA) in a humidified chamber overnight at 4°C. Sections were then treated with primary antibody (Akt, 1:200, Cell Signaling; p-Akt^{Ser473}, 1:50, Cell Signaling; 4EBP1, 1: 1000, Cell Signaling; p-4EBP1$^{Thr37/46}$, 1:1000, Cell Signaling; S6, 1:100, Cell Signaling; p-S6$^{Ser235/236}$, 1:50, Cell Signaling) in 1% BSA and allowed to incubate overnight at 4°C in a humidified chamber. After primary incubation, sections were PBS-washed

before incubating with 1:200 biotinylated goat anti-rabbit secondary antibody (Vector Laboratories) for 1 hour at room temperature. Sections were washed twice in PBS before a 30-minute application of an avidin/biotinylated enzyme complex conjugated to horseradish peroxidase (Vectastain Elite ABC kit, Vector Laboratories). After two washes in PBS, the sections were treated with freshly prepared 3,3′-diaminobenzidine substrate prepared according to the manufacturer's instructions (Vector Laboratories) and allowed to develop. Once a discernible signal was obtained, the reaction was stopped by placing slides in water. Finally, sections were counter-stained with hematoxylin, dehydrated, cleared in xylenes, and mounted in Permount (Fisher Scientific). Images were acquired in color with a Nikon AZ100 Macrofluorescence microscope. NIS-Elements software (Nikon Instruments, Inc.) was used to automatically stitch individual pictures.

2.2.10 Statistical Analysis

The unpaired two-sample t-test was used to compare between two groups. One-way ANOVA, followed by Bonferroni's test was conducted to test for significance among multiple groups. Significance was declared at $p<0.05$ for all tests. All tests were done using GraphPad Prism 5.01, San Diego, CA. Survival probabilities were estimated using Kaplan Meier survival curves, and the treatment groups were compared using the log-rank test.

2.3 Results

2.3.1 The GL261 Glioma Model is Characterized by Heterogeneous Blood-brain Barrier Disruption

Invasiveness of the GL261 model has already been established (Newcomb & Zagzag, 2009) and is even present on a macroscopic scale (**Figure 2.3A**). BBB disruption has been assessed in this model using T1-CE MRI (Leten, Struys, Dresselaers, & Himmelreich, 2014), but microscopic dye-based permeability studies provide a higher spatial resolution of these patterns of BBB disruption. In humans, BBB disruption is not homogeneous within the central tumor mass (**see Figure 2.1, middle panel**); rather, the tumor core displays heterogeneous disruption while the tumor rim, i.e., the invasive edge, demonstrates an intact BBB (Deeken & Loscher, 2007). To determine whether the GL261 model displays comparable deficits, a 3 kDa Texas Red dextran (TRD) permeability marker was injected into mice intravenously and allowed to circulate for 10 minutes. Penetrance of the dye was assessed in proximity to the GFP-positive tumor cells using fluorescence microscopy. Analysis reveals that at all tumor sizes, TRD accumulates heterogeneously at the center of the tumor mass with little to no accumulation at the tumor rim (**Figures 2.3B, 2.3C**). This animal model therefore recapitulates the patterns of BBB disruption seen in human GBM.

2.3.2 GNE-317 Exhibits Similar Cytotoxic Activity and Greater Brain Penetrance than GDC-0980

GNE-317 is an oxetane derivative of GDC-0980 synthesized with the goal of reducing substrate affinity for efflux transporters (Heffron et al., 2012). Despite the molecular changes at the piperizine group, both compounds retain the same molecular backbone including the morpholino and 2-aminopyrimidyl groups (**Figure 2.4A**). *In vitro*, GDC-0980 and GNE-317 demonstrate similar profiles in MTS cytotoxicity experiments using the GL261 cell line. These results suggest that the retained molecular structure common to both drugs allows for similar interactions with PI3K and mTOR targets (**Figure 2.4B**). The steady-state distribution of each drug to the brain was determined in mice implanted with mini-osmotic pumps that provided a continuous intraperitoneal infusion of either GDC-0980 or GNE-317. Both wild-type and TKO (*Mdr1a/b*$^{-/-}$ *Bcrp*$^{-/-}$) mice were used to ascertain the influence of P-gp and BCRP on the transport of drug across the BBB (**Figure 2.5**). After 48 hours of drug exposure, blood and brains were harvested and analyzed via LC-MS/MS.

In animals dosed with GDC-0980, the steady-state brain-to-plasma ratio was 0.1 ± 0.02 in wild-type mice and 1.03 ± 0.27 in TKO mice, a ten-fold increase in brain distribution when both P-gp and BCRP are absent (**Figure 2.4C**). In contrast, the brain-to-plasma ratios in animals dosed with GNE-317 were similar between wild-type and TKO mice (0.81±0.28 vs. 0.98 ± 0.78) (**Figure 2.4D**). Collectively, these data indicate that P-gp and BCRP act in a concerted fashion to efflux GDC-0980, but not GNE-317, and the absence of these transporters in TKO

mice results in a dramatic enhancement in brain distribution of GDC-0980. Further evaluation of GDC-0980 in PKO and BKO mice show that P-gp plays a dominant role in restricting brain distribution over BCRP (**Figure 2.6**).

2.3.3 GNE-317 Penetrates Regions with Invasive Cells More Effectively Than GDC-0980

Brain penetrance of many targeted agents will be expected to differ between regions with a disrupted BBB (like the tumor core) and regions with an intact BBB (like the tumor rim). We sought to determine whether drug distribution might also be affected by affinity for P-gp and BCRP a tumor-bearing animal. C57B6/J mice were intracranially inoculated with GL261-GFP-Luc cells and tumor growth was tracked through bioluminescence imaging. When tumors reached 5e7 radiance, animals were orally administered the maximum tolerated dose of GDC-0980 (7.5 mg/kg), GNE-317 (30 mg/kg) or vehicle once a day for three days. These doses resulted in the same level of total systemic exposure, allowing us to readily compare experimental differences in region-specific brain exposure between treated groups.

Mice were euthanized 1 or 6 hours after the final drug administration and brains were dissected into core, rim, and normal brain as denoted in Fig. 2A and analyzed by LC-MS/MS. Concentrations of GDC-0980 were significantly different between the various regions of the brain. The mean GDC-0980 brain concentration was 720 ± 280 ng/g in the tumor core, 160 ± 100 ng/g in the rim and 78 ± 37 ng/g in the contralateral hemisphere at 1 hr post last oral dose (**Figure 2.7A**). A similar

trend was observed 6 hours after the last drug administration. Concentrations in the tumor core (200 ± 110 ng/g) were higher than in the rim (40± 20 ng/g) and the contralateral hemisphere (70 ± 40 ng/g) (**Figure 2.7A**). Even in the tumor core, the brain-to-plasma ratios demonstrate poor brain penetrance of GDC-0980 (**Figure 2.7C**). In contrast, brain concentrations of GNE-317 were not significantly different in the tumor core, rim and normal brain (**Figure 2.7B**). The corresponding brain-to-plasma ratios at both 1hr and 6 hr for the three regions of the brain suggest that active efflux by both P-gp and BCRP does not influence brain tumor penetrance of GNE-317 (**Figure 2.7D**)**.** Collectively, these data highlight the importance of substrate affinity for efflux transporters as a key determinant of drug penetrance in various regions of malignant glioma, even in the central tumor mass, where there is an impaired BBB.

2.3.4 GNE-317 Inhibits PI3K/mTOR Pathways More Effectively than GDC-0980

To determine whether brain penetrance correlates with inhibition of signaling pathways at the tumor and surrounding rim, we used immunohistochemistry to visualize the ability of each drug to inhibit PI3K and mTOR signaling. Tumor-bearing mice were administered three doses of drug or vehicle over three days once bioluminescence signals reached 5e7 radiance. One hour after the third dose, animals were euthanized and brains were processed and sliced for staining. Immunohistochemistry focused on downstream targets of the PI3K/mTOR signaling pathway (p-Akt^{Ser473}, p-S6$^{Ser235/236}$ and p-4EBP1$^{Thr37/46}$)

(Sami & Karsy, 2013). Representative stained brain slices are shown in **Figure 2.8**. Untreated mice show high intensity staining of p-S6$^{Ser235/236}$, p-4EBP1$^{Thr37/46}$ and, to a lesser extent, p-Akt^{Ser473} within the tumor (**Figure 2.8**). In particular, p-S6$^{Ser235/236}$ staining is more diffuse within the backgrounds of the brain slices, which is consistent with normal brain mTOR activity. Animals treated with GDC-0980 show decreased staining for p-Akt^{Ser473}, but relatively unchanged staining for p-S6$^{Ser235/236}$ and p-4EBP1$^{Thr37/46}$. In contrast, mice treated with GNE-317 show substantial reductions in staining intensity within the tumor across all three phospho-proteins. Importantly, GNE-317 reduced p-S6 staining not only within the tumor, but also in the surrounding normal brain (**Figure 2.8B**). Six hours after dosing, the inhibitory effects of both drugs are largely absent in p-Akt and p-4EBP1 slices, but p-S6 staining is still reduced in mice treated with GNE-317 (**Figure 2.9**). No differences are seen in staining patterns using nonphosphorylated antibodies (Akt, S6, 4EBP1) 1 or 6 hours after dosing (**Figures 2.10 and 2.11**), suggesting that overall protein levels remain the same and the changes seen in levels of phospho-proteins between conditions are accurate. These data suggest that differences in substrate affinity for efflux transporters not only impacts brain penetrance (**Figure 2.7**), and hence, molecular target engagement.

2.3.5 *In Vivo* Efficacy of GDC-0980 and GNE-317

We next sought to determine how the differences in pharmacokinetics and pharmacodynamics observed between GDC-0980 and GNE-317 would impact tumor growth and survival. Seven days after intracranial inoculation with GL261-

GFP-Luc cells, mice were treated once daily with the maximum tolerated dose of GDC-0980 (7.5 mg/kg), GNE-317 (30 mg/kg) or vehicle. For GL261, tumor growth was tracked through bioluminescence imaging on a weekly basis (**Figure 2.12A**). There were no significant changes in GL261 tumor growth among the three groups. In assessing survival benefits in GL261, neither GDC-0980 nor GNE-317 provided survival benefit over the vehicle-treated animals (**Figure 2.12B**). The fact that these drugs were not effective *in vivo* is suggested by the *in vitro* cytotoxicity data showing that the drugs have limited efficacy in inducing cell death in the GL261 cell line (**Figure 2.4B**). Neither drug is effective in the GL261 tumor in spite of greater delivery and enhanced therapeutic targeting efficacy of GNE-317.

2.4 Discussion

The results of this study demonstrate the impact that affinity for efflux transporters can have on chemotherapeutic brain penetrance and molecular target engagement. We first highlight that the GL261 mouse model is an accurate representation of these qualities compared to human GBM pathology (**Figure 2.3**). By experimenting with two PI3K/mTOR analogues that possess the same molecular backbone and targeting capacity (Heffron et al., 2012), and similar physicochemical properties (**Figure 2.13**), we directly measure the influence of efflux transporter substrate affinity in the treatment of GBM. Drug distribution studies in non-tumor and tumor-bearing mice indicate that GNE-317 has better brain penetrance than GDC-0980 because the distribution of GNE-317 is not limited by active efflux at the BBB (**Figures 2.4 & 2.7)**. We also determine that

brain penetrance positively correlates with efficacy in molecular targeting, with GNE-317 being more efficacious than GDC-0980 at down-regulating the PI3K and mTOR pathways (**Figure 2.8**).

Despite the impact these drugs have on inhibition of PI3K/mTOR signaling, there were no demonstrable changes in tumor growth or survival (**Figure 2.12**). These data reinforce another important issue in drug design for GBM, target selection. The inability of these drugs to provide survival benefits is likely specific to the GL261 model, as other glioma models have shown to be sensitive to these agents (Salphati, Heffron et al., 2012). Previous work in conjunction with our *in vitro* data (**Figure 2.4B**) demonstrate that GL261 is at least partially driven by PI3K signaling (Newcomb & Zagzag, 2009), but other pathways likely play parallel roles in tumor growth and development (Szatmari et al., 2006), and combination therapies may be warranted. This failure does not preclude GDC-0980 or more likely, GNE-317, from being more successful in other models or in patients whose gliomas are primarily driven by these other pathways. The increase in brain penetrance and ability to effectively inhibit PI3K/mTOR pathways in our study still confirms that GNE-317 is capable of on target effects *in vivo,* and points to the fact that if combination targeted therapy is used for invasive brain tumors, all drugs in the combination should be brain penetrant.

The current study measuring brain penetrance and target inhibition in both tumor and normal brain provides data that is difficult to obtain in human patients. While clinicians have the ability to measure drug concentration in the homogenized tumor core following surgical resection, data from surrounding brain with invasive

tumor cells is more difficult to obtain. Unfortunately, drug concentration data from the tumor core where the BBB is heterogeneously disrupted do not accurately reflect drug concentrations in other areas of the brain. The lack of biomarkers or imaging techniques capable of indicating successes or failures in drug delivery therefore necessitates that clinicians understand the potential brain penetrance of a drug before its clinical application. This knowledge will help clinicians introduce chemotherapies into clinical trials that have a better chance of success.

The importance of brain penetrance of chemotherapeutics has significant implications regarding the development and evaluation of novel drugs for GBM. Recent attempts to determine drug concentrations and pharmacodynamic responses in tumor and normal brain samples from human patients (Pitz, Desai, Grossman, & Blakeley, 2011) highlights the importance of chemotherapeutic brain penetrance. By eliminating drug delivery issues as a variable in the failures of clinical trials, therapeutic target selection can receive greater attention and consideration. In simplest terms, if we can be assured of adequate delivery, we can then choose drugs based on information about tumor heterogeneity that is not confounded by differences in delivery.

This study also draws attention to the process of drug discovery and development. Beyond the conventional approach of generating novel compounds *de novo*, our study highlights how brain-penetrant targeted agents can be re-designed from existing drugs that have a high substrate affinity for efflux transporters. As elegantly illustrated by (Heffron et al., 2012) and (Salphati et al., 2012) a drug with limited brain penetration can be used as a scaffold to develop

highly brain penetrant analogues with a greater potential for clinical efficacy. At a time when the cost of creating a new drug surpasses $5 billion (Herper, 2013) the ability to modify existing compounds into new agents with potentially drastic changes in targeted bioavailability to sites of action cannot be undervalued.

Figure 2.1

Different imaging modalities visualize tumors residing behind an intact BBB. (A) Patient exhibiting multi-focal GBM with large tumors displayed through ^{18}F-DOPA PET imaging. (B) Another patient 3 weeks post-surgical resection exhibits obvious tumor via ^{18}F-DOPA PET that was missed during surgery.

Figure 2.1

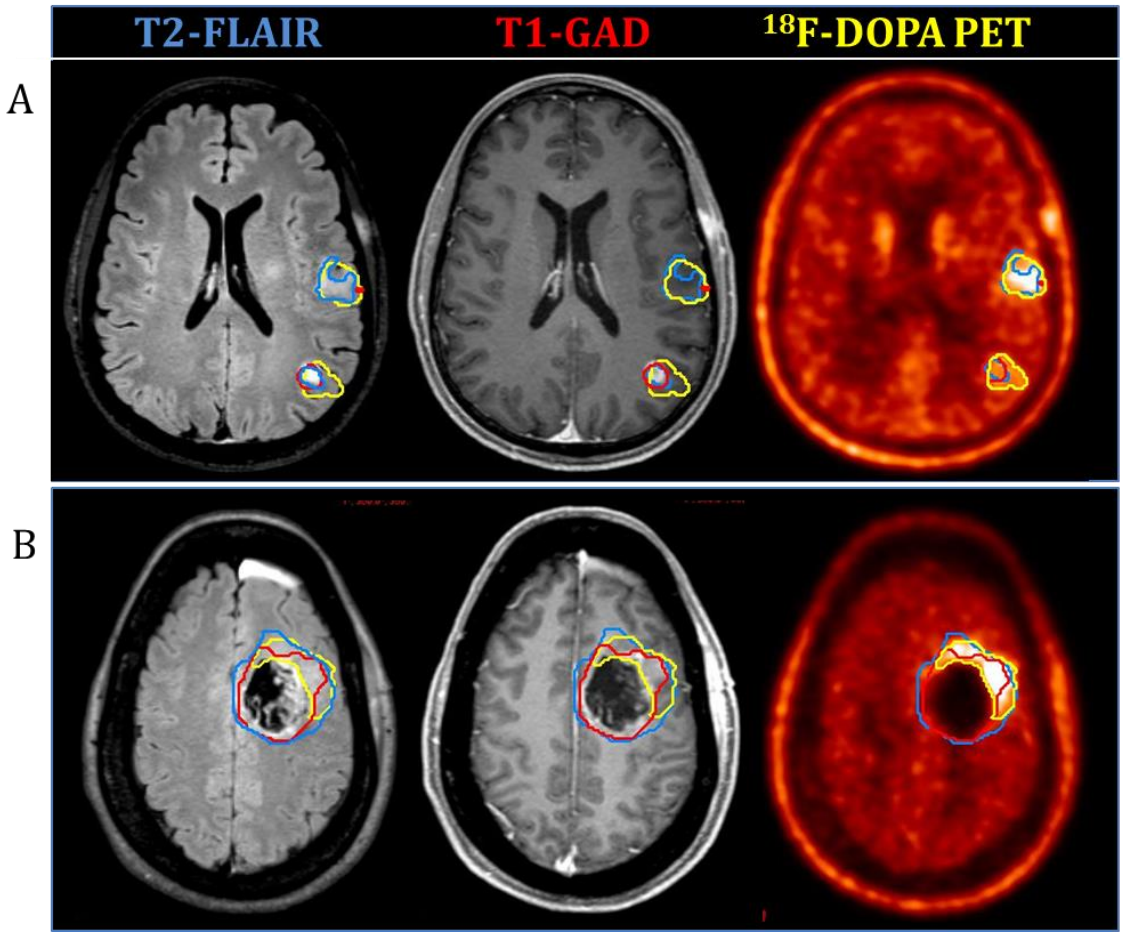

Figure 2.2

Quantified signal volumes for Figure 2.1A and Figure 2.1B. *T1-GAD contour includes post-operative cavity.

Figure 2.2

A

Modality	Contour Volume (cc)	PET Volume outside of T1-GAD (cc)	PET Volume outside of FLAIR (cc)	MR Volume outside of PET (cc)
T1-GAD	10.4	N/A	N/A	4.9
FLAIR	32.0	N/A	N/A	21.7
PET	19.5	13.8	9.1	N/A

B

Modality	Contour Volume (cc)	PET Volume outside of T1-GAD (cc)	PET Volume outside of FLAIR (cc)	MR Volume outside of PET (cc)
T1-GAD	47.7*	N/A	N/A	33.2*
FLAIR	54.3	N/A	N/A	36.4
PET	21.7	7.1	3.8	N/A

Figure 2.3

Characterization of the GL261 murine model. (A) A macroscopic view of GL261-GFP-Luc tumor-bearing brain demonstrates discernible core, rim, and normal brain sections. Scale bar represents 1 mm. (B) and (C) Images of GFP+ tumors and Texas-red dextran infiltration were overlaid to co-localize tumors and heterogeneous BBB disruption. Scale bars represent 1 mm.

Figure 2.3

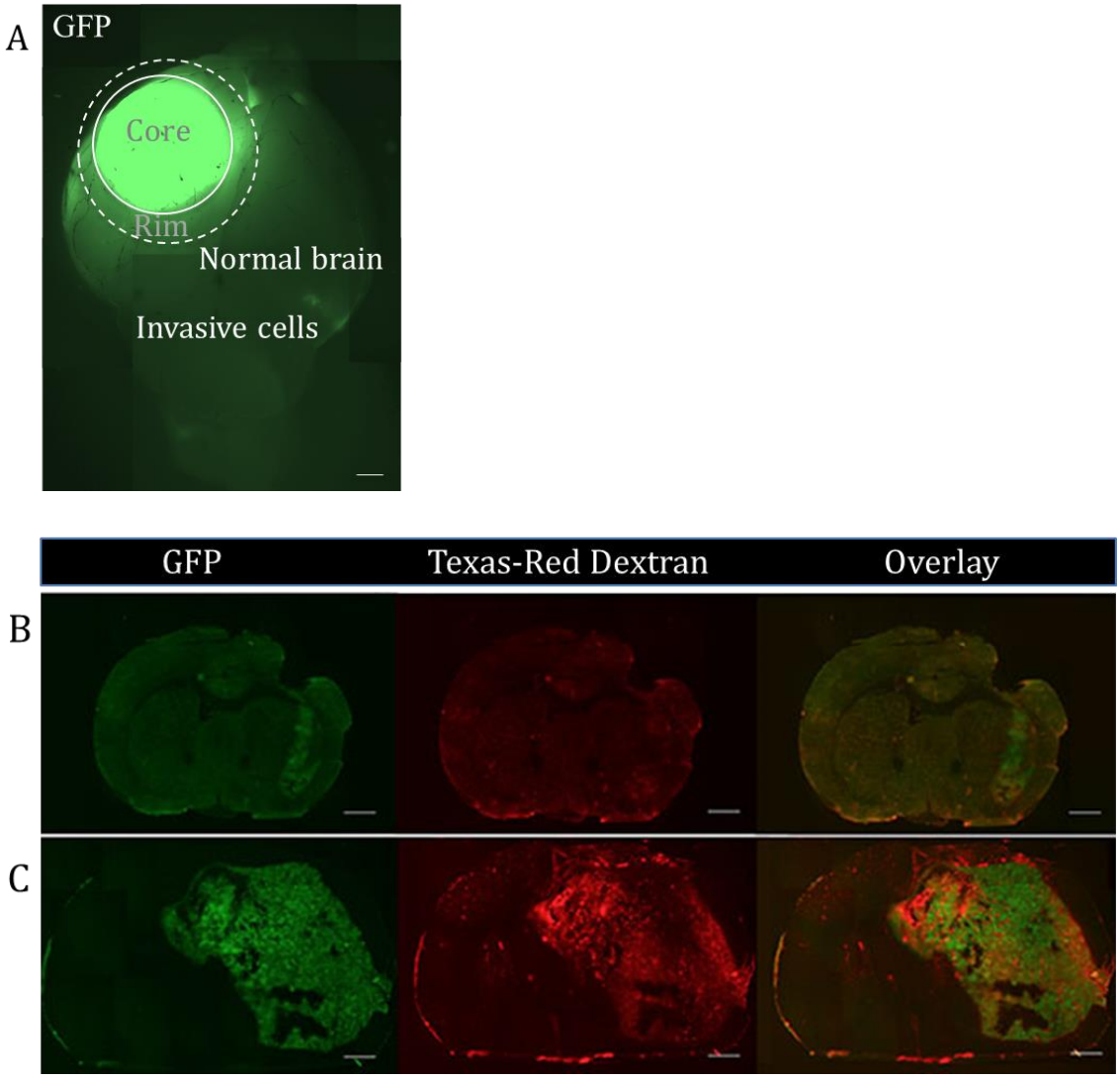
A
GFP
Core
Rim
Normal brain
Invasive cells
GFP
Texas-Red Dextran
Overlay
B
C

Figure 2.4

Cytotoxic and pharmacokinetic comparison of GDC-0980 and GNE-317. (A) Chemical highlight the common molecular backbone and differentiating side chains. (B) Cytotoxicity of GDC-0980 and GNE-317 was assessed in both murine GL261 glioma cell line using the MTS assay. (C) *Mdr1a/b*$^{-/-}$ *Bcrp*$^{-/-}$ triple knockout (TKO) mice treated with GDC-0980 display a significantly higher ($p<.0005$) brain-to-plasma ratio than wild-type mice. (D) *Mdr1a/b*$^{-/-}$ *Bcrp*$^{-/-}$ (TKO) and wild-type mice treated with GNE-317 display comparable brain-to-plasma ratios.

Figure 2.4

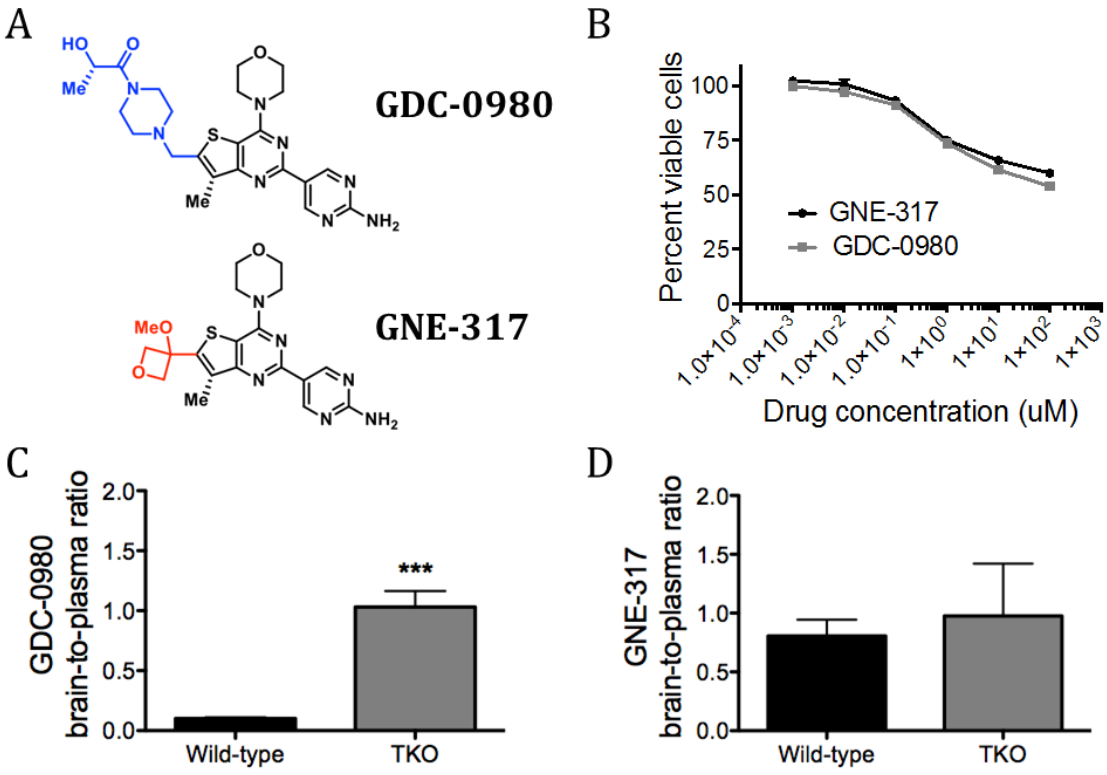
A
GDC-0980
GNE-317
B
Percent viable cells
100
75
50
25
0
GNE-317
GDC-0980
1.0×10-4
1.0×10-3
1.0×10-2
1.0×10-1
1×100
1×101
1×102
1×103
Drug concentration (uM)
C
GDC-0980 brain-to-plasma ratio
2.0
1.5
1.0
0.5
0.0
***
Wild-type
TKO
D
GNE-317 brain-to-plasma ratio
2.0
1.5
1.0
0.5
0.0
Wild-type
TKO

Figure 2.5

Comparison of steady-state kinetics in GDC-0980 and GNE-317 between wild-type FVBn and *Mdr1a/b-/- Bcrp-/-* triple knockout (TKO) mice. (A) and (C) Plasma and brain concentrations of GDC-0980 is significantly increased in TKO mice compared to wild-type ($p<.005$). (B) and (D) Plasma and brain concentrations of GNE-317 is approximately equal between TKO and wild-type mice.

Figure 2.5

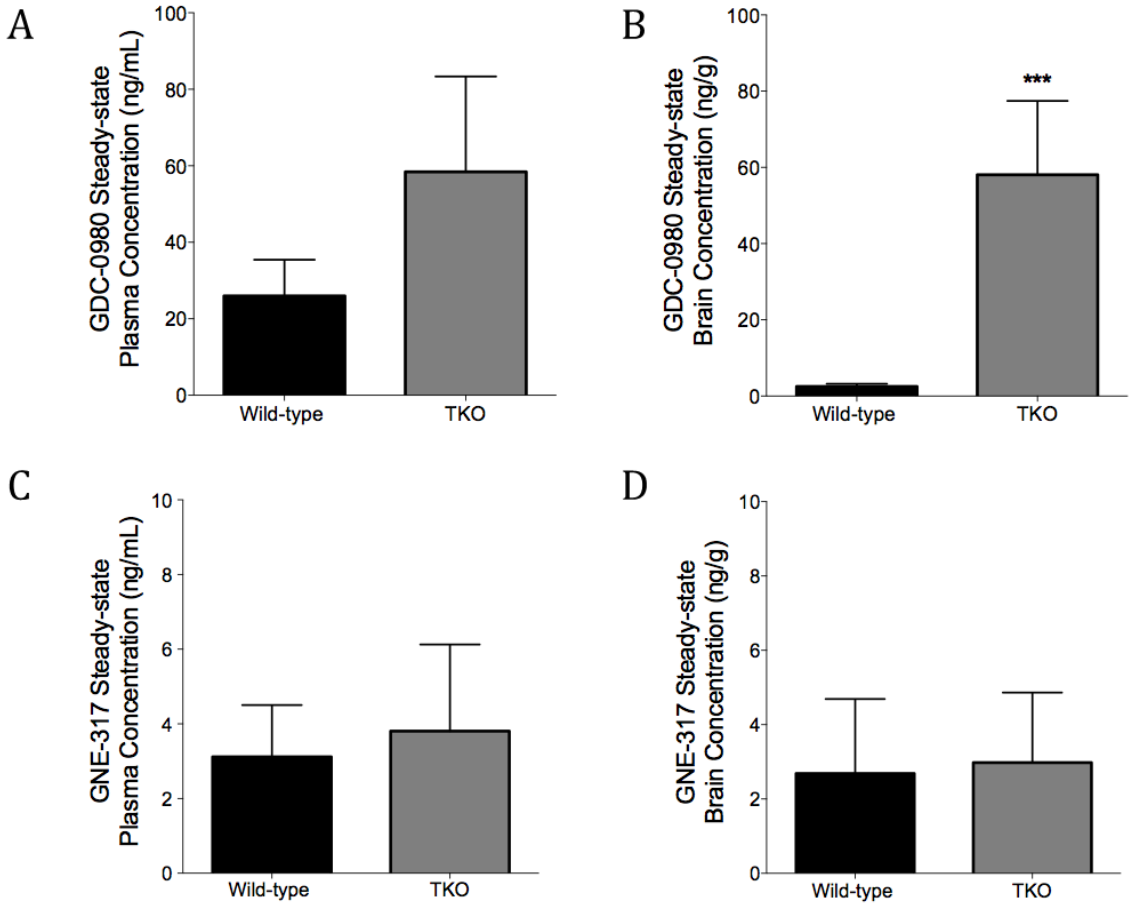
A
GDC-0980 Steady-state Plasma Concentration (ng/mL)
100
80
60
40
20
0
Wild-type
TKO
B
GDC-0980 Steady-state Brain Concentration (ng/g)
***
C
GNE-317 Steady-state Plasma Concentration (ng/mL)
10
8
6
4
2
D
GNE-317 Steady-state Brain Concentration (ng/g)

Figure 2.6

Brain-to-plasma ratios of GDC-0980 in wild-type and efflux transporter knockout mice. Wild-type, *Mdr1a/b*$^{-/-}$ (P-gp knockout (PKO) mice), *Bcrp*$^{-/-}$ (BCRP knockout (BKO) mice), and *Mdr1a/b*$^{-/-}$*Bcrp*$^{-/-}$ mice (triple knockout (TKO) mice).

Figure 2.6

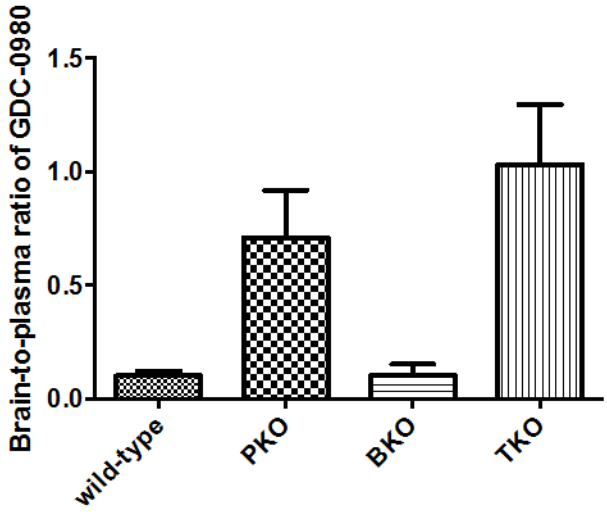
Brain-to-plasma ratio of GDC-0980
1.5
1.0
0.5
0.0
wild-type
PKO
BKO
TKO

Figure 2.7

Regional distribution of GDC-0980 and GNE-317 in a GL261-GFP-Luc tumor-bearing brain. (A) and (C) Regional brain and plasma distributions of GDC-0980 and corroborating brain-to-plasma ratios. (B) and (D) Regional brain and plasma distributions of GNE-317 and corroborating brain-to-plasma ratios.

Figure 2.7

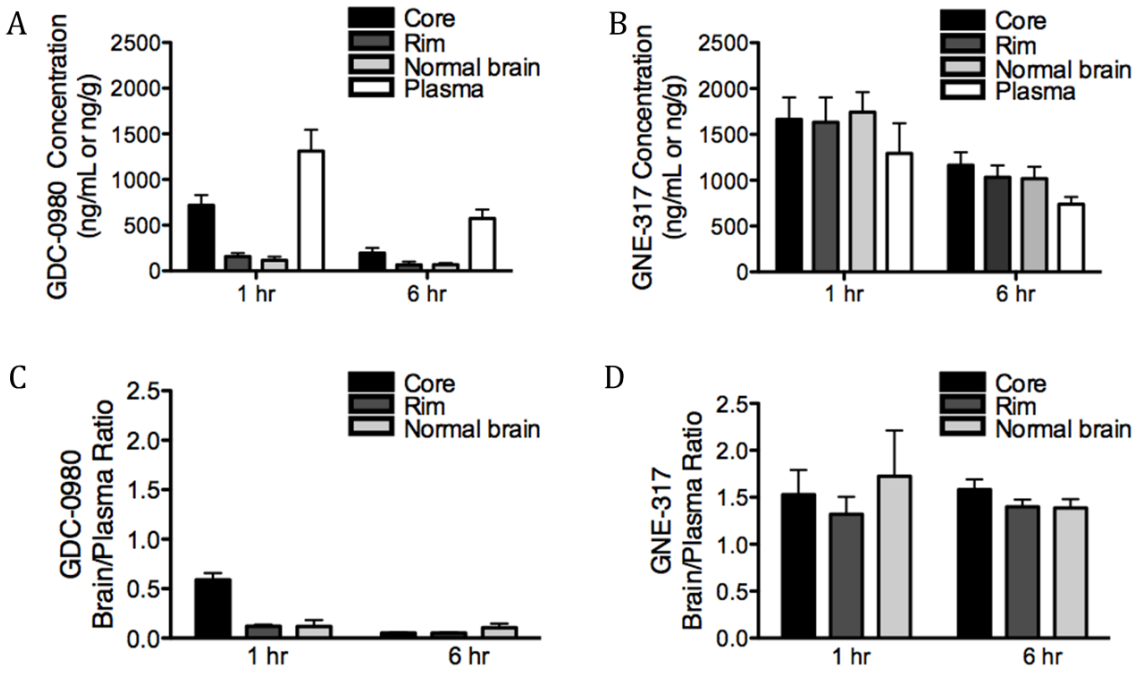
A
GDC-0980 Concentration (ng/mL or ng/g)
2500
2000
1500
1000
500
0
1 hr
6 hr
Core
Rim
Normal brain
Plasma
B
GNE-317 Concentration (ng/mL or ng/g)
2500
2000
1500
1000
500
0
1 hr
6 hr
Core
Rim
Normal brain
Plasma
C
GDC-0980 Brain/Plasma Ratio
2.5
2.0
1.5
1.0
0.5
0.0
1 hr
6 hr
Core
Rim
Normal brain
D
GNE-317 Brain/Plasma Ratio
2.5
2.0
1.5
1.0
0.5
0.0
1 hr
6 hr
Core
Rim
Normal brain

Figure 2.8

Immunohistochemistry of phospho-proteins 1 hour after drug treatment. Scale bars associated with whole slices represent 100 μm while scale bars associated with close-up insets represent 65 μm. (A) p-Akt^{Ser473} staining is reduced in the presence of GNE-317 and to a lesser extent, GDC-0980. (B) p-S6$^{Ser235/236}$ staining is reduced in the presence of GNE-317 but not GDC-0980. (C) p-4EBP1$^{Thr37/46\ staining}$ is reduced in the presence of GNE-317 but not GDC-0980.

Figure 2.8

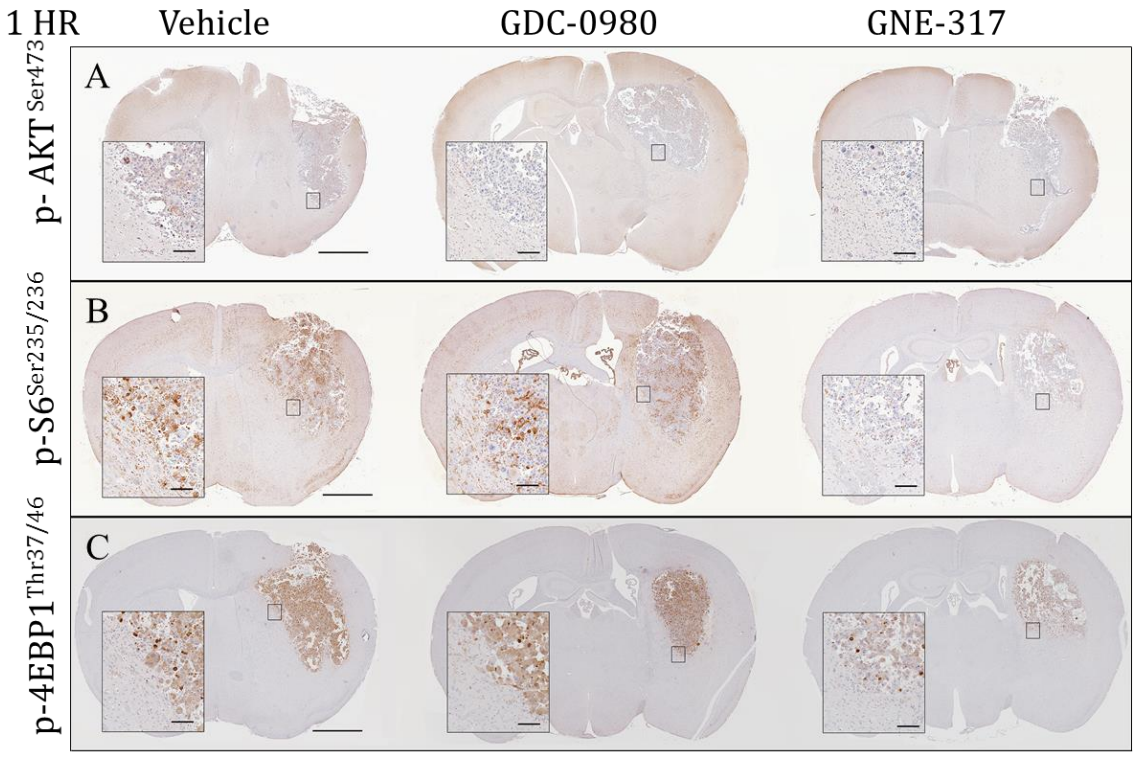
1 HR
Vehicle
GDC-0980
GNE-317
A
p- AKT Ser473
B
p-S6 Ser235/236
C
p-4EBP1 Thr37/46

Figure 2.9

Immunohistochemistry of phosphor proteins 6 hours after drug treatment. Data demonstrates that the inhibitory effects of GNE-317 and GDC-0980 are mostly eliminated. Scale bars associated with whole slices represent 100 μm while scale bars associated with close-up insets represent 65 μm. (A) p-Akt^{Ser473} staining is consistent throughout all groups. (B) p-S6$^{Ser235/236}$ continues to be reduced by GNE-317 and to a lesser extent, by GDC-0980. (C) p-4EBP1$^{Thr37/46\ staining}$ is consistent throughout all groups.

Figure 2.9

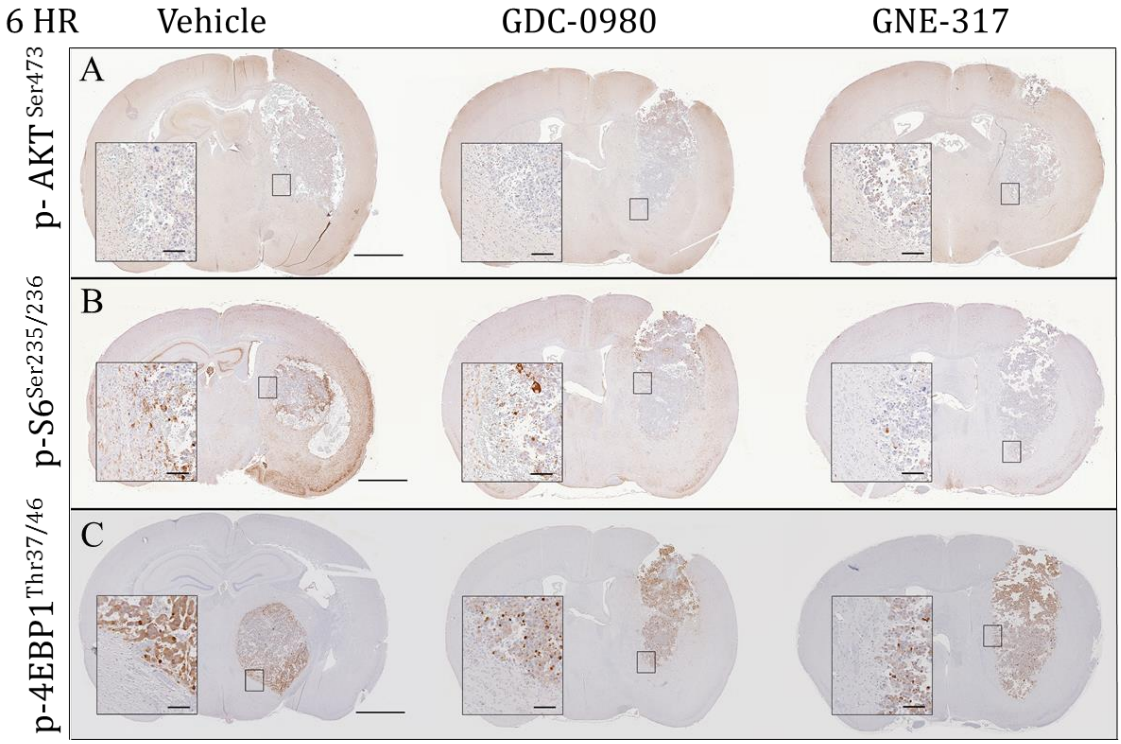
6 HR
Vehicle
GDC-0980
GNE-317
A
p- AKT Ser473
B
p-S6 Ser235/236
C
p-4EBP1 Thr37/46

Figure 2.10

Immunohistochemistry of unphosphorylated proteins 1 hour after drug treatment. (A), (B), and (C) AKT, S6, and 4EBP1 stains are approximately equal between all conditions.

Figure 2.10

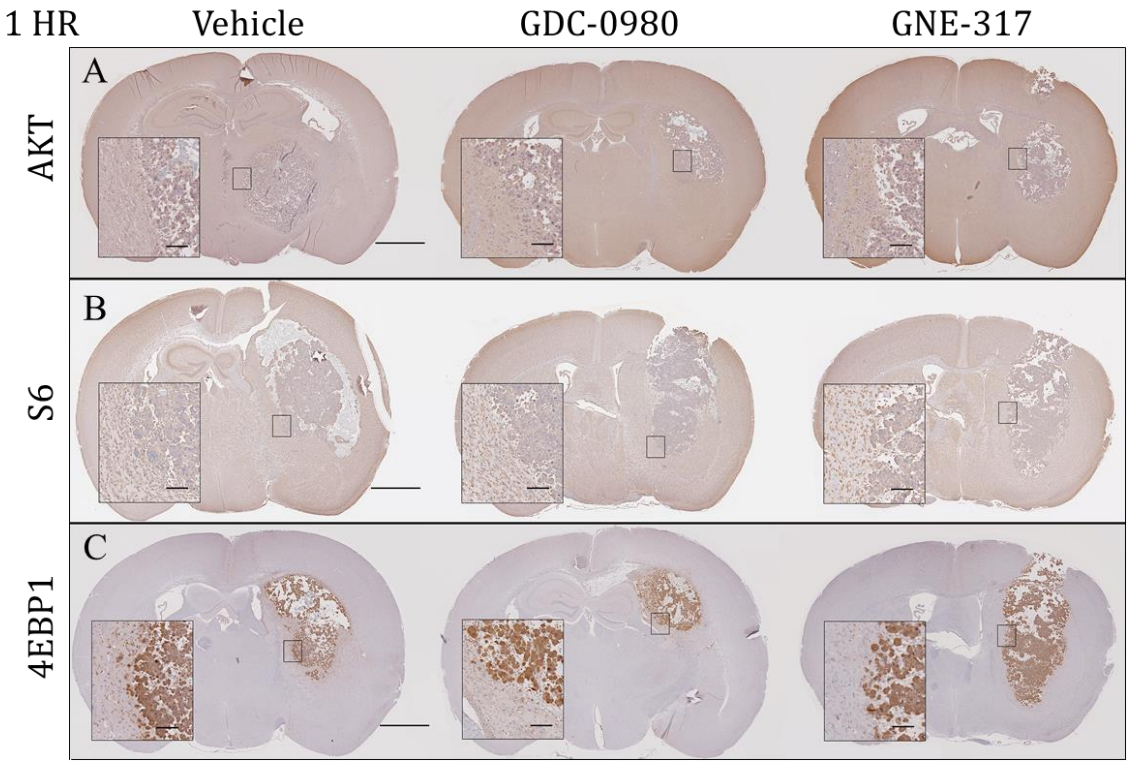

Figure 2.11

Immunohistochemistry 6 hours after drug treatment. (A), (B), and (C) AKT, S6, and 4EBP1 stains are approximately equal between all conditions.

Figure 2.11

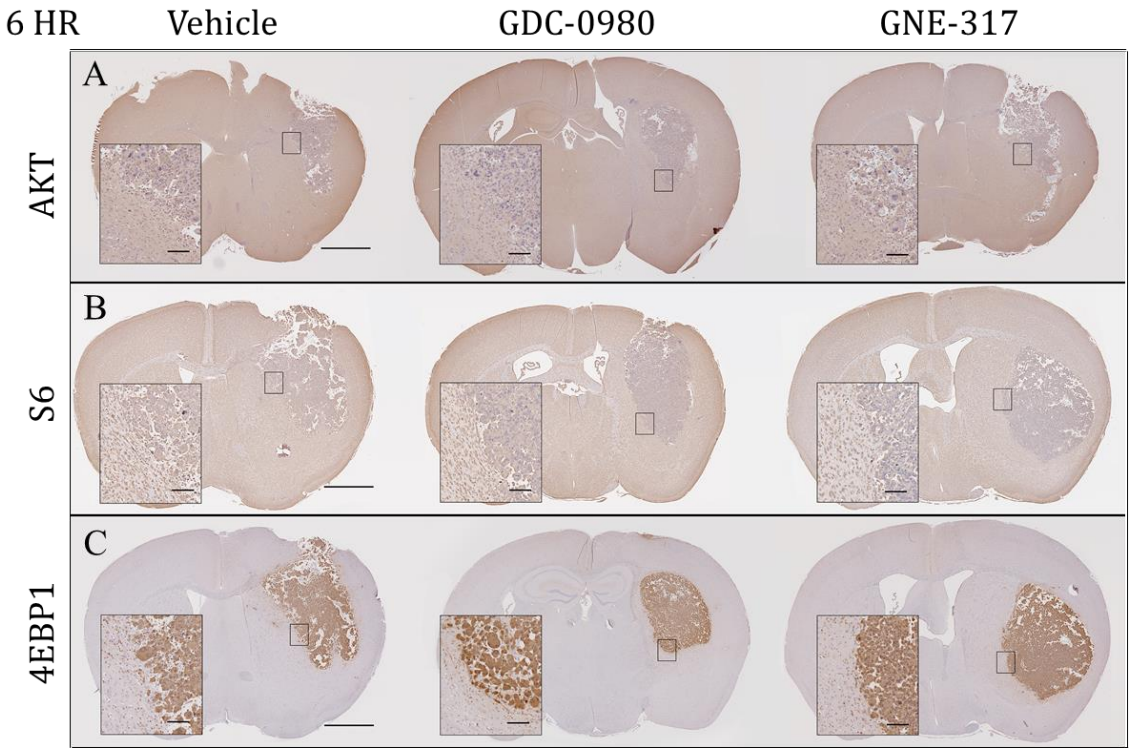

Figure 2.12

In vivo efficacy studies. (A) Tumor progression tracked through bioluminescent imaging shows no demonstrable impact of either GDC-0980 or GNE-317 over vehicle-treated animals. (B) Kaplan-Meier survival curve indicates that neither GDC-0980 nor GNE-317 provide survival benefit over vehicle. (C) Kaplan-Meier survival curve indicates no difference in survival in GNE-317 treated group vs. GDC-0980 treated group ($p=0.12$), but both treatments were significantly different from placebo ($p<0.0005$).

Figure 2.12

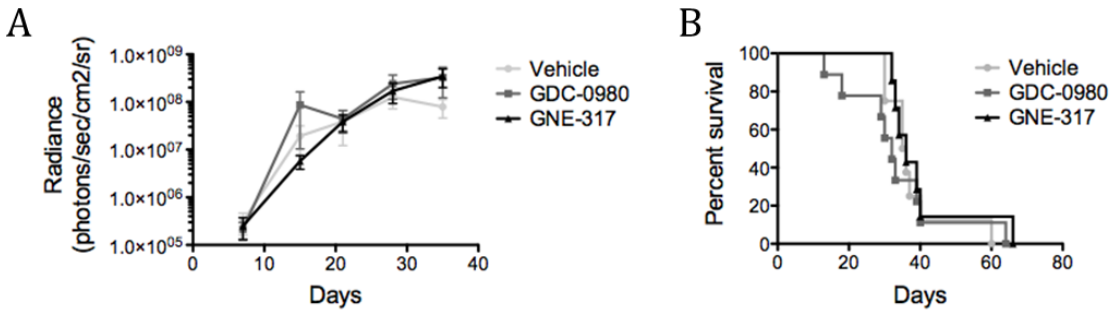
A
Radiance (photons/sec/cm2/sr)
1.0×10^09
1.0×10^08
1.0×10^07
1.0×10^06
1.0×10^05
0
10
20
30
40
Days
Vehicle
GDC-0980
GNE-317
B
Percent survival
100
80
60
40
20
0
0
20
40
60
80
Days
Vehicle
GDC-0980
GNE-317

Figure 2.13

Summary of comparison between GDC-0980 and GNE-317. Comparison of the physicochemical properties, efflux liability and target inhibition of GNE-317 and GDC-0980.

Figure 2.13

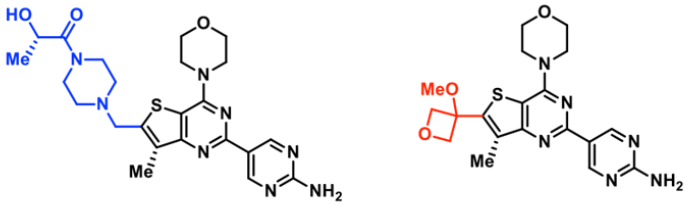

	GDC-0980	GNE-317
MW	498 g/mol	416 g/mol
tPSA	162 A^2	106 A^2
CLogP	2.02	1.25
#H-bond acceptors	11	14
#H-bond donors	2	2
PI3K IC50	5 nM	2 nM
mTOR IC50	17 nM	11 nM
Efflux liability	+++	+
In vivo target inhibition	+	+++

CHAPTER 3

The Influence of Antiangiogenic Therapy on the Distribution and Efficacy of Concurrently Administered Targeted Agents in Malignant Glioma

Rajneet K. Oberoi[1,3,6], Chani M. Becker[2,3,6], Shuangling Zhang[1,6], Jenny L. Pokorny[5], Brett L. Carlson[5], Katrina Bakken[5], Mark A. Schroeder[5], Ann Tuma[5], Stephan J. McFarren[2,3], Olivia Wicker[3,4], John R. Ohlfest[3,4,6], David A. Largaespada[3,4], Jann N. Sarkaria[5, 6] and William F. Elmquist[1,2,3,6]

Affiliations:

1. Department of Pharmaceutics, University of Minnesota, 9-177 Weaver-Densford Hall, 308 Harvard St SE, Minneapolis, MN 55455

2. Department of Neuroscience, University of Minnesota, 6-145 Jackson Hall, 321 Church St SE, Minneapolis, MN 55455

3. Brain Tumor Program, University of Minnesota, 3-115 Cancer & Cardiovascular Research Building, 2231 6th St SE, Minneapolis, MN 55455

4. Department of Pediatrics, University of Minnesota, 6th Floor East Building, 2450 Riverside Ave, Minneapolis, MN 55454

5. Department of Radiation Oncology, Mayo Clinic, 200 First St SW, Rochester, MN 55905

6. Brain Barriers Research Center, University of Minnesota, 9-177 Weaver-Densford Hall, 308 Harvard St SE, Minneapolis, MN 55455

Funding:

National Institute of Neurological Disease and Stroke (NS077921 to WF Elmquist and JN Sarkaria)

Children's Cancer Research Foundation (DA Largaespada)

Keywords: Blood-brain barrier, glioblastoma, bevacizumab, P-gp, antiangiogenic therapy

Conflicts of Interest:

DA Largaespada: co-founder and part owner of two biotechnology companies, Discovery Genomics, Inc and NeoClone Biotechnology; Genentech, Inc. grant recipient.

Author Contributions:

Conception and design: RK Oberoi, JR Ohlfest, JN Sarkaria, WF Elmquist

Development of methodology: RK Oberoi, CM Becker, JL Pokorny

Acquisition of data (provided animals, provided facilities, etc.): RK Oberoi, CM Becker, S Zhang, JL Pokorny, BL Carlson, K Bakken, MA Schroeder, A Tuma

Analysis and interpretation of data (e.g., statistical analysis, biostatistics, computational analysis): RK Oberoi, CM Becker, S Zhang, JL Pokorny, BL Carlson, K Bakken, MA Schroeder, A Tuma

Writing, review, and/or revision of the manuscript: RK Oberoi, CM Becker, DA Largaespada, JN Sarkaria, WF Elmquist

Administrative, technical, or material support (i.e., reporting or organizing data, constructing databases): S Zhang, JL Pokorny, BL Carlson, K Bakken, MA Schroeder, A Tuma

Study supervision: JN Sarkaria, WF Elmquist

3.1 Introduction

Glioblastoma multiforme (GBM) is considered one of the most angiogenic of all solid tumors characterized by extensive vascular proliferation and the diffuse invasion of angiogenic protrusions into the surrounding brain parenchyma (Reardon, 2010). The process of angiogenesis is defined as a highly coordinated, complex development of new blood vessel growth from pre-existing vessels (Fan, Yeh, Leung, Yue, & Wong, 2006). It is initiated and sustained by pro-angiogenic factors such as vascular endothelial growth factor (VEGF) that bind VEGF receptor 2 (VEGFR2) localized on endothelial cells (de Groot & Mandel, 2014). In pathological states, such as chronic inflammatory reactions and in malignant neoplasms, angiogenesis is initiated through the release of pro-angiogenic factors by the tumor itself, leading to extensive vessel development that supports the growing tumor mass (Fan et al., 2006; Plate et al., 1994). Indeed, the formation of new vascular complexes is vital for the proliferation and survival of malignant glioma cells through the provision of survival factors like oxygen and nutrients (de Groot & Mandel, 2014). The novel blood vessels that form during gliomagenesis, however, are leaky. This leakiness results in increased interstitial fluid pressure (IFP) (Weis & Cheresh, 2005). And has been hypothesized to result in deleterious clinical consequences such as compromised drug delivery of cytotoxic agents and enhanced extravasation of tumor cells that invade surrounding tissue (Weis & Cheresh, 2005). Because of these negative effects as well as the desire to prevent or limit the growth of new blood vessels, novel anti-angiogenic therapies (AAT) became an important drug class in cancer treatment.

At an established mechanistic level, AAT addresses many of the negative attributes associated with tumor-induced blood vessel growth. AAT addresses the physical elements of vascular leakiness by effectively re-annealing blood vessels and earlier theories even suggested that AAT could have potential for preventing metastasis by making the restored vasculature impermeable to tumor cells (Le Serve & Hellmann, 1972). Clinically, AAT has proved beneficial in the treatment of a variety conditions, including macular degeneration as well as colorectal, non-small cell lung, ovarian, cervical and kidney cancers. Despite the efficacies in this broad array of cancers, AAT seems to induce deleterious effects in glioma. Beyond restoring the physical elements of the blood-brain barrier, AAT also regenerates the biochemical barrier and reestablishes the activity of efflux transporters (Thompson, Frenkel, & Neuwelt, 2011). Concurrently administered chemotherapeutics that are liable to active efflux at the BBB can permeate the brain through leaky vasculature (Becker et al., 2015), but it is hypothesized that drug delivery could be severely limited in the presence of AAT. Additionally, a growing body of literature suggests that AAT may induce tumor invasion rather than prevent it as originally hypothesized (Pàez-Ribes et al., 2009; Thompson et al., 2011). Histology demonstrates that tumors can adapt to AAT with increased invasiveness and vessel cooption (Thompson et al., 2011; Zuniga et al., 2009) and clinical studies demonstrate that GBM patients treated with AAT develop tumor recurrence at distant rather than local sites from the original tumor compared to patients not given AAT, (Zuniga et al., 2009). More significantly, recent clinical studies in malignant glioma have failed to show a survival benefit with AAT; rather,

the more frequent result is a slight delay in tumor progression (de Groot & Mandel, 2014; Pàez-Ribes et al., 2009).

The lack of therapeutic benefit seen in brain tumors treated with AAT is thought to be due to the normalization of vasculature that restores the restrictive properties of the blood-brain barrier (BBB), including its functional efflux properties (Claes et al., 2008). Two of the most prominent “gatekeepers” at the BBB are the ATP-binding cassette (ABC) transporters, P-glycoprotein (P-gp) and breast cancer resistance protein (BCRP) (Agarwal, Hartz, Elmquist, & Bauer, 2011b). These active efflux transporters are expressed on the luminal side (facing the blood) of endothelial cells at the BBB and function to limit the movement of substrate drugs as they enter the endothelial cells (Agarwal et al., 2011b; Schinkel & Jonker, 2003). Previous studies have shown that many molecularly-targeted agents are substrates for both P-gp and BCRP, including many of the drugs that have been tested against GBM (Tamaki, Ierano, Szakacs, Robey, & Bates, 2011). A more promising therapeutic strategy in malignant glioma, particularly in the context of the continued investigation of AAT, is the utilization of therapeutics with lower efflux liability for P-gp and BCRP. The objective of this study was therefore to evaluate the influence of AAT on the distribution and efficacy of concurrently administered targeted agents with differing liabilities for efflux in a GBM mouse model. Specifically, we hypothesized that concurrent treatment of AAT with other targeted agents would decrease delivery and clinical efficacy, but only in compounds known to be prone to efflux. We found that the VEGF monoclonal antibody, bevacizumab (Genentech Inc’s Avastin) generated a slight decrease in brain penetrance of the

dual PI3K/mTOR inhibitor, GDC-0980 (an established substrate for P-gp and BCRP), but did not affect brain accumulation of the GDC-0980 analogue, GNE-317 (a drug with limited liability for efflux). We further showed that the survival benefit of bevacizumab can only be enhanced with the co-treatment of a brain-penetrant drug like GNE-317. Collectively, these data suggest that AAT-induced BBB normalization is likely to limit the delivery and efficacy of targeted agents that are subject to active efflux.

3.2 Materials & Methods

3.2.1 Animal Care

All procedures were carried out in accordance with the guidelines set by the Principles of Laboratory Animal Care (NIH, Bethesda, MD) and were approved by the Institutional Animal Care and Use Committee (IACUC) of the University of Minnesota (Minneapolis, MN) or the Mayo Clinic. Animals were maintained under temperature controlled conditions with 12 hour dark-12 hour light cycle and were allowed food and water ad libitum. FVB/n wild-type (WT), *Mdr1a/b*$^{-/-}$ (P-gp knockout (PKO) mice), Bcrp$^{-/-}$ (BCRP knockout (BKO) mice), and *Mdr1a/b*$^{-/-}$*Bcrp*$^{-/-}$ mice (triple knockout (TKO) mice) were purchased from Taconic Farms Inc. Female congenitally athymic nude mice (Ncr-*nu/nu*) were purchased from the National Cancer institute.

3.2.2 Chemicals and Reagents

GNE-317, GDC-0980, and bevacizumab (Avastin) were provided by Genentech Inc. (San Francisco, CA). Avastin binds only the human form of VEGF and not the murine form of the molecule (Yu et al., 2008). Texas red dextran 3000 MW (TRD) and fluorescein 332 MW were purchased from Molecular Probes (Invitrogen). For oral administration in mice, drug solutions were prepared in 0.5% methyl cellulose with 0.2% Tween 80. All other chemicals and reagents were of high-performance liquid chromatography grade Ammonium formate and acetonitrile were of HPLC grade and were obtained from Sigma-Aldrich (St. Louis, MO).

3.2.3 Cell Viability Studies

Cell viability assay was carried out for non-GFP labeled GBM10 cells in 96-well plates. The cells were seeded at a density of 5000 cells per well (n=3 plates for each drug, GNE-317 and GDC-0980 in DMSO) and incubated for 24 hours to allow cell attachment. The cells were then incubated with increasing concentrations of GNE-317 or GDC-0980 (0.015uM to 100uM), DMSO control and vehicle control. Following incubation for 48 hours, cells were washed with PBS and 40uL of MTT reagent (3-(4, 5-dimethylthiazol-2-yl)-2, 5-diphenyl tetrazolium bromide) (Alfa Chemical Corp.) (5 mg/mL) was added to each well. The plates were incubated for an additional 3 hours at 37°C at 60 rpm, following which 100µL of DMSO was added to each well. Lastly, the plates were agitated on an orbital shaker for 1 hour at 60 rpm, 37°C. The viability was determined at an absorbance

of 570 nM as the amount of purple formazan produced. The percent survival was determined using drug treated cells normalized to cells treated with DMSO control. The percentage of DMSO was less than 0.01% for all drug solutions.

3.2.4 Xenograft Tumor Implantation

Tumors were generated using GBM10 (Sarkaria et al., 2006) and GBM59 (Carlson et al., 2009), aggressive patient-derived xenografts from the Mayo panel using either orthotopic or flank glioblastoma xenograft models. All patient-derived xenograft cell lines were obtained from patients at the Mayo Clinic and maintained exclusively by serial passage in mice (Carlson et al., 2011). Briefly, flank tumor xenografts were harvested, mechanically disaggregated, and grown for a limited period of time (5-14 days) in DMEM supplemented with 2.5% fetal bovine serum, 1% penicillin, and 1% streptomycin. Cells were harvested following trypsinization and injected in the heads or flanks of nude mice. For flank studies, 2,600,000 GBM10 cells were injected subcutaneously into the right flank in a total volume of 200 ul in phosphate-buffered saline (PBS) under isoflurane sedation. For orthotopic studies, either 600,000 GBM59 cells or 300,000 GBM10 cells were injected into the right striatum in a total volume of 3 ul in PBS during a stereotactic surgery (stereotaxic frame, ASI Instruments). For brain distribution studies, GBM10 cells were transfected with green fluorescent protein (GFP) using methods described previously (Wu et al., 2007). All intracranial tumor-bearing animals used for therapy evaluation were observed daily and euthanized once they reached a moribund condition. Treatment of flank tumor xenografts was essentially the same

with the exception that tumor volume was measured three times weekly. The endpoint for the flank study was time for tumors to reach 1,500 mm^3.

3.2.5 Blood-brain Barrier Imaging

The objectives of BBB imaging studies were two-fold: first, to investigate the degree of heterogeneity in BBB disruption in the non-GFP enhanced GBM10 tumor xenograft mice, and, second, to investigate the effect of bevacizumab as an anti-angiogenic treatment on re-formation of the BBB in GFP-labeled GBM10 tumor xenograft mice. The GFP-labeled GBM10 mice were divided into two groups for BBB imaging purposes: (a) placebo-treated group and (b) bevacizumab-treated group. Animals were treated with an intraperitoneal dose of 5 mg/kg bevacizumab in PBS once a day for either one or two days and then euthanized at either 48 or 72 hours following the last dose. Placebo-treated animals were dosed in equal volumes to the bevacizumab-treated group. Texas-Red dextran (TRD, MW= 3000 kDa) or fluorescein (MW = 332 Da) were used as permeability markers to evaluate the degree of BBB disruption. TRD (1.5 mg/animal) and fluorescein (1.5 mg/animal) were administered together via tail vein and after allowing a circulation time of 10 minutes, the animals were perfused with extracellular fluid buffer (ECF buffer) at a rate of 10 mL/min. Following perfusion, whole brains were harvested, frozen in ice-cold isopentane at -80C and sectioned into 20 micrometer-thick slices using a cryostat. The slices were mounted on glass slides for imaging. The non-GFP labeled GBM10 brains were imaged for with bright field for normal viewing and with fluorescent filters for Texas Red visualization.

The extent of tumor growth was determined by cresyl violet or hematoxylin-eosin (H&E) staining. Cresyl violet staining was performed using 4% paraformaldehyde in phosphate-buffer saline for 10 minutes, followed by 0.1% cresyl violet acetate for 15 minutes. The sections were then processed for dehydration and cleaning in 70% ethanol for 15 seconds followed by 90% ethanol for 10 seconds. Bright field images were then captured using Retiga 2000R camera (Leica DMI 6000B microscope). H&E staining was carried out according to routine laboratory protocols

3.2.6 Plasma and Brain Distribution of GDC-0980 and GNE-317 in FVB Non-Tumor-Bearing Mice

All drug solutions were freshly prepared on the day of the experiment. The dosing solutions for GNE-317 (30 mg/kg) and GDC-0980 (7.5 mg/kg) were prepared as a stable suspension in 0.5% methylcellulose with 0.2% tween 80. Both drugs were orally administered simultaneously using two separate syringes. Mice were euthanized using carbon-dioxide chamber and blood and brain samples were harvested at pre-determined time points, i.e., 1, 4, 6 or 8 and 16 hours post-dose (n=3-4 at each time point). Blood and brain samples were processed as described previously (Oberoi, Mittapalli, Fisher, & Elmquist, 2013).

The data were analyzed using noncompartmental estimation methods using Phoenix WinNonlin 6.1 (Pharsight, Mountain View, CA)The area under the concentration time curve till the last measured time point ($AUC_{0\text{-}tlast}$) was calculated for both plasma and brain concentration time profiles using the log-

linear trapezoidal approximation method. In addition, the brain partition coefficient, Kp, given by the AUC ratio of brain to plasma for both wild-type and TKO mice was determined. Furthermore, the drug targeting index (DTI) was determined. The DTI is defined as the ratio of AUC brain-to-plasma ratio in TKO mice to the AUC brain-to-plasma ratio in the wild-type mice, written as,

$$DTI = AUC_{brain/Plasma\ (TKO)}/AUC_{brain/Plasma\ (wild\text{-}type)}.$$

3.2.7 Regional Brain Distribution of GDC-0980 and GNE-317 in GBM10 Tumor-Bearing Mice

GFP-labeled GBM10 cells were implanted into female athymic nude mice (Ncr-*nu/nu*) (6 weeks old). GFP enabled dissection of the mouse brain into three parts: the tumor core, brain around the tumor (also called the tumor rim), and the contralateral hemisphere. Tumor-bearing mice were divided into two groups (n=6 per group): (a) bevacizumab-treated or (b) placebo (PBS vehicle alone). Because maximum blood flow inhibition after treatment with the anti-angiogenic agent, bevacizumab (or bevacizumab), is achieved 48-72 hours post-dose of the drug (Thompson et al., 2011), we chose this timeframe for our studies in mice. All mice were administered three doses of placebo (vehicle) or bevacizumab (5 mg/kg IP) over a period of eight days, i.e., once every three days. 48 hours after the last dose of bevacizumab, all mice were co-administered GNE-317 (30 mg/kg) and GDC-0980 (7.5 mg/kg) simultaneously. Although there is a 4-fold difference in doses for GNE-317 and GDC-0980, both drugs at these different doses yielded similar plasma concentrations, hence, similar systemic exposures were expected. This

observation of similar exposure levels has been described previously (Becker et al., 2015). Mice were sacrificed 1 hour or 6 hours post-dosing of GDC-0980 and GNE-317 (n=3 at each time point). Plasma and brain samples were harvested and processed as described previously (Becker et al., 2015).

3.2.8 Quantification of GDC-0980 and GNE-317 in Brain and Plasma by LC-MS/MS

The plasma and brain concentrations of GNE-317 and GDC-0980 were determined simultaneously in the same sample using high-performance liquid chromatography-tandem mass spectrometry (LS-MS/MS). On the day of the analysis, frozen brain samples were thawed at room temperature. Brain weights were determined and samples were homogenized using 3 volumes of 5% ice-cold bovine serum albumin prepared in phosphate-buffer saline (PBS) (pH= 7.4). The quantification of GNE-317 and GDC-0980 was performed using a dual gradient method as described below: to 100 μL of plasma sample or 200 μL of brain homogenate sample, 10 μL of 2 μg/mL internal standard, AG1478 (4-[3-chloroanilino]-6,7-dimethoxyquinazoline) was added. Both plasma and brain samples were extracted using 500 μL of ice-cold ethyl acetate. Samples were centrifuged at 7500 rpm at 4°C for 15 minutes, following which 400 μL of the supernatant was transferred to a fresh tube. The extracted supernatant was dried under a gentle stream of nitrogen following which the dried sample were reconstituted in 100μL of mobile phase (72:28:0.1, v/v%, 20mM ammonium formate, pH=3.5 (A): acetonitrile (B): formic acid (A)). 5uL of the sample was

injected into LC-MS/MS. A gradient elution method was used starting at 28% B for 5 minutes (0.25 mL/min), followed by 100% B for 2.5 minutes (0.25 mL/min). A linear gradient was then applied from 7.9 -11.5 minutes (28% B) at a flow rate of 0.5 mL/min, resulting in a total run time of 11 minutes. Chromatographic separation was achieved using Agilent Technologies model 1200 separation system (Santa Clara, CA) using Agilent ZORBAX XDB Eclipse C_{18} column (4.6 x 50 mm, 1.8 μm). The LC-system and TSQ Quantum triple quadrupole mass spectrometer system were linked (Thermo Finnigan, San Jose, CA) and data analysis was performed using Xcalibur software, version 2.0.7. Selected reaction monitoring (SRM) mode with an electrospray ionization source (ESI) was operated in positive ion mode at a spray voltage of 5000 V for both GNE-317 and GDC-0980. The mass-to-charge (m/z) transitions for GDC-0980, GNE-317 and AG1478 were 499.24 → 340.98, 415.11 → 385.13 and 317.03 → 300.98, respectively. The assay was linear over a range of 1.9 ng/ml to 1000 ng/ml with a coefficient of variation lower that 20% throughout the entire range.

3.2.9 Immunohistochemistry

GBM10 cells were implanted in six-to-eight week-old female athymic nude mice (Ncr-*nu/nu*). 20 days after surgery, animals were randomized into one of six treatment groups: (1) placebo (vehicle control), (2) GNE-317 (30 mg/kg administered orally), (3) GDC-0980 (7.5 mg/kg administered orally), and (4) bevacizumab (5 mg/kg administered intraperitoneally), (5) GNE-317 + bevacizumab, or (6) GDC-0980 + bevacizumab (n=5 mice per group). In the

relevant groups, GDC-0980 and GDC-0980 were dosed daily for 5 days while Bevacizumab was dosed on the first and fourth days of treatment. One hour after dosing on the fifth day, all mice were anesthetized with carbon dioxide and perfused with 30 ml PBS. Brains were harvested and stored in 10% buffered formalin for 48 hours and then switched to 70% ethanol until processing. After processing, brains were embedded in paraffin and then sectioned at 5 μm thickness. Tissue slices were heat-fixed onto charged glass slides for staining as described previously (Becker et al., 2015). Briefly, after slides were deparaffinized and rehydrated, antigen epitopes on tissue sections were exposed using an unmasking solution (Vector Laboratories). To remove endogenous peroxidases, slides were then exposed to 3% hydrogen peroxide. Blocking of non-specific staining was achieved with 3% bovine serum albumin (BSA) in a humidified chamber overnight at 4°C. Sections were then treated with primary antibody (p-Akt^{Ser473}, 1:50, Cell Signaling; p-4EBP1$^{Thr37/46}$, 1:1000, Cell Signaling; Ki-67, 1:400, Cell Signaling; p-S6$^{Ser235/236}$, 1:50, Cell Signaling; CD31, 1:100, Cell Signaling) in 1% BSA and allowed to incubate overnight at 4°C in a humidified chamber. Following incubation with the primary anitbody, sections were washed in PBS and then incubated with 1:200 biotinylated goat anti-rabbit secondary antibody (Vector Laboratories) for 1 hour at room temperature. Afterward, sections were washed twice in PBS and then subjected to a 30-minute application of an avidin/biotinylated enzyme complex conjugated to horseradish peroxidase (Vectastain Elite ABC kit, Vector Laboratories). After two washes in PBS, the sections were treated with 3,3′-diaminobenzidine substrate prepared fresh according to the manufacturer's

instructions (Vector Laboratories) and then allowed to develop. Once a discernible signal was obtained, slides were placed in water to stop the reaction. Finally, sections were counter-stained with hematoxylin, dehydrated, cleared in xylenes, and mounted in Permount (Fisher Scientific). Images were acquired in color with an Olympus FluoView FV1000 BX2 Upright Confocal microscope and Panoptiq Digital Slide Imaging System.

3.2.10 Survival Studies in Glioma Models

In-vivo efficacy studies were conducted in both the GBM10 and GBM59 glioma models. All mice were randomized into six groups: (1) placebo (vehicle control), (2) GNE-317 (30 mg/kg administered orally), (3) GDC-0980 (7.5 mg/kg administered orally, was reduced to 6 mg/kg when GBM10-tumor mice showed signs of toxicity), and (4) Bevacizumab (5 mg/kg administered intraperitoneally), (5) GNE-317 + Bevacizumab, or (6) GDC-0980 + bevacizumab (n=10 mice/per group). Animals receiving GDC-0980 or GNE-317 were dosed daily while animals receiving bevacizumab were dosed twice weekly, every 3-4 days. The experimental end point being death or moribund state of mice. GDC-0980 and GNE-317 were prepared in 0.5% methylcellulose and 0.2% tween 80 while bevacizumab was prepared in PBS.

3.2.11 Statistical Analysis

The unpaired two-sample t-test was used to compare between two groups. One-way ANOVA, followed by Bonferroni's test was conducted to test for

significance among multiple groups. Significance was declared at $p<0.05$ for all tests. All tests were done using GraphPad Prism 5.01, San Diego, CA. Survival probabilities were estimated using Kaplan Meier survival curves. The treatment groups were compared using log-rank test.

3.3 Results

3.3.1 The GBM10 Model is Characterized by Heterogeneous Blood-Brain Barrier Disruption and is Similarly Susceptible to GDC-0980 and GNE-317.

BBB disruption in the tumor core is a defining feature in the clinical presentation of glioblastoma multiforme (Pafundi et al., 2013). In contrast, the area of tissue immediately surrounding the core, known as the tumor rim, maintains a relatively intact BBB (Pafundi et al., 2013). In order to effectively recapitulate GBM with accuracy, preclinical mouse models should show these BBB phenotypes in the tumor core and rim. We have previously shown that the GL261 syngeneic glioma model demonstrates a heterogeneously disrupted BBB using Texas Red-dextran (TRD, molecular weight = 3 kDa) as a permeability marker. In the current study, the BBB was evaluated again using TRD in an orthotopic human xenograft GBM model (GBM10) (Sarkaria et al., 2006). Penetrance of the dye was assessed using fluorescence microscopy and the extent of tumor growth was evaluated with cresyl violet staining (**Figure 3.1B**). This analysis demonstrates a heterogeneous pattern of TRD accumulation in the location of the tumor. Importantly, the tumor core demonstrated areas with both large accumulation of TRD (shown bright red) as well as areas with little to no accumulation of TRD (darker red or black) (**Figure**

3.1A). The lack of TRD at the tumor rim and surrounding normal brain suggests an intact BBB capable of protecting invasive glioma cells. This animal model therefore recapitulates the patterns of BBB disruption observed in human GBM.

To ascertain the toxicity of GDC-0980 and GNE-317 against the GBM10 model independent of the drug delivery issues associated with the brain, drugs were tested in both an *in vitro* cytotoxicity assay (**Figure 3.2A**) as well as a flank tumor model (**Figure 3.2B & Figure 3.2C**). In both experiments, GDC-0980 and GNE-317 exhibited similar, albeit limited, efficacy profiles against GBM10. These data suggest that the retained molecular structure common to both drugs allows for similar interactions with their targets, as originally intended (Heffron et al., 2012).

3.3.2 Time Profiles of GDC-0980 and GNE-317 Distributions in Brain and Plasma

Steady state data for brain and plasma exposure to GDC-0980 and GNE-317 have already been reported in Chapter 2, but concentration time profiles are also beneficial to determine the area under the concentration time curve (AUC) and provide additional information regarding distribution kinetics and overall systemic exposure. For this reason, brain distributions of GNE-317 (30 mg/kg) and GDC-0980 (7.5 mg/kg) were determined following a single dose of both drugs in non-tumor bearing FVB wild-type and *Mdr1a/b*$^{(-/)}$*Bcrp1*$^{(-/-)}$ triple knockout mice lacking both forms of P-gp and BCRP mice. The brain and plasma concentration

time profiles of GDC-0980 and GNE-317 in FVB-wild-type and TKO mice are shown in **Figure 3.3**.

The brain concentrations of GDC-0980 were significantly lower than the corresponding plasma concentrations in wild-type mice at all measured time points ($p<0.05$), whereas, brain concentrations in TKO mice were greater than the plasma concentrations, indicating that both P-gp and Bcrp limit brain distribution of GDC-0980 **(Figure 3.3A & Figure 3.3B).** The brain-to-plasma ratio vs. time graph showed an increase before reaching a plateau, suggesting that a pseudo-distributional equilibrium has been achieved **(Figure 3.3C).** The $AUC_{0\text{-tlast}}$ in the wild-type plasma (10.56 ± 1.47 h-µg/ml) and TKO plasma (4.51 ± 1.15 h-µg/mL) were significantly different from each other, although the plasma concentrations at all measured time points except 16 hour were not significantly different **(Table 3.1).** The brain distribution coefficient of GDC-0980 in wild-type animals was 0.05 and increased by ~35 fold to provide a drug targeting index of 1.75 in the TKO mice. Altogether, these data demonstrate that GDC-0980 is subject to efflux by P-gp and BCRP and that brain penetrance can be enhanced when these efflux transporters no longer present as an obstacle.

The brain concentrations of GNE-317 closely followed plasma concentrations in both wild-type and TKO mice, suggesting that neither P-gp nor BCRP influenced the brain distribution of GNE-317 **(Figure 3.3D & Figure 3.3E).** The maximum plasma concentrations were observed at 1 hour in both wild-type and TKO mice. The brain-to-plasma concentration ratios were ~1 at all measured time points in both strains of mice **(Figure 3.3F).** The area under the concentration

time curve to the last measured time point (AUC_{0-t}) in both plasma and brain of the wild-type mice were 10.59 ± 0.81 h-µg/mL and 10.06 ± 0.9 h-µg/mL respectively (**Table 3.1**). In the absence of P-gp and BCRP, the AUC_{0-t} was 11.99 ± 1.65 h-µg/ml and 12.80 ± 1.24 h-µg/ml in the plasma and brain, respectively. Similar AUCs in plasma and brain in both wild-type and TKO mice indicate that GNE-317 brain distribution is not restricted by active efflux at the blood brain barrier. The brain partition coefficient, K_p, given by the AUC ratio in brain to AUC ratio in plasma was ~1 (0.95 in wild-type and 1.07 in TKO), implying that there is equal partitioning in the brain as in the plasma. The observed drug targeting index value for GNE-317 was 1.13, indicating that neither P-gp nor BCRP significantly affect brain distribution of GNE-317.

These data are comparable to previous observations (Salphati et al., 2012; Salphati, Pang et al., 2012), suggesting that the difference in targeting potential of GNE-317 is due to its higher brain penetrance compared to GDC-0980 that is liable to active efflux by P-gp and BCRP at the BBB. These data become more salient when viewed in the context of their similar cytotoxic capabilities (**Figure 3.2**); differences in molecular targeting or efficacy should be attributed to differences in drug delivery to the brain.

3.3.3 GNE-317 Exhibits Greater Brain Penetrance than GDC-0980 in an Orthotopic Xenograft Glioma Model

To investigate the influence of AAT on drug distribution to brain tumors, we administered bevacizumab with either GDC-0980 or GNE-317 in the GFP-labeled

GBM10 orthotopic xenograft model. GDC-0980 has a greater liability for active efflux by P-gp and BCRP at the BBB than GNE-317, so we anticipated differential distribution patterns in the presence of treatment with the anti-angiogenic monoclonal antibody to VEGF, bevacizumab (Ferrara, Hillan, & Novotny, 2005). To validate the optimal dosing of bevacizumab necessary to achieve BBB restoration reported in clinical studies (Thompson et al., 2011), we tested either one or two doses of 5 mg/kg bevacizumab in PBS spaced three days apart. Because a minimum of two doses was needed to produce BBB re-annealing (**Figure 3.4**) and limit the permeation of both small and large molecules (fluorescein and TRD, respectively, in **Figure 3.5**), we chose three bevacizumab doses as a standard for use when evaluating the distribution of other drugs.

To determine the distributions of GDC-0980 and GNE-317 within the tumor core, the brain around the tumor ("rim"), and the contralateral hemisphere ("normal brain"), GFP labeling was essential for the dissection of tumor into these components for subsequent analysis by LC-MS. To generate these tissue samples, bevacizumab was administered twice weekly (total of 3 doses) at 5 mg/kg intraperitoneally to GFP-labeled GBM10 tumor-bearing mice. Forty-eight hours after the last dose of bevacizumab, mice were administered placebo vehicle or GNE-317 (30 mg/kg) and GDC-0980 (7.5 mg/kg) simultaneously via oral gavage. Plasma and brains were harvested one hour or six hours after the dose. Drug concentrations were determined in brain core vs. rim vs. contralateral hemisphere as described previously (Becker et al., 2015). The brain-to-plasma ratios of GNE-317 in the core, rim and contralateral hemisphere were not significantly different to

each other regardless of the presence or absence of bevacizumab (**Figure 3.6).** This pattern was evident both one hour (**Figure 3.6A**) and six hours (**Figure 3.6B**) after dosing of GNE-317. Concentrations of GNE-317 giving rise to these brain-to-plasma ratios are available in **Figure 3.7**.

The brain-to-plasma ratios were significantly reduced for GDC-0980 (**Figure 3.8**) compared to GNE-317 (**Figure 3.6**), due to the extremely low concentrations of GDC-0980 detected in brain tissues (**Figure 3.9**). Importantly, the pattern of brain penetrance in animals treated with either GDC-0980 or GNE-317 were very different. Unlike the consistent accumulation of GNE-317 in the tumor core, rim and normal brain (**Figure 3.6**), GDC-0980 accumulation was significantly greater in the tumor cores of treated animals compared to the tumor rims and normal brains one hour after dosing ($p = <0.05$, **Figure 3.8A**). These patterns of drug accumulation again reinforce the benefit that a disrupted BBB in the tumor core can provide to drugs like GDC-0980 that are not normally brain penetrant. Altogether, these data demonstrate that GNE-317 is more capable of penetrating the brain than GDC-0980. Concurrent treatment with bevacizumab resulted in a trend toward reduced GDC-0980 accumulation in the tumor core, although the decrease was not significant (**Figure 3.8**).

3.3.4 Pharmacodynamic Effects of GNE-317 and GDC-0980 in the GBM10 Brain Tumors

To determine whether brain penetrance correlates with inhibition of signaling pathways at the tumor and surrounding rim, we used

immunohistochemistry to visualize the ability of each drug to inhibit PI3K and mTOR signaling. We further sought to determine the effect of drug treatment on tumor proliferation and vascularization. Toward these ends, GBM10 tumor-bearing mice were administered either 30 mg/kg GNE-317 orally, 7.5 mg/kg GDC-0980 administered orally, 5 mg/kg bevacizumab, a combinations of GDC-0980 and bevacizumab, or a combination of GNE-317 and bevacizumab (n=5 mice per group). GDC-0980 and GDC-0980 were dosed daily for 5 days while bevacizumab was dosed on the first and fourth days of treatment. One hour after dosing on the fifth day, animals were euthanized and brains were processed and sliced for staining. Immunohistochemistry focused on downstream targets of the PI3K/mTOR signaling pathway (p-Akt^{Ser473}, p-S6$^{Ser235/236}$ and p-4EBP1$^{Thr37/46}$) as well as markers of proliferation (Ki67) and vascularity (CD31). Representative stained brain slices are shown in **Figure 3.10A** while random portions of the tumor were chosen for greater magnification **(Figure 3.10B)**. We anticipated that staining for phospho-proteins would be reduced in GNE-317-treated xenografted tumors compared to GDC-0980 because GNE-317 has greater brain penetrance, but staining was did not demonstrate any appreciable differences between groups (**Figure 10**). Similarly, there were no significant differences in staining for Ki67 or CD31. Potential reasons explaining these data are described in the discussion of this chapter.

3.3.5 Bevacizumab Modulates Survival in Brain Tumor-Bearing Animals Treated with Concurrent Therapeutics

Despite the lack of significant differences in staining intensity between groups, we sought to determine how bevacizumab would modulate survival of animals treated with either GDC-0980 or GNE-317. The non-significant staining data and limited efficacy against GBM10 cells in vitro (**Figure 3.3A**) led us to introduce another human xenograft glioma (GBM59) into our survival studies that may show greater susceptibility to PI3K/mTOR inhibition. The use of this patient-derived cell line is already well established (Carlson et al., 2009). Seven days after intracranial inoculation with GBM10 or GBM59 cells, mice were treated with a daily dose of either GNE-317 (30 mg/kg administered orally) or GDC-0980 (7.5 mg/kg, reduced to 6 mg/kg after one week of treatment due to signs of toxicity) alone or in combination with bevacizumab (5 mg/kg, administered intraperitoneally). Bevacizumab was dosed twice weekly, every 3-4 days. Bevacizumab provided a survival benefit alone in all cases, but that survival benefit was significantly enhanced during co-treatment with GNE-317 (p=.0395 in **Figure 3.11A**, p=.0017 in **Figure 3.12A**). Similarly, the efficacy of GNE-317 was also significantly enhanced during concurrent treatment with bevacizumab (p=<.0001 in **Figure 3.11A**, p=.0048 in **Figure 3.12A**). In animals treated with bevacizumab, there was no enhanced survival benefit of concurrent treatment with GDC-0980 (**Figure 3.11B** and **Figure 3.12B**). Treatment with bevacizumab did extend the lifespan of tumor-bearing animals compared to animals treated with GDC-0980 alone (p=.0097 in **Figure 3.11B** and p=.0326 in **Figure 3.12B**). These data collectively

suggest that Bevacizumab may enhance the survival benefit of concurrently administered targeted agents, but that improvements over bevacizumab therapy alone is most significant in the presence of a brain-penetrant chemotherapeutic.

3.4 Discussion

The results of this study demonstrate the influence that AAT can have on brain penetrance and efficacy of concurrently administered targeted agents. We first describe that the GBM10 xenograft glioma model accurately recapitulates the heterogeneous pattern of BBB disrupted seen in human pathology (**Figure 3.1**). Through our experiments with GDC-0980 and GNE-317, we validated and further characterized previous data from Chapter 2 that described how GDC-0980 has limited brain penetration due to active efflux compared to GNE-317 (**Figure 3.3**, **Table 3.1**) (Becker et al., 2015). Due to these difference, these drugs were considered ideal candidates to investigate the influence of anti-angiogenic therapy with bevacizumab on brain delivery of co-administered agents. We hypothesized that restoration of the BBB would not alter the brain distribution of GNE-317, but would decrease tumor core concentrations of GDC-0980 because the drug is liable to efflux when the BBB is intact. Our data demonstrating that bevacizumab does not influence distribution of the more brain penetrant compound, GNE-317 (**Figure 3.6**), was therefore expected, but our findings that bevacizumab did not significantly influence the distribution of GDC-0980 (**Figure 3.8**) was unanticipated. These data are particularly surprising in the context of other work

having successfully demonstrated a decrease in delivery of concurrently administered chemotherapeutics in the presence of AAT (Goldwirt et al., 2015).

Our staining data demonstrating no appreciable differences between treatment groups (**Figure 3.10**) was also unexpected; these data in the GBM10 mouse model contrast from the strong differences in staining intensities seen in the GL261 mouse model in Chapter 2 (Becker et al., 2015). These effects may be model-dependent, however, as patient-derived tumors maybe driven by different genetic mutations that could be more or less susceptible to treatment with PI3K/mTOR inhibition. The similarity in staining across all groups for phospho-proteins may have resulted because of a lack of efficacy in the GBM10 cell line, which reflects the limited efficacy seen in the *in vitro* cytotoxicity assay (**Figure 3.3A**). Lack of differences in staining intensity for Ki67 and CD31 may alternatively suggest that five days of treatment is an insufficient duration of therapy to induce demonstrable changes in these proliferation and the extent of vascularization. Despite any significant changes in staining intensity between treatment groups, there were significant survival benefits to multiple therapies in both the GBM10 and GBM59 xenograft glioma models (**Figure 3.11**& **Figure 3.12**). Such benefits may be due to prolonged treatment or to anti-tumor mechanisms outside the PI3K/mTOR pathway. In our xenograft models, bevacizumab enhanced the survival benefit of concurrently administered targeted agents. Our data suggests improvements from bevacizumab therapy by itself is most significant in the presence of a brain-penetrant chemotherapeutic like GNE-317, compared to a compound with great efflux liability for P-gp and BCRP, like GDC-0980.

Although the xenograft model showed significant survival benefits following the treatment of GDC-0980, GNE-317, and bevacizumab, these data were not mirrored in flank studies. The purpose of the experiments was to ascertain efficacy against the tumor in the presence or absence of the delivery-modifying BBB. Despite these intents, the flank provides a different microenvironment than the brain, which can modify not only tumor growth, but also angiogenesis and invasion (Antunes et al., 2000). The changes to the tumor between microenvironment niches should therefore lead to differences in sensitivity to therapeutics and limit the translation between GBM flank and orthotopic models.

From a broader perspective, the results from this study show that although AAT normalizes tumor vasculature, which could improve drug delivery of co-administered cytotoxic drugs, this effect is “paradoxical” (Thompson et al., 2011). By normalizing and maturing the brain tumor vasculature, AAT restores the previously disrupted BBB. Restoration of the disrupted BBB may regenerate its structural and functional properties, in particular, the presence of active efflux transporters (Thompson et al., 2011). Although our data do not support a significant reduction in the distribution of GDC-0980, other drugs may demonstrate greater susceptibility to this effect (Tamaki et al., 2011). The variability of drug delivery in the context of AAT highlights the unpredictability of the treatment regimen.

The clinical decision about whether AAT represents an appropriate treatment strategy in GBM, either alone or in combination with other therapeutics, is further influenced by the potential ramifications of stopping such therapy.

Beyond the potential propensity for enhanced invasiveness referenced earlier (Pàez-Ribes et al., 2009; Thompson et al., 2011), "tumor rebound" (Batchelor et al., 2007; Cacheux et al., 2008; Stein et al., 2008; Stein, Yang, Bates, & Fojo, 2008), the emergence of a more aggressive disease (Ellis & Reardon, 2009; Greenberg et al., 2008), and rapid revascularization (Mancuso et al., 2006) have all been reported following discontinuation of AAT. Consideration to include AAT in the standard treatment of GBM should therefore be considered carefully.

Figure 3.1

Characterization of the BBB properties associated with the GBM10 orthotopic xenograft model. The same tumor is imaged in three different pictures: (A) TRD accumulation to demonstrate the extent of BBB disruption. (B) cresyl violet staining to confirm the tumor boundaries and (C) a bright field (BF) image for control purposes.

Figure 3.1

Figure 3.2

Comparison of the cytotoxic effects of GDC-0980 and GNE-317 independent of the brain's influence on drug delivery. (A) *In vitro* MTT cytotoxicity assay demonstrates similar potency and efficacy of GDC-0980 and GNE-317 against GBM10 cells. (B) *In vivo* subcutaneous flank model of GBM10 shows GDC-0980 and GNE-317 act to produce a similar delay in tumor growth. Growth was assessed via the physical measurement of the tumor with calipers at three dimensions. Points are the mean of all subjects, no SEM included for visualization purposes. (C) *In vivo* subcutaneous flank model of GBM10 shows GDC-0980 and GNE-317 have similar survival patterns (animals were euthanized when their tumors reached 1500 mm^3).

Figure 3.2

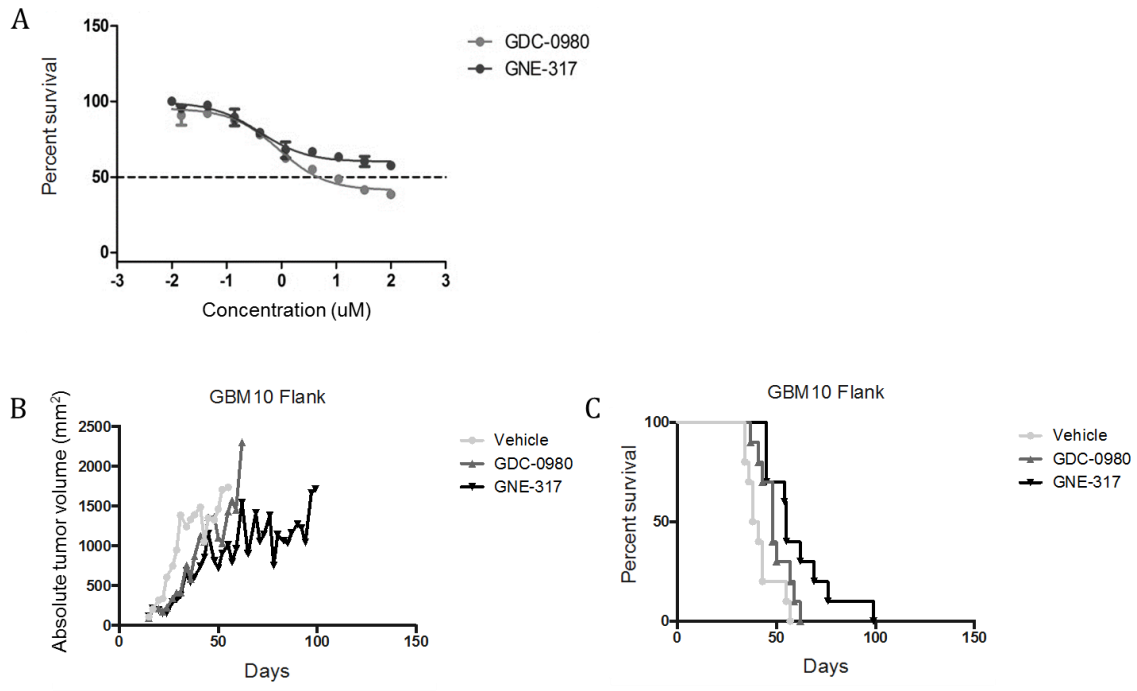
A
Percent survival
150
100
50
0
-3
-2
-1
0
1
2
3
Concentration (uM)
GDC-0980
GNE-317
B
GBM10 Flank
Absolute tumor volume (mm2)
2500
2000
1500
1000
500
0
0
50
100
150
Days
Vehicle
GDC-0980
GNE-317
C
GBM10 Flank
Percent survival
100
50
0
0
50
100
150
Days
Vehicle
GDC-0980
GNE-317

Figure 3.3

Time profiles of GDC-0980 and GNE-317 distributions in brain and plasma. Measurements were ascertained following a single simultaneous oral dose of GNE-317 (30 mg/kg) and GDC-0980 (7.5 mg/kg). Plasma and brain concentration time profiles of GNE-317 are shown in FVBn wild-type (A) and in triple knockout (TKO) mice (B). Corresponding brain-to-plasma ratios with respect to time are shown in (C) for both wild-type and TKO mice. Plasma and brain concentration-time profiles of GDC-0980 (7.5 mg/kg) are shown in FVBn wild-type (D) and TKO mice (E). Corresponding brain-to-plasma ratios with respect to time are shown in (F) for both wild-type and TKO mice. Data represent mean ± S.D. (n= 3-4 at each time point).

Figure 3.3

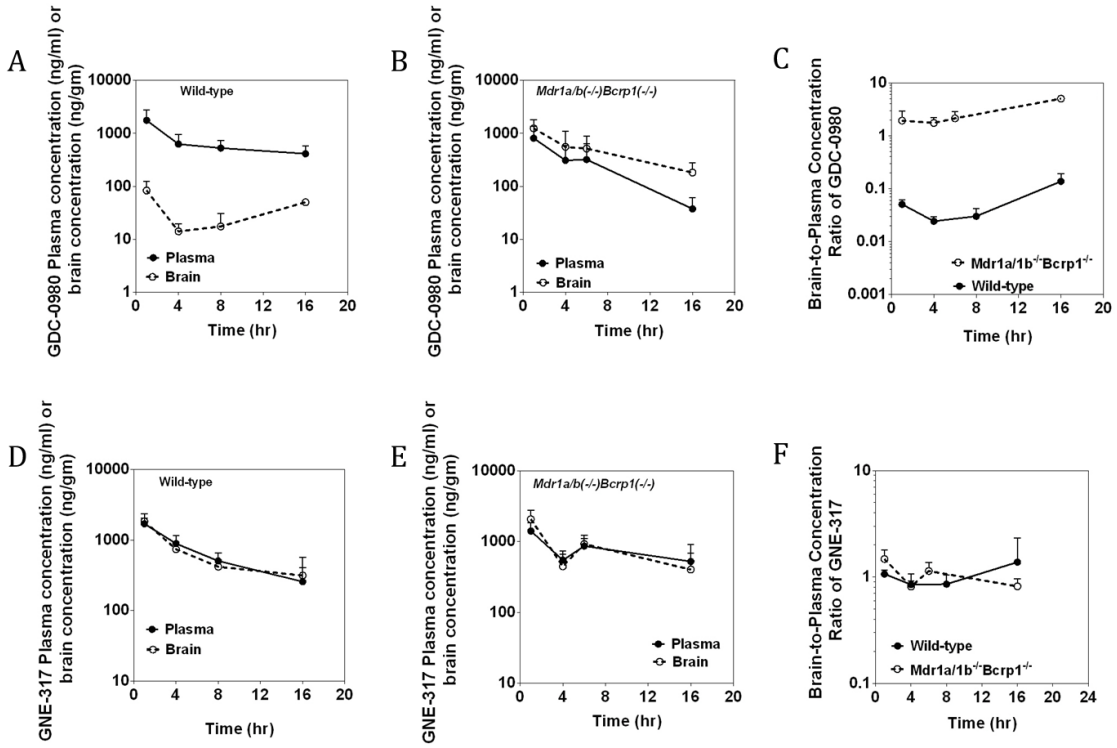
A
GDC-0980 Plasma concentration (ng/ml) or brain concentration (ng/gm)
Wild-type
Plasma
Brain
Time (hr)
B
GDC-0980 Plasma concentration (ng/ml) or brain concentration (ng/gm)
Mdr1a/b(-/-)Bcrp1(-/-)
Plasma
Brain
Time (hr)
C
Brain-to-Plasma Concentration Ratio of GDC-0980
Mdr1a/1b-/-Bcrp1-/-
Wild-type
Time (hr)
D
GNE-317 Plasma concentration (ng/ml) or brain concentration (ng/gm)
Wild-type
Plasma
Brain
Time (hr)
E
GNE-317 Plasma concentration (ng/ml) or brain concentration (ng/gm)
Mdr1a/b(-/-)Bcrp1(-/-)
Plasma
Brain
Time (hr)
F
Brain-to-Plasma Concentration Ratio of GNE-317
Wild-type
Mdr1a/1b-/-Bcrp1-/-
Time (hr)

Table 3.1

Plasma and brain pharmacokinetics of GNE3-17 and GDC-0980. PK data were determined by non-compartmental analysis after simultaneous administration of a single oral dose of GNE-317 (30 mg/kg) and GDC-0980 (7.5 mg/kg) in wild-type and *Mdr1a/b*$^{(-/-)}$*Bcrp1*$^{(-/-)}$ mice. Results are expressed as mean ± S.D. *n* = 3 - 4.

Table 3.1

		GNE-317		GDC-0980	
	Parameter (units)	Wild-type	*Mdr1a/b(-/-)Bcrp1(-/-)*	Wild-type	*Mdr1a/b(-/-)Bcrp1(-/-)*
Plasma	C_{max} (µg/mL)	1.7 ± 0.20	1.41 ± 0.21	1.76 ± 0.58	0.81 ± 0.27
	T_{max} (hr)	1	1	1	1
	$AUC_{0\text{-tlast}}$ (h.µg/mL)	10.59 ± 0.81	11.99 ± 1.65	10.56 ± 1.47	4.51 ± 1.15
Brain	C_{max} (µg/mL)	1.84 ± 0.29	2.07 ± 0.36	0.083 ±0.023	1.25 ± 0.27
	T_{max} (hr)	1	1	1	1
	$AUC_{0\text{-tlast}}$ (h.µg/mL)	10.06 ± 0.9	12.80 ± 1.24	0.52 ± 0.06	7.91 ± 1.44
	K_p = AUC_{brain} /AUC_{plasma}	0.95	1.07	0.05	1.75
	DTI	1.13		35	

Figure 3.4

Dosing of bevacizumab and its effects on TRD accumulation. Top panels (A-D) show fluorescence imaging of TRD and bottom panels (E-G) show corresponding brain slices stained with Cresyl Violet and imaged under bright field. TRD accumulates more readily in vehicle treated animals (A & E), less readily in animals treated with a single dose of bevacizumab (B & F), and little-to-none in animals treated with two doses of bevacizumab and euthanized either 24 or 72 hours later (C & G, D & H). Outlines generated manually on the basis of subjective tumor extent via cresyl violet staining.

Figure 3.4

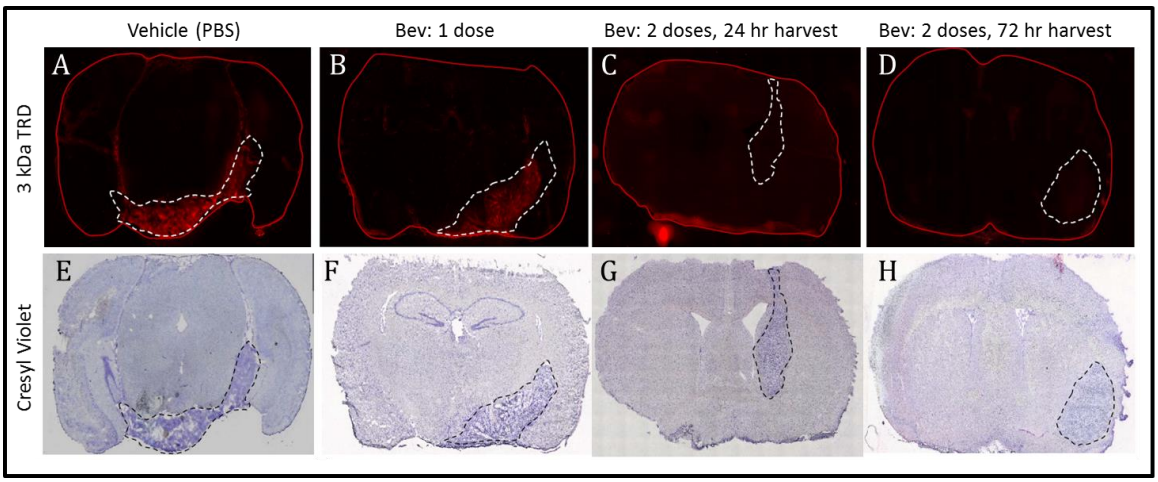
Vehicle (PBS)
Bev: 1 dose
Bev: 2 doses, 24 hr harvest
Bev: 2 doses, 72 hr harvest
3 kDa TRD
Cresyl Violet
A
B
C
D
E
F
G
H

Figure 3.5

Dosing of bevacizumab seals the BBB to restrict dye permeation. Top panels (A-B) show fluorescence imaging of TRD; middle panels (C-D) show corresponding brain slices with fluorescence imaging of fluorescein; bottom panels (E-G) show corresponding brain slices stained in H&E and imaged using bright field. Dye accumulate more readily in vehicle-treated animals (A & C) and less readily in animals treated with bevacizumab (B & D). Tumor outlines generated manually on the basis of subjective tumor extent via H&E staining.

Figure 3.5

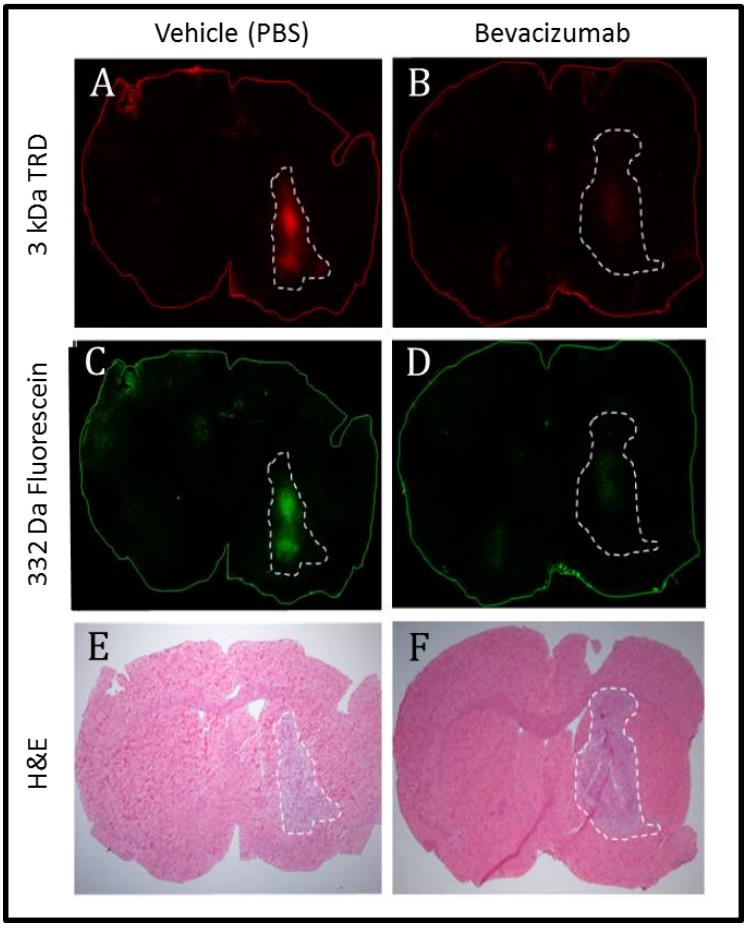
Vehicle (PBS)
Bevacizumab
3 kDa TRD
332 Da Fluorescein
H&E
A
B
C
D
E
F

Figure 3.6

Influence of bevacizumab on tumor and brain distribution of GNE-317. Brain-to-plasma ratios of GNE-317 distribution are approximately equal both one hour (A) and six hours (B) after dosing with GNE-317.

Figure 3.6

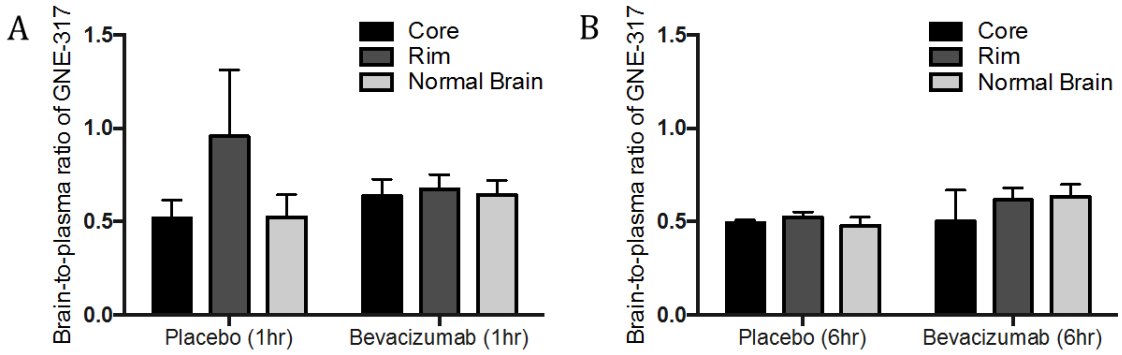
A
Brain-to-plasma ratio of GNE-317
1.5
1.0
0.5
0.0
Core
Rim
Normal Brain
Placebo (1hr)
Bevacizumab (1hr)
B
Brain-to-plasma ratio of GNE-317
1.5
1.0
0.5
0.0
Core
Rim
Normal Brain
Placebo (6hr)
Bevacizumab (6hr)

Figure 3.7

Influence of bevacizumab on tumor and brain concentrations of GNE-317. Raw data describing the amount of drug present in tissue or plasma are provided in both placebo- and bevacizumab-treated animals at both 1- and 6-hour time points after dosing with GNE-317.

Figure 3.7

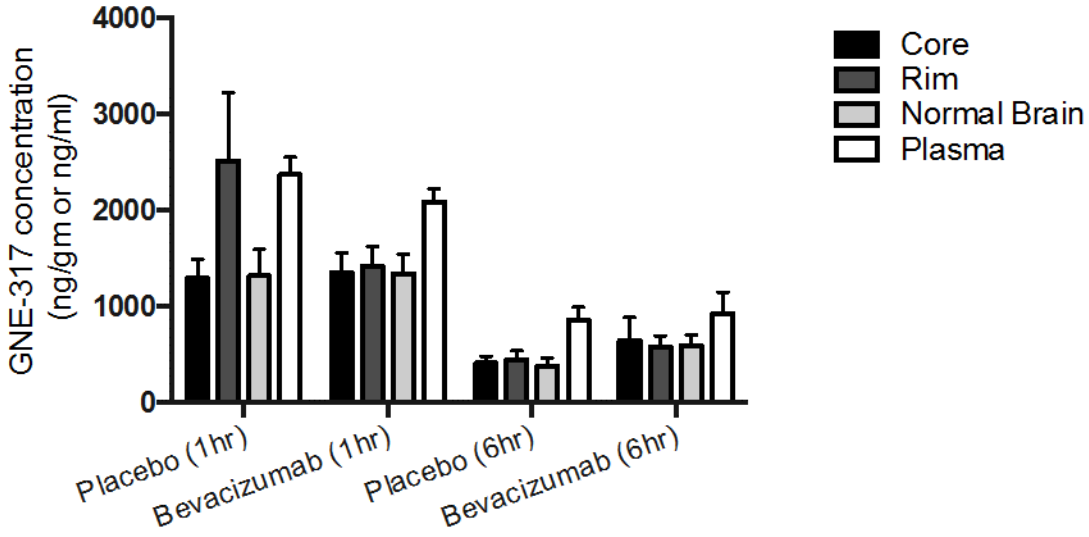
GNE-317 concentration (ng/gm or ng/ml)
4000
3000
2000
1000
0
Placebo (1hr)
Bevacizumab (1hr)
Placebo (6hr)
Bevacizumab (6hr)
Core
Rim
Normal Brain
Plasma

Figure 3.8

Influence of bevacizumab on tumor and brain distribution of GDC-0980. Brain-to-plasma ratios of GDC-0980 distribution are approximately equal both one hour (A) and six hours (B) after dosing with GDC-0980.

Figure 3.8

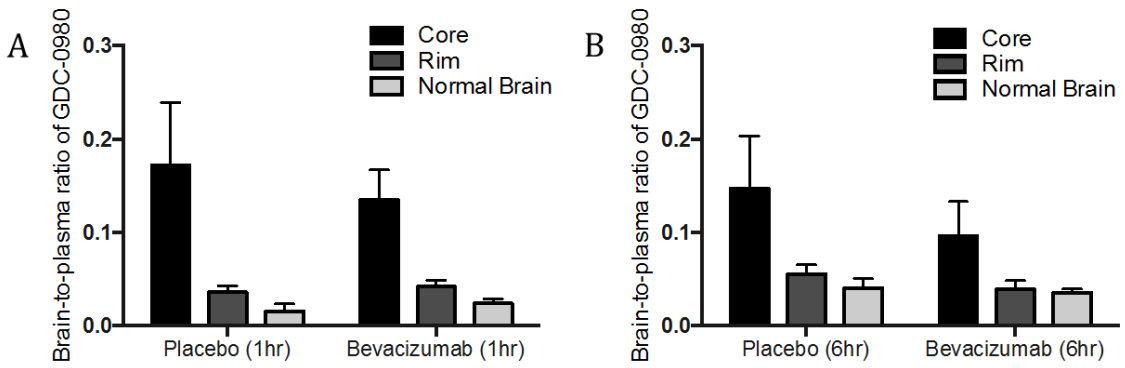
A
Brain-to-plasma ratio of GDC-0980
0.3
0.2
0.1
0.0
Core
Rim
Normal Brain
Placebo (1hr)
Bevacizumab (1hr)
B
Brain-to-plasma ratio of GDC-0980
0.3
0.2
0.1
0.0
Core
Rim
Normal Brain
Placebo (6hr)
Bevacizumab (6hr)

Figure 3.9

Influence of bevacizumab on tumor and brain concentrations of GDC-0980. Raw data describing the amount of drug present in tissue or plasma are provided in both placebo- and bevacizumab-treated animals at both 1- and 6-hour time points after dosing with GDC-0980.

Figure 3.9

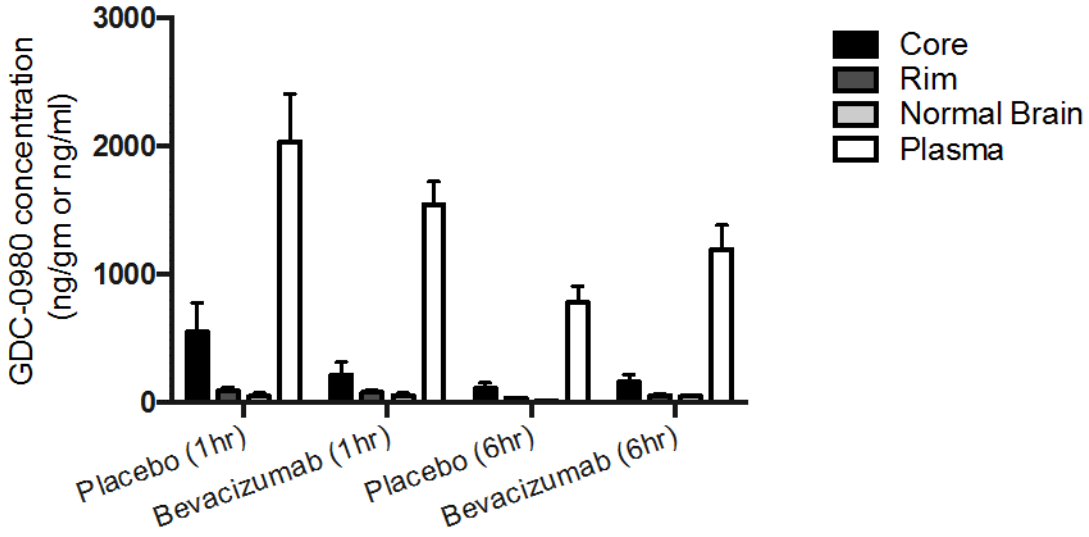
GDC-0980 concentration (ng/gm or ng/ml)
3000
2000
1000
0
Placebo (1hr)
Bevacizumab (1hr)
Placebo (6hr)
Bevacizumab (6hr)
Core
Rim
Normal Brain
Plasma

Figure 3.10

Immunohistochemistry one hour after treatment with bevacizumab, GDC-0980 or GNE-317 or in combination. Representative images of whole brains are shown in (A) while magnified portions of those brains are shown in (B). Scale bar in (A) = 650um, scale bar in (B) = 100 um. Staining intensities were not significantly different between groups.

Figure 3.10

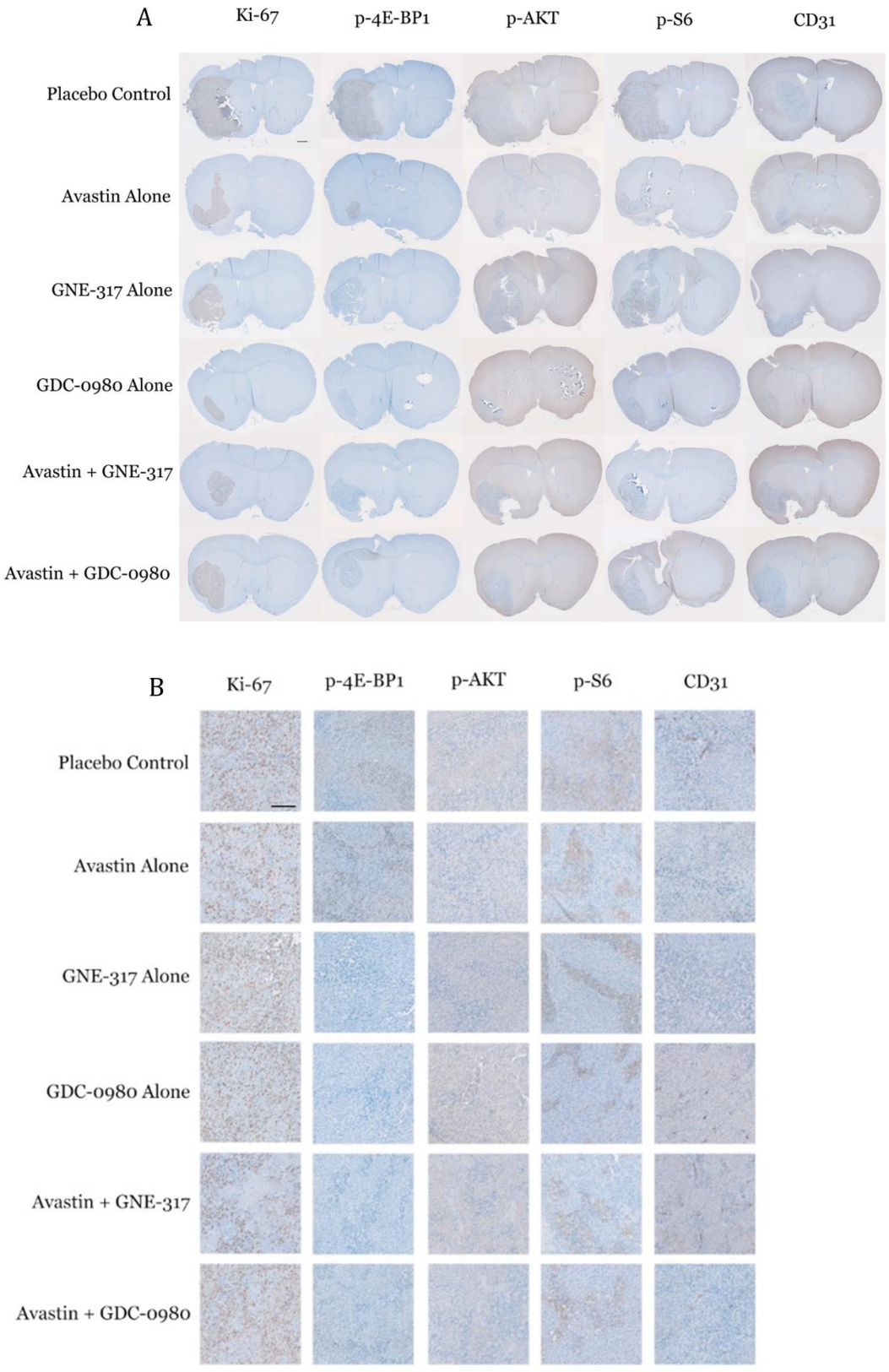
A
Ki-67
p-4E-BP1
p-AKT
p-S6
CD31
Placebo Control
Avastin Alone
GNE-317 Alone
GDC-0980 Alone
Avastin + GNE-317
Avastin + GDC-0980
B
Ki-67
p-4E-BP1
p-AKT
p-S6
CD31
Placebo Control
Avastin Alone
GNE-317 Alone
GDC-0980 Alone
Avastin + GNE-317
Avastin + GDC-0980

Figure 3.11

In vivo efficacy studies in the GBM10 orthotopic xenograft glioma model. (A) Kaplan Meier survival curves indicate that treatment with GNE-317 + bevacizumab is more significant than treatment with GNE-317 alone (p=<.0001) or bevacizumab alone (p=.0395). (B) Kaplan Meier survival curves indicate that treatment with GDC-0980 + bevacizumab is more significant than treatment with GDC-0980 alone (p=.0097) but not more significant than treatment with bevacizumab alone).

Figure 3.11

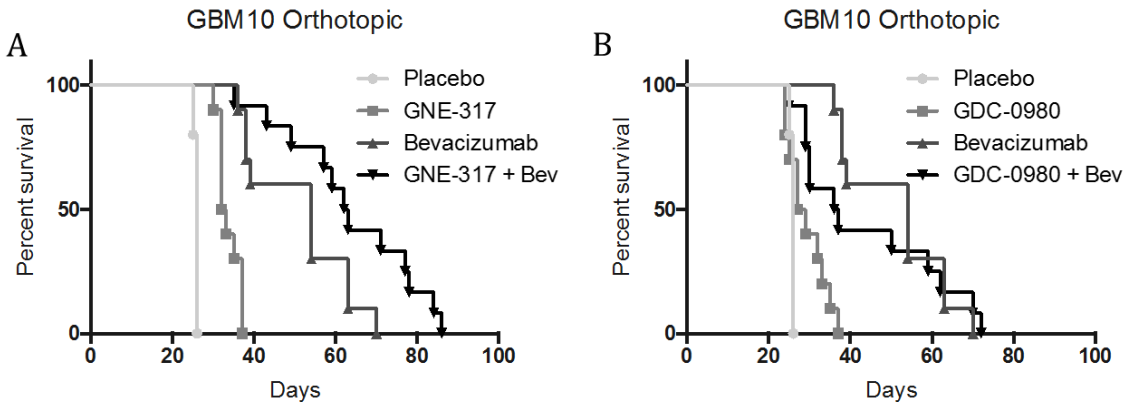
A
GBM10 Orthotopic
Placebo
GNE-317
Bevacizumab
GNE-317 + Bev
Percent survival
Days
B
GBM10 Orthotopic
Placebo
GDC-0980
Bevacizumab
GDC-0980 + Bev
Percent survival
Days

Figure 3.12

In vivo efficacy studies in the GBM59 orthotopic xenograft glioma model. (A) Kaplan Meier survival curves indicate that treatment with GNE-317 + bevacizumab is more significant than treatment with GNE-317 alone (p=<.0048) or bevacizumab alone (p=.0017). (B) Kaplan Meier survival curves indicate that treatment with GDC-0980 + bevacizumab is more significant than treatment with GDC-0980 alone (p=.0326) but not more significant than treatment with bevacizumab alone).

Figure 3.12

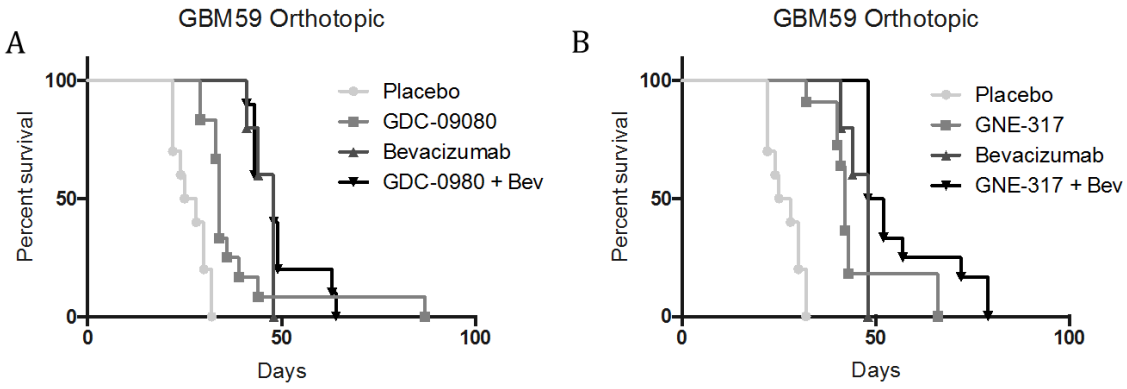
A
GBM59 Orthotopic
Percent survival
100
50
0
0
50
100
Days
Placebo
GDC-09080
Bevacizumab
GDC-0980 + Bev
B
GBM59 Orthotopic
Percent survival
100
50
0
0
50
100
Days
Placebo
GNE-317
Bevacizumab
GNE-317 + Bev

CHAPTER 4

The Therapeutic Potential of the Parthenolide Derivative, LC-1 in the Targeting of Glioma Stem Cells

Joseph K. Hexum[1*], Chani M. Becker[2*], Aaron M. Kempema[1], John R. Ohlfest[3,4], David A. Largaespada[3,4], and Daniel A. Harki[,1,4,5]

Adapted by permission from Elsevier

Chani M. Becker et al., Parthenolide prodrug LC-1 slows growth of intracranial glioma, Bioorganic & Medicinal Chemistry Letters (2015) 25 (12): 2493-2495

*JK Hexum and CM Becker contributed equally to this work and share first authorship

Affiliations:

1. Department of Medicinal Chemistry, University of Minnesota, 8-101 Weaver Densford Hall, 308 Harvard Street SE, Minneapolis, MN 55455

2. Department of Neuroscience, University of Minnesota, 6-145 Jackson Hall, 321 Church St SE, Minneapolis, MN 55455

3. Department of Pediatrics, University of Minnesota, 6th Floor East Building, 2450 Riverside Ave, Minneapolis, MN 55454

4. Masonic Cancer Center, University of Minnesota, 425 E River Pkwy #754, Minneapolis, MN 55455

5. Stem Cell Institute, University of Minnesota, 2001 6th Street SE, Minneapolis, MN 55455

Funding:

Hyundai Hope on Wheels (Hope Grant Award, JR Ohlfest & DA Harki),
The V Foundation for Cancer Research (V Scholar Award, DA Largaespada)
Children's Cancer Research Foundation (DA Largaespada)

Keywords: Blood-brain barrier, glioblastoma, LC-1, Parthenolide, Pharmacokinetics

Conflicts of Interest:

DA Largaespada: co-founder and part owner of two biotechnology companies, Discovery Genomics, Inc and NeoClone Biotechnology; Genentech, Inc. grant recipient.

Author Contributions:

Conception and design: CM Becker, JK Hexum, JR Ohlfest, DA Harki

Development of methodology: CM Becker, JK Hexum

Acquisition of data (provided animals, provided facilities, etc.): CM Becker, JK Hexum

Analysis and interpretation of data (e.g., statistical analysis, biostatistics, computational analysis): CM Becker, JK Hexum

Writing, review, and/or revision of the manuscript: CM Becker, JK Hexum, DA Largaespada, DA Harki

Administrative, technical, or material support (i.e., reporting or organizing data, constructing databases): JK Hexum

Study supervision: JR Ohlfest, DA Largaespada, DA Harki

4.1 Introduction

Glioblastoma multiforme (GBM) is the most aggressive form of glioma (Ostrom, Gittleman, Stetson, Virk, & Barnholtz-Sloan, 2015; Parsons et al., 2008) and currently, a lethal disease with only a 15 month survival prognosis (Parsons et al., 2008). Individuals diagnosed with GBM are treated using a combination of therapeutic measures including surgical resection, radiation therapy and chemotherapy with temozolomide (Stupp et al., 2005). As described in Chapter 1, this disease is difficult to treat due to several factors including among other factors, its invasiveness and genetic heterogeneity (Bonavia, Inda, Cavenee, & Furnari, 2011; Ortensi, Setti, Osti, & Pelicci, 2013; Pardridge, 2003). Many of the failures in recent clinical trials can be attributed to poor targeting that does adequately address these qualities. Appropriate target selection is therefore a crucial component towards the development and application of successful chemotherapeutics in the treatment of GBM.

Glioma stem cells comprise one of the most compelling targets in the treatment of GBM. Beyond roles in the initiation and propagation of brain tumors, cancer stem cells (CSCs) have also been described as a population of drug- and radiation-resistant cells that are central to tumor recurrence (Rich & Eyler, 2008; Singh et al., 2004; Yuan et al., 2004). While the exact mechanisms surrounding these phenomena are still relatively unproven, a combination of slow cell cycle kinetics, low levels of reactive oxygen species, improved DNA repair capacity, and high expression levels of anti-apoptotic genes and efflux transporters all likely play roles in resistance (Bao et al., 2006; Diehn et al., 2009; M. Jackson, Hassiotou, &

Nowak, 2015; G. Liu et al., 2006). These data suggest that targeting CSCs that provide such beneficial properties to the tumor may be of tremendous advantage in the treatment of GBM.

Parthenolide (PTL; **Figure 4.1**), a sesquiterpene lactone natural product isolated from the feverfew plant (*Tanacetum parthenium*), has been shown to exhibit broad-spectrum anti-cancer activity (Ghantous, Sinjab, Herceg, & Darwiche, 2013). This small molecule exhibits anti-proliferative activity against a variety of cancer cell lines, including leukemia, glioma, breast cancer, and prostate cancer cells (Anderson & Bejcek, 2008; Guzman et al., 2005; Guzman et al., 2007). In addition, PTL has been shown to selectively target acute myelogenous leukemia (AML) stem cells, while sparing hematopoietic stem cells (Guzman et al., 2007). The mechanism of action of this activity is complex due to the variety of cellular processes that PTL affects, including NF-κB signaling, microtubule detyrosination, DNA methylation, and reactive oxygen species generation (Fonrose et al., 2007; Kwok, Koh, Ndubuisi, Elofsson, & Crews, 2001; Z. Liu et al., 2009; Shanmugam et al., 2010). Additionally, while PTL has been shown to inhibit the activation of NF-κB by binding to IKKβ in HeLa cells (Kwok et al., 2001), there is evidence that PTL does not inhibit NF-κB in GBM cells (Anderson & Bejcek, 2008). An additional feature of PTL that complicates its clinical development is its low water solubility and bioavailability. These poor molecular attributes led to the development of prodrugs, including LC-1 (also known as DMAPT or dimethylamino-parthenolide; **Figure 4.1**), which is over 1000-fold more soluble in water than PTL (Guzman et al., 2007; Neelakantan, Nasim, Guzman, Jordan, &

Crooks, 2009). LC-1 has also been shown to be considerably more bioavailable than PTL in mice and canine studies (Guzman et al., 2007). Based on the evidence that GBM populations contain drug-resistant brain tumor stem cells and that PTL has been shown to target AML stem cells (Guzman et al., 2005), we hypothesized that LC-1 may possess anti-proliferative efficacy against GBM *in vivo*. Therefore, we evaluated LC-1 for brain penetrance in addition to *in vitro* and *in vivo* anti-proliferative efficacy in GBM models.

4.2 Materials & Methods

4.2.1 LC-1 Preparation and PTL Purification

LC-1 (also known as dimethylamino-parthenolide, DMAPT) was synthesized as previously described(Neelakantan et al., 2009). Parthenolide (PTL) was purchased from Enzo Life Sciences and was purified by SiO_2 chromatography (gradient 0-30% ethyl acetate in hexanes) prior to biological testing.

4.2.2 Preparation of PTL and LC-1 Stock Solutions

PTL and LC-1 stock solutions for cytotoxicity assays were prepared in DMSO (either 20 mM or 40 mM concentration) and stored at -20 °C when not in use. Compound purities were assessed frequently by analytical reverse-phase HPLC analysis and fresh solutions were prepared as needed.

4.2.3 Cell Culture

All cell lines were maintained in a humidified 5% CO_2 environment at 37 °C. U-87 MG cells were cultured as described previously (B. Wen, Hexum, Widen, Harki, & Brummond, 2013). GBM6 cells were cultured in DMEM/F-12 (1:1) media with L-glutamine, without HEPES (Thermo Scientific) supplemented with B-27 supplement (1X, Gibco), N-2 supplement (1X, Gibco), Normocin (0.1 mg/mL, InvivoGen), human epidermal growth factor (EGF, 20 ng/mL, PeproTech), human fibroblast growth factor-basic (FGF-basic, 20 ng/mL, PeproTech), penicillin (50 I.U./mL, Cellgro), and streptomycin (50 µg/mL, Cellgro). GL261 murine glioma cells were transfected with green fluorescent protein (GFP) and luciferase (Luc) from separate plasmids using methods described previously (Wu et al., 2007). GL261-GFP-Luc cells were cultured in hypoxic conditions (5% oxygen)(Olin et al., 2010) in DMEM media (Cellgro) supplemented with 10% FBS (Gibco), penicillin (100 I.U./mL, ATCC), and streptomycin (100 µg/mL, ATCC) along with puromycin (10 µg/mL, Gibco) and G418 (500 µg/mL, InvivoGen) selection reagents. U-87 MG and GL261-GFP-Luc cells were dissociated from flask/plate surfaces using 0.25% trypsin/EDTA solution (Gibco) and GBM6 cells were dissociated using TrypLE Express (Gibco) solution.

4.2.4 Alamar Blue Cytotoxicity Assays

Cytotoxicity assays were performed as described previously (Hexum, Tello-Aburto, Struntz, Harned, & Harki, 2012; B. Wen et al., 2013). The IC_{50} value for PTL in U-87 MG cells was obtained previously (B. Wen et al., 2013). U-87 MG,

GBM6, and GL261-GFP-Luc cells were seeded at a density of 5,000 cells/well in cell culture media (50 µL) in standard 96-well plates (Costar) 24 hours prior to treatment. Blank (no cells) wells and control (vehicle control treated) wells were prepared with each experiment. Compounds were serially diluted in pre-warmed media and dosed to cells (final volume = 100 µL; final DMSO concentration = 0.5%). Approximately 2 hours before the end of the treatment period (48 hours), Alamar Blue (Invitrogen) cell viability reagent was added to each well (10 µL). After the 48 hour treatment period, the fluorescence of each well was read using a BioTek Synergy H1 plate reader. Cytotoxicity curves (sigmoidal dose response) were generated using GraphPad Prism (v. 5.0).

4.2.5 Animal Care

For the C57BL/6J mouse studies, all procedures were carried out in accordance with the guidelines set by the Principles of Laboratory Animal Care (NIH, Bethesda, MD) and were approved by the Institutional Animal Care and Use Committee (IACUC) of the University of Minnesota (Minneapolis, MN). Female C57BL/6J mice aged 6-8 weeks were purchased from Jackson Laboratories. C57BL/6J mice were allowed food and water *ad libitum*. In survival studies, mice that became moribund were euthanized by CO_2 asphyxiation. Pharmacokinetic studies performed by Apredica LLC using CD-1 mice were in compliance with the Animal Welfare Act, The Guide for the Care and Use of Laboratory Animals, and the Office of Laboratory Animal Welfare.

4.2.6 Pharmacokinetic Studies

The pharmacokinetic studies were carried out by Apredica LLC (now Cyprotex PLC). Briefly, six CD-1 male mice (three mice for each time point) were provided a single dose of 100 mg/kg LC-1 (p.o.; formulated in 0.5% methylcellulose) and were sacrificed after either one or four hours. Blood samples were collected in K_2EDTA microtainer tubes for plasma separation. The blood samples were then centrifuged at 6,000 rpm for 5 minutes at 4 °C. Brains were perfused and collected. Mouse plasma and brain samples were stored at -80 °C. Plasma and brain samples were thawed on ice and were maintained at 4° C during processing. Brain tissues were homogenized in 50 mM potassium phosphate (pH 7.4). The plasma or homogenized brain tissue was then mixed with three volumes of methanol, incubated on ice for 5 minutes, and centrifuged. The supernatant was then used for the analysis. Drug concentrations were measured in perfused brain samples and in plasma by LC-MS/MS using an Agilent 6410 mass spectrometer coupled with an Agilent 1200 HPLC and a CTC PAL chilled autosampler, all controlled by MassHunter software (Agilent). Separation was performed using a C18 reverse phase HPLC column and an acetonitrile-water gradient system. After separation, peaks were analyzed by mass spectrometry using ESI ionization in MRM mode. Calibration curves were obtained by first preparing a working dilution of LC-1 in DMSO at 50 times the final concentration. Serial dilutions were prepared from the working dilution. The serial dilutions were then diluted 50-fold into mouse plasma or brain homogenate and processed as described above. The resulting pharmacokinetic data (perfused brain and plasma concentrations of PTL and LC-

1) were analyzed using Microsoft Excel to calculate mean concentrations and standard deviations (S.D.).

4.2.7 LC-1 Toxicity Study in Healthy Mice

Twelve 6-8-week old female C57BL/6 mice were split equally into four groups (40 mg/kg LC-1, 100 mg/kg LC-1, vehicle control, and phlebotomy control). The groups other than the phlebotomy group were dosed (p.o.) with vehicle alone or LC-1 (40 mg/kg or 100 mg/kg) daily for 30 days. LC-1 was formulated for oral dosing in 0.3 M 2-hydroxypropyl-β-cyclodextrin (HP-β-CD; vehicle) at 40 mg/kg and 100 mg/kg. HP-β-CD and other cyclodextrin derivatives form non-covalent complexes with hydrophobic molecules, enhancing their solubility in aqueous solutions (Challa, Ahuja, Ali, & Khar, 2005; Gould & Scott, 2005). Solid HP-β-CD was purchased from Santa Cruz Biotechnology. Vehicle solutions were prepared by dissolving HP-β-CD in Milli-Q Millipore water and mixing well (using sonication if necessary) to achieve a final concentration of 0.3 M. Blood samples were drawn via orbital eye bleeds (50 µL per read) from each mouse on days 0, 12, 21, and 30. The blood samples were collected into EDTA-coated vessels using capillary tubes and eyes were alternated between reads. Complete blood counts (white and red blood cell counts, hemoglobin levels, and platelet levels) were obtained for the mice using a Hemavet 850FS (Drew Scientific, Oxford, CT).

4.2.8 Intracranial Tumor Implantation

Brain tumors were established through intracranial inoculation of 30,000 GL261-GFP-Luc cells in PBS (1 µL) to 6-8-week old female C57BL/6J mice as previously described.[8] Briefly, cells were cultured to subconfluence then washed in phosphate-buffered saline (PBS), trypsinized, filtered through a 40 µm mesh, and resuspended in sterile PBS. Mice were anesthetized with a ketamine/xylazine cocktail (53.7 mg/mL ketamine and 9.26 mg/mL xylazine delivered 1 mL/kg via intraperitoneal injection) before surgery. Cells were injected into the right ventral striatum based on coordinates 2.5 mm lateral and 0.5 mm anterior from bregma at a ventral depth of 3 mm from the surface of the brain. Using an automated pump, cells were injected at a continuous rate of 0.2 µL/min over 5 minutes (Stoelting Co. Quintessential Stereotaxic Injector). Tumor growth was determined through bioluminescence imaging using the IVIS50 system (Caliper Life Sciences) and quantified in radiance units (photons/second/cm^2/radian^2) using Living Image software (PerkinElmer) following an i.p. injection of D-luciferin (100 µL, 28.5 mg/mL in PBS) 10 minutes before imaging (substrate for luciferase enzyme, Gold Biotechnology). Animals were sedated using 2-5% isoflurane in oxygen provided by nose cones within the imager.

4.2.9 LC-1 Survival Study in Tumor-Bearing Mice

Starting seven days after intracranial inoculation with GL261-GFP-Luc cells, mice were treated once daily with either 100 mg/kg LC-1 dissolved in 0.3 M HP-β-CD or vehicle alone (Das, Lin, Ho, & Ng, 2008; H. Lin & Ho, 2011). Statistical

significance for the comparison between the LC-1 and vehicle survival curves (Kaplan-Meier) was determined using a log-rank test performed using GraphPad Prism software (v. 5.0).

4.3 Results

4.3.1 LC-1 Demonstrates a Similar Cytotoxicity Profile to Parthenolide

In order to determine the *in vitro* anti-glioma activity of PTL and prodrug, LC-1, we performed cytotoxicity assays using U-87 MG, GBM6, and GL261-GFP-Luc cells (**Figure 4.2**). U-87 MG is a frequently utilized human GBM cell line that has recently been genetically sequenced (M. J. Clark et al., 2010). GBM6, a human patient-derived GBM cell line (Swaminathan et al., 2010), contains a population of $CD133^+$ cells, a marker commonly associated with the stem cell population of glioma cells (Singh et al., 2004). GL261-GFP-Luc is a GL261 murine glioma cell line that was stably transfected with green fluorescent protein (GFP) and luciferase (Luc) plasmids that permit the kinetics of tumor growth to be monitored by bioluminescent imaging (Wu et al., 2007). The IC_{50} value for PTL against U-87 MG cells was obtained previously by our group (B. Wen et al., 2013). PTL and LC-1 were found to be similarly active against U-87 MG cells (IC_{50} values of 8.8 µM and 8.8 µM, respectively), GBM6 cells (3.4 µM and 3.5 µM), and GL261-GFP-Luc cells (7.6 µM and 6.9 µM) (**Table 4.1**).

4.3.2 LC-1 Brain Penetrance

Given our promising *in vitro* anti-proliferative activity data of LC-1 against multiple GBM cell culture models, we next sought to explore the pharmacokinetic properties of LC-1. We deemed it critical to determine the extent to which LC-1 could penetrate the blood-brain barrier (BBB) in healthy mice prior to efficacy studies in glioma-bearing mice. We speculated that LC-1 could penetrate the brain because of its low molecular weight (293.4 Da) and minimal hydrogen bonding donors/acceptors with water (4 H-bond acceptors) as the free base, which are established features of brain-penetrant drugs (predictive for brain-penetrant small molecules: < 400 Da molecular weight and < 8 total H-bonds with water) (Pardridge, 2007; Upadhyay, 2014). Additionally, LC-1 has a positive charge under biological conditions due to the basic dimethylamino group and it has been suggested that the presence of a positive charge on a molecule at pH 7-8 is favorable for brain permeation (D. E. Clark, 2003).

Pharmacokinetic (PK) data was obtained by dosing CD-1 male mice with LC-1 (100 mg/kg) and harvesting organ and blood samples after either one or four hours following drug administration. Concentrations of LC-1 and its elimination product, PTL, in perfused brain tissue and plasma were then quantified using liquid chromatography-mass spectrometry (**Table 4.2**). Concentrations in plasma after one hour were determined to be 2,965 ng/mL (LC-1) and 2,142 ng/mL (PTL), whereas even higher levels were observed in perfused brain at the same time point: 6,251 ng/g (LC-1) and 2,402 ng/g (PTL). After four hours, the concentrations of LC-1 and PTL in plasma (115 and 211 ng/mL, respectively) and perfused brain

(342 and 113 ng/g, respectively) were considerably diminished. The perfused brain concentration for LC-1 (one hour time point) corresponds to a concentration of approximately 21 μM (assuming a brain tissue density of 1 g/mL), which is well above the measured IC_{50} values for LC-1 and PTL in glioma cell lines (**Table 4.1**). Brain-to-plasma LC-1 concentration ratios were 2.1 (one hour) and 3.0 (four hours) and demonstrate the penetrance of this molecule through the BBB. In general, compounds with brain-to-plasma ratios >1 are considered to be able to freely cross the BBB (Mensch, Oyarzabal, Mackie, & Augustijns, 2009). Our data is consistent with a previous study of LC-1 that measured a half-life of 0.63 hours in mouse serum (Guzman et al., 2007). Our data is consistent with a previous study of LC-1 that measured a half-life of 0.63 hours in mouse serum (Guzman et al., 2007). Taken together, these PK data suggest that LC-1 has the potential to penetrate the BBB and accumulate to significant concentrations in brain tissue. This conclusion is further supported by recent PK data obtained with structurally related dimethylamino-micheliolide (DMAMCL) in adult Wistar rats, which revealed brain-to-plasma ratios of 1.84 (30 minutes) and 1.91 (three hours) (An et al., 2015).

4.3.3 LC-1 is Well-Tolerated in Animal Toxicity Studies

Previous studies have shown that LC-1 is well tolerated in mice and canines at high doses (100 mg/kg) (Guzman et al., 2007; Hassane et al., 2010). In order to obtain an oral toxicity profile of LC-1 in C57BL/6 mice, we tested their tolerance to 40 mg/kg and 100 mg/kg doses of LC-1. The mice for this experiment (12 total) were split into four groups (40 mg/kg LC-1, 100 mg/kg LC-1, vehicle control, and

phlebotomy control). LC-1 was formulated for oral dosing in 0.3 M 2-hydroxypropyl-β-cyclodextrin (HP-β-CD; vehicle) (Das et al., 2008; H. Lin & Ho, 2011). [31, 32] HP-β-CD forms non-covalent complexes with hydrophobic molecules, thereby enhancing their solubility in aqueous solutions (Challa et al., 2005; Gould & Scott, 2005). The phlebotomy control mice were given no treatment. The other three mice groups were either dosed (p.o.) with vehicle alone or LC-1 (40 mg/kg or 100 mg/kg in HP-β-CD vehicle) daily for 30 days. Blood samples were drawn from each mouse on days 0, 12, 21, and 30. Complete blood counts (CBC) of white blood cells (WBC), red blood cells (RBC), hemoglobin, and platelets were measured for each sample. These hematological parameters were specifically chosen because they provide indications of health status. No significant differences were observed between the groups in the CBC panel (**Figure 4.3**), suggesting the drug demonstrates a robust safety profile in hematological measurements.

4.3.4 *In Vivo* Efficacy of LC-1

After establishing that LC-1 accumulates to biologically relevant concentrations in brain tissue and is non-toxic following continuous dosing for several weeks, we then studied whether LC-1 could extend survival of glioma-bearing mice as a single agent. We chose the syngeneic murine GL261 model due to its pathological similarity to human GBM (Newcomb & Zagzag, 2009), and the specific cells used in our study, GL261-GFP-Luc, permit tumor growth to be monitored by bioluminescence imaging (Wu et al., 2007). In addition, the high dose of LC-1 (100 mg/kg) was chosen due to the lack of *in vivo* toxicity. Following

establishment of GL261-GFP-Luc tumors in mice, animals were randomized and treated daily with either LC-1 (100 mg/kg in HP-β-CD vehicle) or vehicle alone. Weekly bioluminescence imaging revealed a delay in tumor growth kinetics in LC-1-treated mice in comparison to vehicle-treated control mice (**Figure 4.4A**). This delay in tumor growth properties also corresponded to increased survival, with Kaplan-Meier curves revealing a statistically significant (p=0.01) extension of survival in the LC-1-treated group in comparison to vehicle control (**Figure 4.4B**).

4.4 Discussion

The results of this study demonstrate the impact of glioma stem cells as a target in anti-GBM chemotherapeutics. We first highlight that the parthenolide analogue, LC-1 has potent and efficacious cytotoxic effects against multiple glioma cell lines (**Table 4.1** and **Figure 4.2**). By ascertaining the pharmacokinetics of LC-1 in the brain and plasma, we demonstrate drug's brain penetrant capabilities (**Table 4.2**). Extended oral dosing suggests the drug is relatively non-toxic even after repeated exposure (**Figure 4.3**) and significantly improves survival in a mouse model of GBM (**Figure 4.4**). The impact of a benefit to survival should not be underappreciated, as previous chapters demonstrate that these data are not easy to generate, even with the most promising therapeutics.

This study validates the importance of adequate target selection and drug delivery in the treatment of GBM. Oftentimes, research efforts are narrowed at one of these dimensions, but only when a compound can address both fields can a drug really hold therapeutic promise in a clinical setting. Given the success in the

GL261 model, the parthenolide derivative, LC-1, should be further tested in other animal models of glioma to validate the beneficial effects of the drug in multiple contexts. Importantly, additional research in this area should also help to characterize the mechanism of action of the drug, including whether the cytotoxic effects and survival benefit seen in this study coincide with a demonstrable reduction in the cancer stem cell population. RNA sequencing in untreated and treated cells *in vitro* or in tumor-bearing animals can provide greater insight into the molecular pathways activated in the presence and absence of drug, while flow cytometry or immunohistochemistry using antibodies specific for cancer stem cells can help determine the effect of a drug on that specific population. Currently, no therapeutic agent has been approved in the treatment of cancer that has been shown to target cancer stem cells specifically, so additional research into this mechanism of action could be extremely valuable.

Figure 4.1

Molecular Structures of parthenolide (PTL) and LC-1.

Figure 4.1

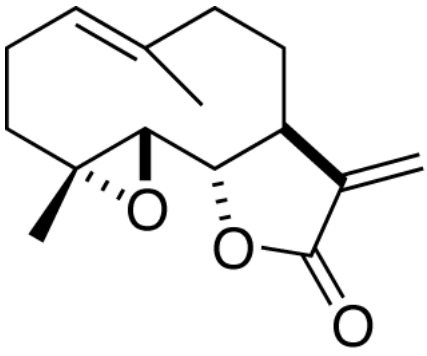

PTL

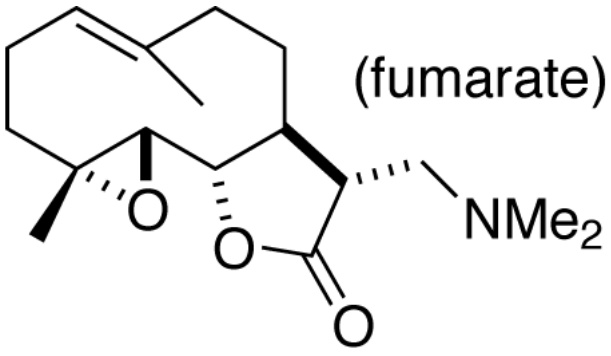

LC-1

Table 4.1

Cytotoxicity of parthenolide and LC-1 against glioma cell lines.

Table 4.1

Cytotoxicity of parthenolide and LC-1 against glioma cell lines

Compound	IC_{50} Values for Glioma Cell Lines[a]		
	U-87 MG	GBM6	GL261-GFP-Luc
PTL	8.8 ± 2.1[b]	3.4 ± 1.1	7.6 ± 2.2
LC-1	8.8 ± 1.9	3.5 ± 1.1	6.9 ± 1.7

[a]Mean IC_{50} values are in μM ± S.D (n ≥ 3 replicates). [b]Obtained previously (B. Wen et al., 2013).

Table 4.2

Pharmacokinetic (PK) data for LC-1 in non-tumor-bearing mice.

Table 4.2

Pharmacokinetic (PK) data for LC-1.[a]

	1 Hour[b]		4 Hours	
	LC-1	Elimination Product (PTL)	LC-1	Elimination Product (PTL)
Plasma	2965 ± 899	2142 ± 885	115 ± 2[c]	211 ± 28
Perfused Brain	6251 ± 1774	2402 ± 387	342 ± 208	113 ± 73
Brain-to-Plasma Ratio	2.1	1.1	3.0	0.5

[a]Values for plasma (ng/mL) and perfused brain (ng/g) are shown as mean concentration ± S.D. These experiments were run in triplicate unless otherwise noted. [b]n = 2. [c]The measured LC-1 concentration for one of the 4 hour plasma samples was below the lower limit of quantification (LLOQ) of 0.5 ng/mL (n = 2).

Figure 4.2

Dose-response cytotoxic profiles with PTL and LC-1 in glioma cell lines. Representative IC_{50} curves for PTL (open circles) and LC-1 (closed triangles) against (A) U-87 MG, (B) GBM6, and (C) GL261-GFP-Luc cells. Viability was determined via Alamar Blue assay. Error bars represent the standard deviation (S.D.) of triplicate data.

Figure 4.2

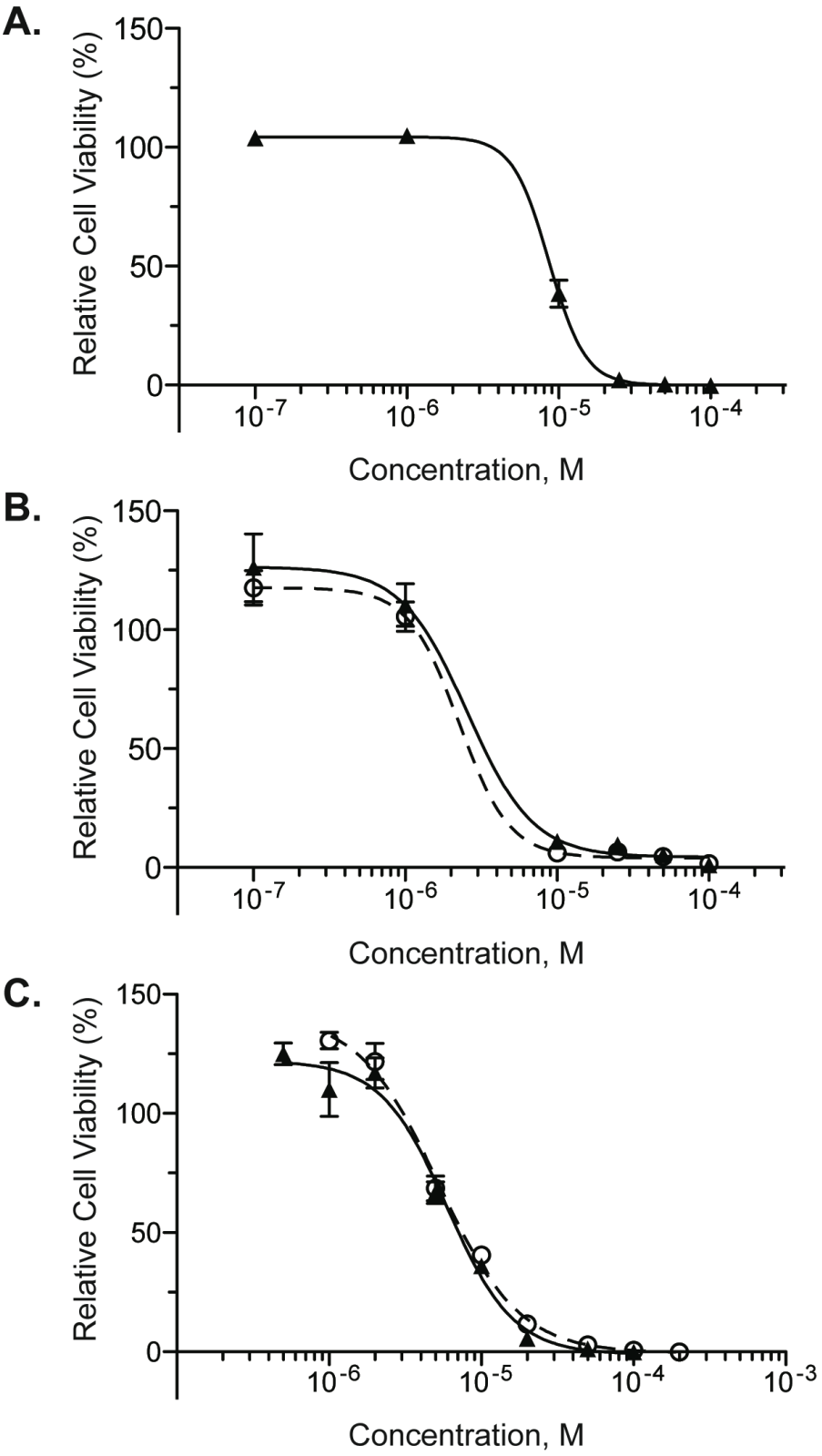
A.
Relative Cell Viability (%)
150
100
50
0
10-7
10-6
10-5
10-4
Concentration, M
B.
Relative Cell Viability (%)
150
100
50
0
10-7
10-6
10-5
10-4
Concentration, M
C.
Relative Cell Viability (%)
150
100
50
0
10-6
10-5
10-4
10-3
Concentration, M

Figure 4.3

CBC data from non-tumor bearing mice treated with LC-1 mouse. These data include counts of (A) white blood cells (WBCs), (B) red blood cells (RBCs), (C) hemoglobin, and (D) platelets. Vehicle = 0.3 M HP-β-CD. Phlebotomy control mice were untreated. Data are shown as the mean count ± SEM. For these experiments, n = 3 except the vehicle and phlebotomy control groups on day 0 (n = 2). No statistical significance was observed among the groups in any of the conditions (one-way repeated measures ANOVA; 95% confidence level).

Figure 4.3

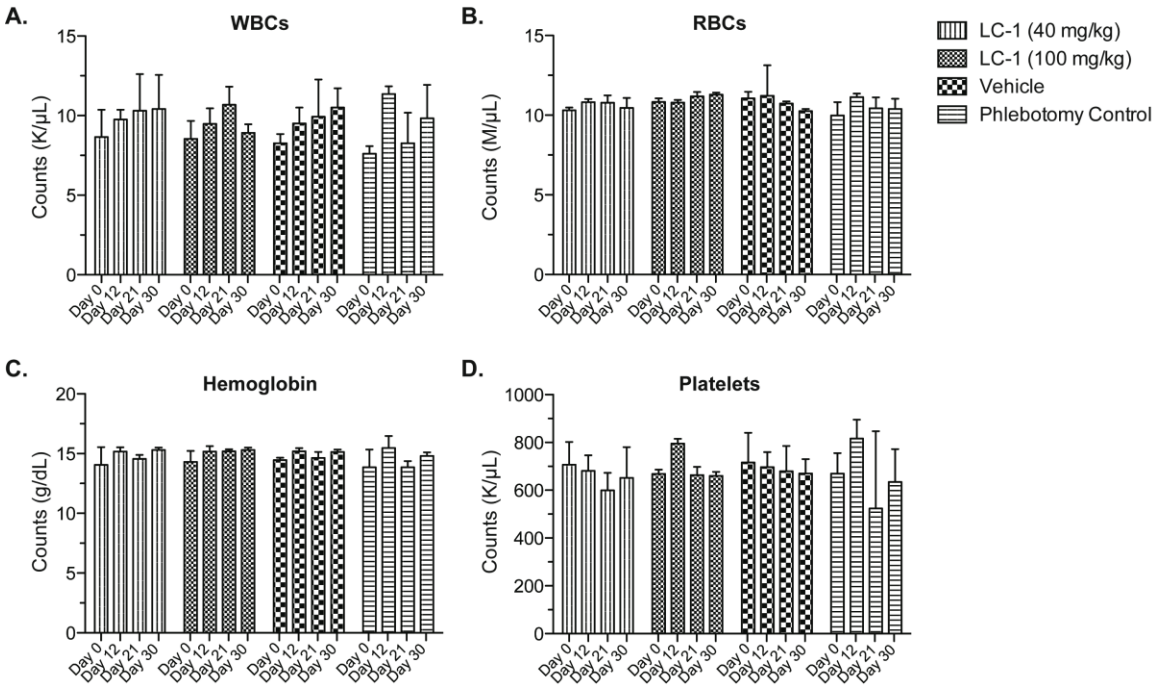
A.
WBCs
Counts (K/µL)
B.
RBCs
Counts (M/µL)
C.
Hemoglobin
Counts (g/dL)
D.
Platelets
Counts (K/µL)
Day 0
Day 12
Day 21
Day 30
LC-1 (40 mg/kg)
LC-1 (100 mg/kg)
Vehicle
Phlebotomy Control

Figure 4.4

In vivo survival data. (A) *In vivo* bioluminescent imaging of GL261-GFP-Luc glioma-bearing mice treated with either LC-1 (100 mg/kg; n = 10) or vehicle (0.3 M 2-hydroxypropyl-β-cyclodextrin; n = 6). Data points are shown as mean log-normalized bioluminescence values ± SEM. (B) Kaplan-Meier survival curves for the tumor-bearing mice treated with LC-1 or vehicle (p = 0.01).

Figure 4.4

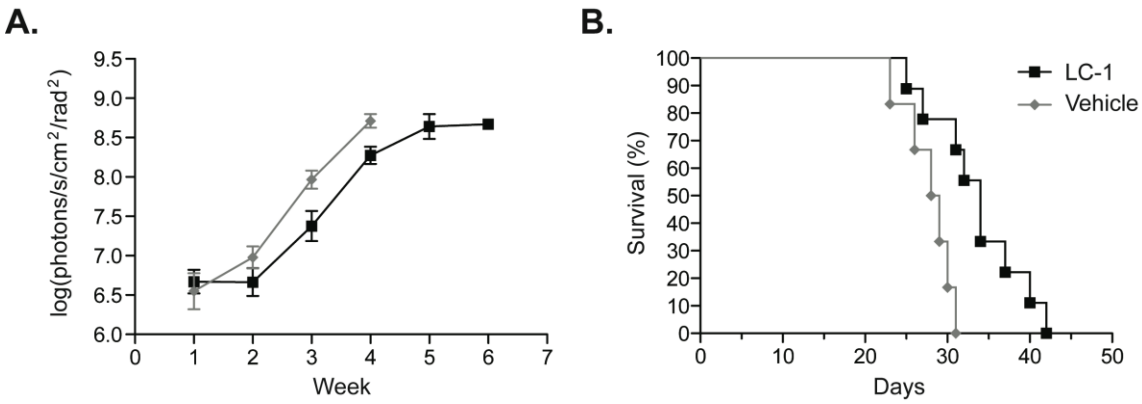
A.
log(photons/s/cm^2/rad^2)
9.5
9.0
8.5
8.0
7.5
7.0
6.5
6.0
0
1
2
3
4
5
6
7
Week
B.
Survival (%)
100
90
80
70
60
50
40
30
20
10
0
0
10
20
30
40
50
Days
LC-1
Vehicle

CHAPTER 5

Recapitulation and Future Directions

5.1 Molecular mechanisms underlying the failures of targeted agents in the treatment of malignant glioma

Glioblastoma Multiforme is a deadly disease. During two hundred years of medical advances and scientific breakthroughs, the best treatments for GBM provide only five months' survival benefit. At this time, the standard of care is limited to surgical resection, radiation therapy, and temozolomide, although the use of Avastin (bevacizumab) remains disputed. It was the intent of this thesis to characterize the molecular mechanisms that preclude or limit the efficacy of brain tumor chemotherapeutics. Both internal characteristics of the tumor and external attributes of tested therapeutic agents were assessed to gain a clearer understanding of the treatment paradigm associated with glioblastoma multiforme.

The data provided in previous chapters highlight the following molecular mechanisms that contribute to the challenges in treating GBM: (1) the invasiveness of the disease that increases the area to which treatment must extend, (2) genetic heterogeneity that makes an obstacle for target selection, and (3) insufficient delivery of drugs through the blood-brain barrier that limits the ability of many compounds to reach the tumor. Addressing and mitigating these obstacles to the extent possible during drug development should increase the potential for therapeutic success in patients.

Chapter 2 demonstrated the importance of brain penetrance of targeted agents in the treatment of GBM. The GL261 mouse glioma model was selected for this study because of its ability to accurately recapitulate the invasiveness and heterogeneous pattern of BBB disruption seen in human imaging studies. Brain

penetrance of GDC-0980 and GNE-317 were assessed in wildtype and *Mdr1a/b-/- Bcrp-/-* triple knockout (TKO) mice and showed that GDC-0980, but not GNE-317, demonstrates significant liability to efflux by P-gp and BCRP transporters. This finding was particularly salient in the context of the drugs' similar cytotoxicity profiles. In the GL261 model, GNE-317 accumulated to a much greater extent than GDC-0980 in not only the tumor core, but also in the tumor rim and normal brain where invasive cells are known to exist.

To test the influence of differential brain penetrance on therapeutic efficacy including molecular targeting capacity and benefits to survival, GL261-tumor bearing animals were treated with either drug before measuring for demonstrable effects. Unlike GDC-0980, GNE-317 was able to successfully decrease the downstream signaling of PI3K and mTOR. Unexpectedly, these data did not translate in survival studies and neither drug was able to delay tumor growth or prolong the lives of GL261 tumor-bearing mice. This effect highlights the challenges presented by the tumor's genetic heterogeneity and the consequences of inadequate target selection. Brain tumor therapeutics must therefore be brain penetrant, exhibit little liability for efflux, and be well matched to each tumor's genetic signature.

Following up on the work from Chapter 2, Chapter 3 assessed the impact of anti-angiogenic therapy (AAT) on delivery and efficacy of concurrently administered targeted agents in the treatment of malignant glioma. In the GBM10 and GBM59 orthotopic xenograft models utilized in this study, GDC-0980 and GNE-317 again demonstrated similar efficacy profiles both *in vitro* and in GBM

flank tumors. Because the blood-brain barrier did not present an obstacle in these conditions, such experiments established a baseline for subsequent drug studies in the brain. Following several doses of bevacizumab to normalize the leaky vasculature normally present within tumors, the distribution of GDC-0980 and GNE-317 was assessed. Bevacizumab was shown to decrease the distribution of GDC-0980, although not significantly; in contrast, bevacizumab did not modify the accumulation of GNE-317. These data suggest that AAT-induced BBB normalization limits the delivery of targeted agents that are subject to active efflux, but not targeted agents that are already brain penetrant.

The impact of AAT on survival benefits to concurrently administered targeted therapies was also investigated. Bevacizumab alone provided a survival benefit in all cases, but the survival benefit was only found to be significantly enhanced during co-treatment with a brain penetrant drug like GNE-317. The benefits to survival in intracranial tumor models were unanticipated in the context of earlier experiments demonstrating limited efficacy in *in vitro* and flank tumor experiments. This paradoxical effect can be explained by the changes in molecular presentation of tumor cells cultivated in different environments that may give rise to differences in susceptibility to targeted agents. Such effects create additional complications to creating accurate brain tumor models.

Chapter 4 further explored the importance of appropriate target selection in GBM using parthenolide and its derivative, LC-1. Both analogues are known to target cancer stem cells that are thought to give rise to tumors, although LC-1 is considered a more bioavailable form the parthenolide parent drug. Effectively

killing cancer stem cells is an important goal in brain tumor research because this cell population is considered very difficult to target; CSCs are highly resistant to drug treatment because of their slow cell cycle kinetics, low levels of reactive oxygen species, improved DNA repair capacity, and high expression levels of anti-apoptotic genes and efflux transporters. *In vitro* studies of parthenolide and LC-1 in several glioma cell lines demonstrated that both drugs exhibited similar cytotoxicity profiles and were able to induce total cell death at higher concentrations, unlike in experiments from Chapters 2 and 3 with GDC-0980 and GNE-317, which could not completely kill the glioma cell lines in which they were tested. LC-1 was also shown to be brain penetrant and non-toxic after prolonged exposure. Importantly, the drug produced a demonstrable delay in tumor growth and significant benefits to survival. For these reasons, glioma stem cells remain a compelling therapeutic target for future clinical therapies.

5.2 Strategies to improve drug delivery of targeted agents

The blood-brain barrier presents a significant obstacle to the delivery of drugs to brain tumors like glioblastoma multiforme. Because many chemotherapeutics are liable to efflux by P-gp and BCRP at the BBB, there have been many attempts to manipulate transporters to reduce efflux activity. As Chapter 2 describes, targeted agents can be modified to limit their liabilities for efflux, but this process can be expensive and time-consuming. An alternate strategy for improving delivery of a drug without chemical modification may be through the concurrent administration of efflux pump inhibitors. Efflux pump

inhibitors have been applied to cancer therapies as early as 1981 (Krishna & Mayer, 2000). In cancers outside the brain, such drugs enhanced parenchymal penetrance of targeted therapies, but these effects did not translate to a clinical benefit (Robey et al., 2010). Indeed, they usually produced toxicity in patients because of the changes in systemic exposure of co-administered therapeutics (Krishna & Mayer, 2000). More recently developed inhibitors have been reported to be better tolerated and less disruptive to other co-administered drugs, but their successes both pre-clinically and clinically remain limited (Bates, Amiri-Kordestani, & Giaccone, 2012; Robey et al., 2010). Although several efflux pump inhibitors have been approved by the Food and Drug Administration (FDA), no compound has improved drug delivery to the brain; research in this area therefore remains ongoing.

Rather than modulate the biochemical component of the BBB, additional strategies have sought to address the physical components of the BBB. Ironically, both BBB restoration and BBB disruption methodologies have been tested to improve drug delivery to the brain. The first type of therapy, BBB restoration, occurs through the administration of a VEGF inhibitor like bevacizumab (Avastin). As discussed in Chapter 3, bevacizumab is known to repair the disrupted BBB seen in various pathologies; although postulated to increase drug delivery, bevacizumab can actually decrease drug delivery by reestablishing the function of efflux transporters. This effect may, therefore, be deleterious in the treatment of GBM if a co-administered therapeutic is susceptible to efflux by such transporters.

The second therapeutic methodology, termed “blood-brain barrier disruption (BBBD) therapy” uses osmotic, mechanical or pharmacological manipulation to transiently increase permeability at the tight junctions. Osmotic BBBD therapy uses hypertonic solutions capable of shrinking endothelial cells and physically interrupt tight junction complexes that create gaps for paracellular diffusion of molecules (Rapoport, 2000). In contrast, mechanical disruption occurs through the application of focused ultrasound that, when delivered transcranially, results in the temporary opening of tight junctions (H. Liu et al., 2010). Pharmacological agents including bradykinin and bradykinin-like compounds (histamines and leukotrienes) work via a third mechanism: the activation of the G-protein coupled receptor, bradykinin receptor B_2, induces second messenger systems that transiently increase cytosolic calcium that opens tight junctions (Kemper, Boogerd, Thuis, Beijnen, & van Tellingen, 2004). Despite the suggested mechanisms of action, these techniques vary in their efficacy toward BBB disruption and enhanced delivery of concurrently administered therapeutics. Further research is therefore needed in BBBD before such a strategy becomes a standard of care for GBM.

Because of the challenges associated with systemically administered therapies, local strategies and carrier methods have become additional areas of interest in the treatment of brain tumors. Convention-enhanced delivery (CED) is one such technique in which a pump provides a prolonged slow infusion of drug directly into brain parenchyma (Groothuis et al., 1999). Despite direct delivery into the brain, the diffusion of drug through the tissue has typically been limited, often

sparing regions of the brain distant from the infusion source where invasive glioma cells may be present (Fiandaca, Forsayeth, Dickinson, & Bankiewicz, 2008). From the carrier perspective, both nanoparticles and peptide linkers can help facilitate the delivery of drugs (Blasi, Giovagnoli, Schoubben, Ricci, & Rossi, 2007; Hervé, Ghinea, & Scherrmann, 2008) to the brain. Investigation into these approaches continues as the associated technologies and reagents improves over time.

5.3 Alternative treatments with therapeutic potential for malignant glioma

An understanding of the molecular mechanisms behind the failures of targeted agents in the treatment of glioblastoma multiforme should help inform future drug development. The invasive nature and genetically heterogeneous qualities of glioma necessitate that small molecule therapeutics be efficacious at targeting and killing all tumor cells, including glioma stem cells. To ensure adequate drug delivery, targeted agents must be designed so as not to be substrates for efflux pumps. Finally, AAT may be a promising therapeutic strategy if it is combined with other targeted agents that are not susceptible to efflux from an intact blood-brain barrier.

Given the overwhelming failures in chemotherapy-based clinical trials and the challenges faced in improving drug design in glioma, an alternative treatment strategy may be beneficial. To circumvent many of the limitations associated with drug-based treatment strategies, scientists and clinicians are turning to immunotherapies. Brain tumors possess a variety of mutated proteins that should give rise to immunogenic tumor-specific neoantigens (McLendon et al., 2008b).

Despite the presence of such neoantigens, the immune system rarely attacks CNS cancers. Glioma patients exhibit a competent immune system, but the CNS maintains a relative and specialized form of immune privilege that prevents immune responses in the brain (Muldoon et al., 2012). Indeed, immunosuppressed patients who receive organ transplants from individuals with a non-metastatic primary brain tumor frequently develop cancer of brain origin in the donated organ. This observation suggests that glioma patients maintain an active immune system peripherally that is able to disable or prevent tumor growth of circulating glioma cells (Collignon, Holland, & Feng, 2004). Efforts to activate the immune system within the CNS occur in the forms of vaccine-based platforms and NK- or T-cell based immunocellular strategies (Bielamowicz, Khawja, & Ahmed, 2013; C. M. Jackson, Lim, & Drake, 2014; Perez-Diez & Marincola, 2002). Many such immunotherapies have entered clinical trials (Bielamowicz et al., 2013; C. M. Jackson et al., 2014; Xu, Chow, Lim, & Li, 2014), yet patient responses have been mixed (Gomez & Kruse, 2006). The optimization of immunotherapies in GBM therefore remains a significant goal within the field of neuro-oncology.

BIBLIOGRAPHY

Abbott, N. J. (2005). Dynamics of CNS barriers: Evolution, differentiation, and modulation. *Cellular and Molecular Neurobiology, 25*(1), 5-23.

Abbott, N. J., Rönnbäck, L., & Hansson, E. (2006). Astrocyte–endothelial interactions at the blood–brain barrier. *Nature Reviews Neuroscience, 7*(1), 41-53.

Adams, P. D., Jasper, H., & Rudolph, K. L. (2015). Aging-induced stem cell mutations as drivers for disease and cancer. *Cell Stem Cell, 16*(6), 601-612.

Agarwal, S., Hartz, A. M., Elmquist, W. F., & Bauer, B. (2011a). Breast cancer resistance protein and P-glycoprotein in brain cancer: Two gatekeepers team up. *Current Pharmaceutical Design, 17*(26), 2793-2802. doi:BSP/CPD/E-Pub/000567 [pii]

Agarwal, S., Hartz, A. M., Elmquist, W. F., & Bauer, B. (2011b). Breast cancer resistance protein and P-glycoprotein in brain cancer: Two gatekeepers team up. *Current Pharmaceutical Design, 17*(26), 2793-2802. doi:BSP/CPD/E-Pub/000567 [pii]

Agarwal, S., Mittapalli, R. K., Zellmer, D. M., Gallardo, J. L., Donelson, R., Seiler, C., . . . Ohlfest, J. R. (2012). Active efflux of dasatinib from the brain limits efficacy against murine glioblastoma: Broad implications for the clinical use of molecularly targeted agents. *Molecular Cancer Therapeutics, 11*(10), 2183-2192. doi:10.1158/1535-7163.MCT-12-0552 [doi]

Agarwal, S., Sane, R., Oberoi, R., Ohlfest, J. R., & Elmquist, W. F. (2011). Delivery of molecularly targeted therapy to malignant glioma, a disease of

the whole brain. *Expert Reviews in Molecular Medicine, 13*, e17. doi:10.1017/S1462399411001888 [doi]

Alvarez, J. I., Dodelet-Devillers, A., Kebir, H., Ifergan, I., Fabre, P. J., Terouz, S., . . . Prat, A. (2011). The hedgehog pathway promotes blood-brain barrier integrity and CNS immune quiescence. *Science (New York, N.Y.), 334*(6063), 1727-1731. doi:10.1126/science.1206936 [doi]

An, Y., Guo, W., Li, L., Xu, C., Yang, D., Wang, S., . . . Zhai, J. (2015). Micheliolide derivative DMAMCL inhibits glioma cell growth in vitro and in vivo.

Anderson, K. N., & Bejcek, B. E. (2008). Parthenolide induces apoptosis in glioblastomas without affecting NF-. KAPPA. B. *Journal of Pharmacological Sciences, 106*(2), 318-320.

Antunes, L., Angioi-Duprez, K. S., Bracard, S. R., Klein-Monhoven, N. A., Le Faou, A. E., Duprez, A. M., & Plenat, F. M. (2000). Analysis of tissue chimerism in nude mouse brain and abdominal xenograft models of human glioblastoma multiforme: What does it tell us about the models and about glioblastoma biology and therapy? *The Journal of Histochemistry and Cytochemistry : Official Journal of the Histochemistry Society, 48*(6), 847-858.

Bao, S., Wu, Q., McLendon, R. E., Hao, Y., Shi, Q., Hjelmeland, A. B., . . . Rich, J. N. (2006). Glioma stem cells promote radioresistance by preferential activation of the DNA damage response. *Nature, 444*(7120), 756-760.

Batchelor, T. T., Sorensen, A. G., di Tomaso, E., Zhang, W., Duda, D. G., Cohen, K. S., . . . Zhu, M. (2007). AZD2171, a pan-VEGF receptor tyrosine kinase inhibitor, normalizes tumor vasculature and alleviates edema in glioblastoma patients. *Cancer Cell, 11*(1), 83-95.

Bates, S. E., Amiri-Kordestani, L., & Giaccone, G. (2012). Drug development: Portals of discovery. *Clinical Cancer Research : An Official Journal of the American Association for Cancer Research, 18*(1), 23-32. doi:10.1158/1078-0432.CCR-11-1001 [doi]

Becker, C. M., Oberoi, R. K., McFarren, S. J., Muldoon, D. M., Pafundi, D. H., Pokorny, J. L., . . . Elmquist, W. F. (2015). Decreased affinity for efflux transporters increases brain penetrance and molecular targeting of a PI3K/mTOR inhibitor in a mouse model of glioblastoma. *Neuro-Oncology, 17*(9), 1210-1219. doi:10.1093/neuonc/nov081 [doi]

Begley, D. J., & Brightman, M. W. (2003). Structural and functional aspects of the blood-brain barrier. *Peptide transport and delivery into the central nervous system* (pp. 39-78) Springer.

Bell, C., Dowson, N., Puttick, S., Gal, Y., Thomas, P., Fay, M., . . . Rose, S. (2015). Increasing feasibility and utility of 18 F-FDOPA PET for the management of glioma. *Nuclear Medicine and Biology, 42*(10), 788-795.

Berens, M. E., & Giese, A. (1999). "... Those left behind." biology and oncology of invasive glioma cells. *Neoplasia, 1*(3), 208-219.

Bergmann, O., Spalding, K. L., & Frisen, J. (2015). Adult neurogenesis in humans. *Cold Spring Harbor Perspectives in Biology, 7*(7), a018994. doi:10.1101/cshperspect.a018994 [doi]

Bielamowicz, K., Khawja, S., & Ahmed, N. (2013). Adoptive cell therapies for glioblastoma. *Frontiers in Oncology, 3*

Blasi, P., Giovagnoli, S., Schoubben, A., Ricci, M., & Rossi, C. (2007). Solid lipid nanoparticles for targeted brain drug delivery. *Advanced Drug Delivery Reviews, 59*(6), 454-477.

Bogomolny, D. L., Petrovich, N. M., Hou, B. L., Peck, K. K., Kim, M. J., & Holodny, A. I. (2004). Functional MRI in the brain tumor patient. *Topics in Magnetic Resonance Imaging, 15*(5), 325-335.

Bonavia, R., Inda, M. M., Cavenee, W. K., & Furnari, F. B. (2011). Heterogeneity maintenance in glioblastoma: A social network. *Cancer Research, 71*(12), 4055-4060. doi:10.1158/0008-5472.CAN-11-0153 [doi]

Brandner, S. (2013). Mouse models of glioma pathogenesis: History and state of the art. *Emerging concepts in neuro-oncology* (pp. 87-107) Springer.

Cacheux, W., Boisserie, T., Staudacher, L., Vignaux, O., Dousset, B., Soubrane, O., . . . Goldwasser, F. (2008). Reversible tumor growth acceleration following bevacizumab interruption in metastatic colorectal cancer patients scheduled for surgery. *Annals of Oncology : Official Journal of the European Society for Medical Oncology / ESMO, 19*(9), 1659-1661. doi:10.1093/annonc/mdn540 [doi]

Candolfi, M., Curtin, J. F., Nichols, W. S., Muhammad, A. G., King, G. D., Pluhar, G. E., . . . Moore, P. F. (2007). Intracranial glioblastoma models in preclinical neuro-oncology: Neuropathological characterization and tumor progression. *Journal of Neuro-Oncology, 85*(2), 133-148.

Carlson, B. L., Grogan, P. T., Mladek, A. C., Schroeder, M. A., Kitange, G. J., Decker, P. A., . . . James, C. D. (2009). Radiosensitizing effects of temozolomide observed in vivo only in a subset of O6-methylguanine-DNA methyltransferase methylated glioblastoma multiforme xenografts. *International Journal of Radiation Oncology* Biology* Physics, 75*(1), 212-219.

Carlson, B. L., Pokorny, J. L., Schroeder, M. A., & Sarkaria, J. N. (2011). Establishment, maintenance, and in vitro and in vivo applications of primary human glioblastoma multiforme (GBM) xenograft models for translational

biology studies and drug discovery. *Current Protocols in Pharmacology,* , 14.16. 1-14.16. 23.

Challa, R., Ahuja, A., Ali, J., & Khar, R. (2005). Cyclodextrins in drug delivery: An updated review. *Aaps Pharmscitech, 6*(2), E329-E357.

Chang, S. M., Parney, I. F., Huang, W., Anderson, F. A., Asher, A. L., Bernstein, M., . . . Laws, E. R. (2005). Patterns of care for adults with newly diagnosed malignant glioma. *Jama, 293*(5), 557-564.

Chen, J., McKay, R. M., & Parada, L. F. (2012). Malignant glioma: Lessons from genomics, mouse models, and stem cells. *Cell, 149*(1), 36-47.

Chen, L., Zhang, Y., Yang, J., Hagan, J. P., & Li, M. (2013). Vertebrate animal models of glioma: Understanding the mechanisms and developing new therapies. *Biochimica Et Biophysica Acta (BBA)-Reviews on Cancer, 1836*(1), 158-165.

Claes, A., Wesseling, P., Jeuken, J., Maass, C., Heerschap, A., & Leenders, W. P. (2008). Antiangiogenic compounds interfere with chemotherapy of brain tumors due to vessel normalization. *Molecular Cancer Therapeutics, 7*(1), 71-78. doi:10.1158/1535-7163.MCT-07-0552 [doi]

Clark, D. E. (2003). In silico prediction of blood–brain barrier permeation. *Drug Discovery Today, 8*(20), 927-933.

Clark, M. J., Homer, N., O'connor, B. D., Chen, Z., Eskin, A., Lee, H., . . . Nelson, S. F. (2010). U87MG decoded: The genomic sequence of a cytogenetically aberrant human cancer cell line. *PLoS Genet, 6*(1), e1000832.

Collignon, F. P., Holland, E. C., & Feng, S. (2004). Organ donors with malignant gliomas: An update. *American Journal of Transplantation, 4*(1), 15-21.

Dai, C., & Holland, E. C. (2001). Glioma models. *Biochimica Et Biophysica Acta (BBA)-Reviews on Cancer, 1551*(1), M19-M27.

Dai, H., Marbach, P., Lemaire, M., Hayes, M., & Elmquist, W. F. (2003). Distribution of STI-571 to the brain is limited by P-glycoprotein-mediated efflux. *The Journal of Pharmacology and Experimental Therapeutics, 304*(3), 1085-1092. doi:10.1124/jpet.102.045260 [doi]

Das, S., Lin, H., Ho, P. C., & Ng, K. (2008). The impact of aqueous solubility and dose on the pharmacokinetic profiles of resveratrol. *Pharmaceutical Research, 25*(11), 2593-2600.

de Groot, J. F., & Mandel, J. J. (2014). Update on anti-angiogenic treatment for malignant gliomas. *Current Oncology Reports, 16*(4), 1-7.

Deeken, J. F., & Loscher, W. (2007). The blood-brain barrier and cancer: Transporters, treatment, and trojan horses. *Clinical Cancer Research : An Official Journal of the American Association for Cancer Research, 13*(6), 1663-1674. doi:13/6/1663 [pii]

Diehn, M., Cho, R. W., Lobo, N. A., Kalisky, T., Dorie, M. J., Kulp, A. N., . . . Wong, M. (2009). Association of reactive oxygen species levels and radioresistance in cancer stem cells. *Nature, 458*(7239), 780-783.

Eckley, M., & Wargo, K. A. (2010). A review of glioblastoma multiforme. *US Pharm, 35*(5), 3-10.

Edfeldt, F. N., Folmer, R. H., & Breeze, A. L. (2011). Fragment screening to predict druggability (ligandability) and lead discovery success. *Drug Discovery Today, 16*(7), 284-287.

Ehrlich, P. (1904). Über die beziehung chemischer konstitution. *Verteilung, Und Pharmakologischer Wirkung,*

Ellingson, B. M., Cloughesy, T. F., Lai, A., Nghiemphu, P. L., Lalezari, S., Zaw, T., . . . Pope, W. B. (2012). Quantification of edema reduction using differential quantitative T2 (DQT2) relaxometry mapping in recurrent glioblastoma treated with bevacizumab. *Journal of Neuro-Oncology, 106*(1), 111-119.

Ellis, L. M., & Reardon, D. A. (2009). Cancer: The nuances of therapy. *Nature, 458*(7236), 290-292.

Fan, T., Yeh, J., Leung, K. W., Yue, P. Y., & Wong, R. N. (2006). Angiogenesis: From plants to blood vessels. *Trends in Pharmacological Sciences, 27*(6), 297-309.

Fazeny-Dörner, B., Wenzel, C., Veitl, M., Piribauer, M., Rössler, K., Dieckmann, K., . . . Marosi, C. (2003). Survival and prognostic factors of patients with unresectable glioblastoma multiforme. *Anti-Cancer Drugs, 14*(4), 305-312.

Ferrara, N., Hillan, K. J., & Novotny, W. (2005). Bevacizumab (avastin), a humanized anti-VEGF monoclonal antibody for cancer therapy. *Biochemical and Biophysical Research Communications, 333*(2), 328-335.

Fiandaca, M. S., Forsayeth, J. R., Dickinson, P. J., & Bankiewicz, K. S. (2008). Image-guided convection-enhanced delivery platform in the treatment of neurological diseases. *Neurotherapeutics, 5*(1), 123-127.

Fink, J. R., Muzi, M., Peck, M., & Krohn, K. A. (2015). Multimodality brain tumor imaging: MR imaging, PET, and PET/MR imaging. *Journal of Nuclear Medicine : Official Publication, Society of Nuclear Medicine, 56*(10), 1554-1561. doi:10.2967/jnumed.113.131516 [doi]

Fiveash, J. B., & Spencer, S. A. (2003). Role of radiation therapy and radiosurgery in glioblastoma multiforme. *Cancer Journal (Sudbury, Mass.), 9*(3), 222-229.

Fonrose, X., Ausseil, F., Soleilhac, E., Masson, V., David, B., Pouny, I., . . . Lafanechere, L. (2007). Parthenolide inhibits tubulin carboxypeptidase activity. *Cancer Research, 67*(7), 3371-3378. doi:67/7/3371 [pii]

Friedman, H. S., Kerby, T., & Calvert, H. (2000). Temozolomide and treatment of malignant glioma. *Clinical Cancer Research : An Official Journal of the American Association for Cancer Research, 6*(7), 2585-2597.

Gabathuler, R. (2010). Approaches to transport therapeutic drugs across the blood-brain barrier to treat brain diseases. *Neurobiology of Disease, 37*(1), 48-57. doi:10.1016/j.nbd.2009.07.028 [doi]

Ghantous, A., Sinjab, A., Herceg, Z., & Darwiche, N. (2013). Parthenolide: From plant shoots to cancer roots. *Drug Discovery Today, 18*(17), 894-905.

Giese, A., Bjerkvig, R., Berens, M. E., & Westphal, M. (2003). Cost of migration: Invasion of malignant gliomas and implications for treatment. *Journal of Clinical Oncology : Official Journal of the American Society of Clinical Oncology, 21*(8), 1624-1636. doi:10.1200/JCO.2003.05.063 [doi]

Gil-Gil, M. J., Mesia, C., Rey, M., & Bruna, J. (2013). Bevacizumab for the treatment of glioblastoma. *Clinical Medicine Insights.Oncology, 7*, 123.

Goldman, S. A., & Sim, F. (2005). Neural progenitor cells of the adult brain. Paper presented at the *Novartis found Symp, , 265* 66-80.

Goldmann, E. (1913). Vitalfärbung am zentralnervensystem: Beitrag zur physiopathologie des plexus choriodeus und der hirnhäute. abh. preuss. *Akad.Wiss., Phys.-Math.Kl,* (1)

Goldwirt, L., Beccaria, K., Carpentier, A., Idbaih, A., Schmitt, C., Levasseur, C., . . . Fernandez, C. (2015). Preclinical impact of bevacizumab on brain and tumor distribution of irinotecan and temozolomide. *Journal of Neuro-Oncology, 122*(2), 273-281.

Gomez, G. G., & Kruse, C. A. (2006). Mechanisms of malignant glioma immune resistance and sources of immunosuppression. *Gene Therapy & Molecular Biology, 10*(A), 133-146.

Gonçalves, C. S., Xavier-Magalhães, A., Costa, B. M., Pojo, M., & Lourenço, T. (2013). *Mechanisms of aggressiveness in glioblastoma: Prognostic and potential therapeutic insights* INTECH Open Access Publisher.

Gould, S., & Scott, R. C. (2005). 2-hydroxypropyl-β-cyclodextrin (HP-β-CD): A toxicology review. *Food and Chemical Toxicology, 43*(10), 1451-1459.

Greaves, M., & Maley, C. C. (2012). Clonal evolution in cancer. *Nature, 481*(7381), 306-313.

Greenberg, J. I., Shields, D. J., Barillas, S. G., Acevedo, L. M., Murphy, E., Huang, J., . . . Angle, N. (2008). A role for VEGF as a negative regulator of pericyte function and vessel maturation. *Nature, 456*(7223), 809-813.

Groothuis, D. R., Ward, S., Itskovich, A. C., Dobrescu, C., Allen, C. V., Dills, C., & Levy, R. M. (1999). Comparison of 14C-sucrose delivery to the brain by

intravenous, intraventricular, and convection-enhanced intracerebral infusion. *Journal of Neurosurgery, 90*(2), 321-331.

Guzman, M. L., Rossi, R. M., Karnischky, L., Li, X., Peterson, D. R., Howard, D. S., & Jordan, C. T. (2005). The sesquiterpene lactone parthenolide induces apoptosis of human acute myelogenous leukemia stem and progenitor cells. *Blood, 105*(11), 4163-4169. doi:2004-10-4135 [pii]

Guzman, M. L., Rossi, R. M., Neelakantan, S., Li, X., Corbett, C. A., Hassane, D. C., . . . Jordan, C. T. (2007). An orally bioavailable parthenolide analog selectively eradicates acute myelogenous leukemia stem and progenitor cells. *Blood, 110*(13), 4427-4435. doi:blood-2007-05-090621 [pii]

Haar, C. P., Hebbar, P., Wallace, G. C.,4th, Das, A., Vandergrift, W. A.,3rd, Smith, J. A., . . . Banik, N. L. (2012). Drug resistance in glioblastoma: A mini review. *Neurochemical Research, 37*(6), 1192-1200. doi:10.1007/s11064-011-0701-1 [doi]

Hanahan, D., & Weinberg, R. A. (2000). The hallmarks of cancer. *Cell, 100*(1), 57-70.

Hanahan, D., & Weinberg, R. A. (2011). Hallmarks of cancer: The next generation. *Cell, 144*(5), 646-674.

Hassane, D. C., Sen, S., Minhajuddin, M., Rossi, R. M., Corbett, C. A., Balys, M., . . . Jordan, C. T. (2010). Chemical genomic screening reveals synergism

between parthenolide and inhibitors of the PI-3 kinase and mTOR pathways. *Blood, 116*(26), 5983-5990. doi:10.1182/blood-2010-04-278044 [doi]

Hedden, J. (2014). Glioblastoma multiforme: Pipeline. *Datamonitor,*

Heffron, T. P., Salphati, L., Alicke, B., Cheong, J., Dotson, J., Edgar, K., . . . Zhang, X. (2012). The design and identification of brain penetrant inhibitors of phosphoinositide 3-kinase alpha. *Journal of Medicinal Chemistry, 55*(18), 8007-8020. doi:10.1021/jm300867c [doi]

Hegi, M. E., Diserens, A., Gorlia, T., Hamou, M., de Tribolet, N., Weller, M., . . . Mariani, L. (2005). MGMT gene silencing and benefit from temozolomide in glioblastoma. *New England Journal of Medicine, 352*(10), 997-1003.

Herper, M. (2013, 8/11/2013). **The cost of creating A new drug now $5 billion, pushing big pharma To Change**. *Forbes,*

Hervé, F., Ghinea, N., & Scherrmann, J. (2008). CNS delivery via adsorptive transcytosis. *The AAPS Journal, 10*(3), 455-472.

Hexum, J. K., Tello-Aburto, R., Struntz, N. B., Harned, A. M., & Harki, D. A. (2012). Bicyclic cyclohexenones as inhibitors of NF-κB signaling. *ACS Medicinal Chemistry Letters, 3*(6), 459-464.

Hoelzinger, D. B., Mariani, L., Weis, J., Woyke, T., Berens, T. J., McDonough, W., . . . Berens, M. E. (2005). Gene expression profile of glioblastoma

multiforme invasive phenotype points to new therapeutic targets. *Neoplasia, 7*(1), 7-16.

Holland, E. C. (2001). Gliomagenesis: Genetic alterations and mouse models. *Nature Reviews Genetics, 2*(2), 120-129.

Huether, S. E., & McCance, K. L. (2013). *Understanding pathophysiology* Elsevier Health Sciences.

Hulleman, E., & Helin, K. (2005). Molecular mechanisms in gliomagenesis. *Advances in Cancer Research, 94*, 1-27.

Inda, M., Bonavia, R., & Seoane, J. (2014). Glioblastoma multiforme: A look inside its heterogeneous nature. *Cancers, 6*(1), 226-239.

Iwamoto, F. M., Reiner, A. S., Panageas, K. S., Elkin, E. B., & Abrey, L. E. (2008). Patterns of care in elderly glioblastoma patients. *Annals of Neurology, 64*(6), 628-634.

Jackson, C. M., Lim, M., & Drake, C. G. (2014). Immunotherapy for brain cancer: Recent progress and future promise. *Clinical Cancer Research,* , clincanres. 2057.2013.

Jackson, M., Hassiotou, F., & Nowak, A. (2015). Glioblastoma stem-like cells: At the root of tumor recurrence and a therapeutic target. *Carcinogenesis, 36*(2), 177-185. doi:10.1093/carcin/bgu243 [doi]

Jacobs, V. L., Valdes, P. A., Hickey, W. F., & De Leo, J. A. (2011). Current review of in vivo GBM rodent models: Emphasis on the CNS-1 tumour model. *ASN Neuro, 3*(3), e00063. doi:10.1042/AN20110014 [doi]

Johnson, B. E., Mazor, T., Hong, C., Barnes, M., Aihara, K., McLean, C. Y., . . . Costello, J. F. (2014). Mutational analysis reveals the origin and therapy-driven evolution of recurrent glioma. *Science (New York, N.Y.), 343*(6167), 189-193. doi:10.1126/science.1239947 [doi]

Karunanithi, S., Sharma, P., Kumar, A., Khangembam, B. C., Bandopadhyaya, G. P., Kumar, R., . . . Bal, C. (2013). Comparative diagnostic accuracy of contrast-enhanced MRI and 18F-FDOPA PET-CT in recurrent glioma. *European Radiology, 23*(9), 2628-2635.

Kegelman, T. P., Hu, B., Emdad, L., Das, S. K., Sarkar, D., & Fisher, P. B. (2014). In vivo modeling of malignant glioma: The road to effective therapy. *ADVANCES IN CANCER RESEARCH, VOL 121, 121*, 261-330.

Keles, G. E., Anderson, B., & Berger, M. S. (1999). The effect of extent of resection on time to tumor progression and survival in patients with glioblastoma multiforme of the cerebral hemisphere. *Surgical Neurology, 52*(4), 371-379.

Kemper, E. M., Boogerd, W., Thuis, I., Beijnen, J. H., & van Tellingen, O. (2004). Modulation of the blood–brain barrier in oncology: Therapeutic opportunities

for the treatment of brain tumours? *Cancer Treatment Reviews, 30*(5), 415-423.

Kreso, A., & Dick, J. E. (2014). Evolution of the cancer stem cell model. *Cell Stem Cell, 14*(3), 275-291.

Krishna, R., & Mayer, L. D. (2000). Multidrug resistance (MDR) in cancer: Mechanisms, reversal using modulators of MDR and the role of MDR modulators in influencing the pharmacokinetics of anticancer drugs. *European Journal of Pharmaceutical Sciences, 11*(4), 265-283.

Kwok, B. H., Koh, B., Ndubuisi, M. I., Elofsson, M., & Crews, C. M. (2001). The anti-inflammatory natural product parthenolide from the medicinal herb feverfew directly binds to and inhibits IκB kinase. *Chemistry & Biology, 8*(8), 759-766.

Le Serve, A. W., & Hellmann, K. (1972). Metastases and the normalization of tumour blood vessels by ICRF 159: A new type of drug action. *British Medical Journal, 1*(5800), 597-601.

Lefranc, F., Brotchi, J., & Kiss, R. (2005). Possible future issues in the treatment of glioblastomas: Special emphasis on cell migration and the resistance of migrating glioblastoma cells to apoptosis. *Journal of Clinical Oncology : Official Journal of the American Society of Clinical Oncology, 23*(10), 2411-2422. doi:23/10/2411 [pii]

Leten, C., Struys, T., Dresselaers, T., & Himmelreich, U. (2014). In vivo and ex vivo assessment of the blood brain barrier integrity in different glioblastoma animal models. *Journal of Neuro-Oncology,* , 1-10.

Levatic, J., Curak, J., Kralj, M., Smuc, T., Osmak, M., & Supek, F. (2013). Accurate models for P-gp drug recognition induced from a cancer cell line cytotoxicity screen. *Journal of Medicinal Chemistry, 56*(14), 5691-5708. doi:10.1021/jm400328s [doi]

Lin, H., & Ho, P. C. (2011). Preclinical pharmacokinetic evaluation of resveratrol trimethyl ether in sprague-dawley rats: The impacts of aqueous solubility, dose escalation, food and repeated dosing on oral bioavailability. *Journal of Pharmaceutical Sciences, 100*(10), 4491-4500.

Lin, N., Yan, W., Gao, K., Wang, Y., Zhang, J., & You, Y. (2014). Prevalence and clinicopathologic characteristics of the molecular subtypes in malignant glioma: A multi-institutional analysis of 941 cases. *PloS One, 9*(4), e94871.

Liu, H., Hua, M., Chen, P., Chu, P., Pan, C., Yang, H., . . . Wei, K. (2010). Blood-brain barrier disruption with focused ultrasound enhances delivery of chemotherapeutic drugs for glioblastoma treatment 1. *Radiology, 255*(2), 415-425.

Liu, G., Yuan, X., Zeng, Z., Tunici, P., Ng, H., Abdulkadir, I. R., . . . Yu, J. S. (2006). Analysis of gene expression and chemoresistance of CD133+ cancer stem cells in glioblastoma. *Molecular Cancer, 5*, 67. doi:1476-4598-5-67 [pii]

Liu, Z., Liu, S., Xie, Z., Pavlovicz, R. E., Wu, J., Chen, P., . . . Chan, K. K. (2009). Modulation of DNA methylation by a sesquiterpene lactone parthenolide. *The Journal of Pharmacology and Experimental Therapeutics, 329*(2), 505-514. doi:10.1124/jpet.108.147934 [doi]

Llaguno, S. A., Chen, Y., McKay, R. M., & Parada, L. F. (2011). Stem cells in brain tumor development. *Cancer Dev, 90*, 15-44.

Lobo, N. A., Shimono, Y., Qian, D., & Clarke, M. F. (2007). The biology of cancer stem cells. *Annu.Rev.Cell Dev.Biol., 23*, 675-699.

Maher, E. A., Furnari, F. B., Bachoo, R. M., Rowitch, D. H., Louis, D. N., Cavenee, W. K., & DePinho, R. A. (2001). Malignant glioma: Genetics and biology of a grave matter. *Genes & Development, 15*(11), 1311-1333. doi:10.1101/gad.891601 [doi]

Mancuso, M. R., Davis, R., Norberg, S. M., O'Brien, S., Sennino, B., Nakahara, T., . . . McDonald, D. M. (2006). Rapid vascular regrowth in tumors after reversal of VEGF inhibition. *The Journal of Clinical Investigation, 116*(10), 2610-2621. doi:10.1172/JCI24612 [doi]

Mariani, L., McDonough, W. S., Hoelzinger, D. B., Beaudry, C., Kaczmarek, E., Coons, S. W., . . . Berens, M. E. (2001). Identification and validation of P311 as a glioblastoma invasion gene using laser capture microdissection. *Cancer Research, 61*(10), 4190-4196.

McLendon, R., Friedman, A., Bigner, D., Van Meir, E. G., Brat, D. J., Mastrogianakis, G. M., . . . Aldape, K. (2008a). Comprehensive genomic characterization defines human glioblastoma genes and core pathways. *Nature, 455*(7216), 1061-1068.

McLendon, R., Friedman, A., Bigner, D., Van Meir, E. G., Brat, D. J., Mastrogianakis, G. M., . . . Aldape, K. (2008b). Comprehensive genomic characterization defines human glioblastoma genes and core pathways. *Nature, 455*(7216), 1061-1068.

Mensch, J., Oyarzabal, J., Mackie, C., & Augustijns, P. (2009). In vivo, in vitro and in silico methods for small molecule transfer across the BBB. *Journal of Pharmaceutical Sciences, 98*(12), 4429-4468.

Molina, E. S., Pillat, M. M., Moura-Neto, V., Lah, T. T., & Ulrich, H. (2014). Glioblastoma stem-like cells: Approaches for isolation and characterization. *Journal of Cancer Stem Cell Research, 2*, e1007.

Molina, J. R., Hayashi, Y., Stephens, C., & Georgescu, M. (2010). Invasive glioblastoma cells acquire stemness and increased akt activation. *Neoplasia, 12*(6), 453-IN5.

Mukherjee, S. (2011). *The emperor of all maladies: A biography of cancer* Simon and Schuster.

Muldoon, L. L., Alvarez, J. I., Begley, D. J., Boado, R. J., del Zoppo, G. J., Doolittle, N. D., . . . Ohlfest, J. R. (2012). Immunologic privilege in the central nervous system and the blood–brain barrier. *Journal of Cerebral Blood Flow & Metabolism, 33*(1), 13-21.

Nagy, R., Sweet, K., & Eng, C. (2004). Highly penetrant hereditary cancer syndromes. *Oncogene, 23*(38), 6445-6470.

Neelakantan, S., Nasim, S., Guzman, M. L., Jordan, C. T., & Crooks, P. A. (2009). Aminoparthenolides as novel anti-leukemic agents: Discovery of the NF-κB inhibitor, DMAPT (LC-1). *Bioorganic & Medicinal Chemistry Letters, 19*(15), 4346-4349.

Newcomb, E. W., & Zagzag, D. (2009). The murine GL261 glioma experimental model to assess novel brain tumor treatments. *CNS cancer* (pp. 227-241) Springer.

Nobusawa, S., Watanabe, T., Kleihues, P., & Ohgaki, H. (2009). IDH1 mutations as molecular signature and predictive factor of secondary glioblastomas. *Clinical Cancer Research : An Official Journal of the American Association for Cancer Research, 15*(19), 6002-6007. doi:10.1158/1078-0432.CCR-09-0715 [doi]

Noell, S., Mack, A. F., Wolburg, H., Wolburg-Buchholz, K., & Fallier-Becker, P. (2011). *The blood-brain barrier in brain tumours* INTECH Open Access Publisher.

Oberoi, R. K., Mittapalli, R. K., Fisher, J., & Elmquist, W. F. (2013). Sunitinib LC–MS/MS assay in mouse plasma and brain tissue: Application in CNS distribution studies. *Chromatographia, 76*(23-24), 1657-1665.

Oberoi, R. K., Mittapalli, R. K., & Elmquist, W. F. (2013). Pharmacokinetic assessment of efflux transport in sunitinib distribution to the brain. *The Journal of Pharmacology and Experimental Therapeutics, 347*(3), 755-764. doi:10.1124/jpet.113.208959 [doi]

Ohgaki, H., & Kleihues, P. (2007). Genetic pathways to primary and secondary glioblastoma. *The American Journal of Pathology, 170*(5), 1445-1453.

Ohgaki, H., & Kleihues, P. (2013). The definition of primary and secondary glioblastoma. *Clinical Cancer Research : An Official Journal of the American Association for Cancer Research, 19*(4), 764-772. doi:10.1158/1078-0432.CCR-12-3002 [doi]

Ohlfest, J. R., Demorest, Z. L., Motooka, Y., Vengco, I., Oh, S., Chen, E., . . . Largaespada, D. A. (2005). Combinatorial antiangiogenic gene therapy by nonviral gene transfer using the sleeping beauty transposon causes tumor regression and improves survival in mice bearing intracranial human glioblastoma. *Molecular Therapy : The Journal of the American Society of Gene Therapy, 12*(5), 778-788. doi:S1525-0016(05)01429-2 [pii]

Olin, M. R., Andersen, B. M., Zellmer, D. M., Grogan, P. T., Popescu, F. E., Xiong, Z., . . . Ohlfest, J. R. (2010). Superior efficacy of tumor cell vaccines

grown in physiologic oxygen. *Clinical Cancer Research : An Official Journal of the American Association for Cancer Research, 16*(19), 4800-4808. doi:10.1158/1078-0432.CCR-10-1572 [doi]

Omuro, A., & DeAngelis, L. M. (2013). Glioblastoma and other malignant gliomas: A clinical review. *Jama, 310*(17), 1842-1850.

Ortensi, B., Setti, M., Osti, D., & Pelicci, G. (2013). Cancer stem cell contribution to glioblastoma invasiveness. *Stem Cell Research and Therapy, 4*(1), 18-29.

Ostrom, Q. T., Gittleman, H., Stetson, L., Virk, S. M., & Barnholtz-Sloan, J. S. (2015). Epidemiology of gliomas. *Current understanding and treatment of gliomas* (pp. 1-14) Springer.

Pàez-Ribes, M., Allen, E., Hudock, J., Takeda, T., Okuyama, H., Viñals, F., . . . Casanovas, O. (2009). Antiangiogenic therapy elicits malignant progression of tumors to increased local invasion and distant metastasis. *Cancer Cell, 15*(3), 220-231.

Pafundi, D. H., Laack, N. N., Youland, R. S., Parney, I. F., Lowe, V. J., Giannini, C., . . . Brinkmann, D. H. (2013). Biopsy validation of 18F-DOPA PET and biodistribution in gliomas for neurosurgical planning and radiotherapy target delineation: Results of a prospective pilot study. *Neuro-Oncology, 15*(8), 1058-1067. doi:10.1093/neuonc/not002 [doi]

Pardridge, W. M. (2007). Blood–brain barrier delivery. *Drug Discovery Today, 12*(1), 54-61.

Pardridge, W. M. (2003). Blood-brain barrier drug targeting: The future of brain drug development. *Molecular Interventions, 3*(2), 90-105, 51. doi:10.1124/mi.3.2.90 [doi]

Parsons, D. W., Jones, S., Zhang, X., Lin, J. C., Leary, R. J., Angenendt, P., . . . Kinzler, K. W. (2008). An integrated genomic analysis of human glioblastoma multiforme. *Science (New York, N.Y.), 321*(5897), 1807-1812. doi:10.1126/science.1164382 [doi]

Patel, M. N., Halling-Brown, M. D., Tym, J. E., Workman, P., & Al-Lazikani, B. (2013). Objective assessment of cancer genes for drug discovery. *Nature Reviews Drug Discovery, 12*(1), 35-50.

Paz, M. F., Yaya-Tur, R., Rojas-Marcos, I., Reynes, G., Pollan, M., Aguirre-Cruz, L., . . . Esteller, M. (2004). CpG island hypermethylation of the DNA repair enzyme methyltransferase predicts response to temozolomide in primary gliomas. *Clinical Cancer Research : An Official Journal of the American Association for Cancer Research, 10*(15), 4933-4938. doi:10.1158/1078-0432.CCR-04-0392 [doi]

Perez-Diez, A., & Marincola, F. (2002). Immunotherapy against antigenic tumors: A game with a lot of players. *Cellular and Molecular Life Sciences CMLS, 59*(2), 230-240.

Pitz, M. W., Desai, A., Grossman, S. A., & Blakeley, J. O. (2011). Tissue concentration of systemically administered antineoplastic agents in human brain tumors. *Journal of Neuro-Oncology, 104*(3), 629-638.

Plate, K. H., Breier, G., Weich, H. A., Mennel, H. D., & Risau, W. (1994). Vascular endothelial growth factor and glioma angiogenesis: Coordinate induction of VEGF receptors, distribution of VEGF protein and possible in vivo regulatory mechanisms. *International Journal of Cancer, 59*(4), 520-529.

Ramaswamy, V., & Taylor, M. D. (2015). The amazing and deadly glioma race. *Cancer Cell, 28*(3), 275-277.

Rapoport, S. I. (2000). Osmotic opening of the blood–brain barrier: Principles, mechanism, and therapeutic applications. *Cellular and Molecular Neurobiology, 20*(2), 217-230.

Reardon, D. A. (2010). Antiangiogenic therapy for glioblastoma: New directions. *The Angiogenesis Foundation, Spring*

Rich, J. N., & Eyler, C. E. (2008). Cancer stem cells in brain tumor biology. *Cold Spring Harbor Symposia on Quantitative Biology, 73*, 411-420. doi:10.1101/sqb.2008.73.060 [doi]

Robey, R. W., Massey, P. R., Amiri-Kordestani, L., & Bates, S. E. (2010). ABC transporters: Unvalidated therapeutic targets in cancer and the CNS. *Anti-*

Cancer Agents in Medicinal Chemistry, 10(8), 625-633. doi:BSP/ACAMC/E-Pub/ 00103 [pii]

Rong, Y., Durden, D. L., Van Meir, E. G., & Brat, D. J. (2006). 'Pseudopalisading'necrosis in glioblastoma: A familiar morphologic feature that links vascular pathology, hypoxia, and angiogenesis. *Journal of Neuropathology & Experimental Neurology, 65*(6), 529-539.

Salphati, L., Heffron, T. P., Alicke, B., Nishimura, M., Barck, K., Carano, R. A., . . . Phillips, H. S. (2012). Targeting the PI3K pathway in the brain--efficacy of a PI3K inhibitor optimized to cross the blood-brain barrier. *Clinical Cancer Research : An Official Journal of the American Association for Cancer Research, 18*(22), 6239-6248. doi:10.1158/1078-0432.CCR-12-0720 [doi]

Salphati, L., Pang, J., Plise, E. G., Lee, L. B., Olivero, A. G., Prior, W. W., . . . Zhang, X. (2012). Preclinical assessment of the absorption and disposition of the phosphatidylinositol 3-kinase/mammalian target of rapamycin inhibitor GDC-0980 and prediction of its pharmacokinetics and efficacy in human. *Drug Metabolism and Disposition: The Biological Fate of Chemicals, 40*(9), 1785-1796. doi:10.1124/dmd.112.046052 [doi]

Sami, A., & Karsy, M. (2013). Targeting the PI3K/AKT/mTOR signaling pathway in glioblastoma: Novel therapeutic agents and advances in understanding. *Tumour Biology : The Journal of the International Society for*

Oncodevelopmental Biology and Medicine, 34(4), 1991-2002. doi:10.1007/s13277-013-0800-5 [doi]

Sancar, A., Lindsey-Boltz, L. A., Ünsal-Kaçmaz, K., & Linn, S. (2004). Molecular mechanisms of mammalian DNA repair and the DNA damage checkpoints. *Annual Review of Biochemistry, 73*(1), 39-85.

Sarkaria, J. N., Carlson, B. L., Schroeder, M. A., Grogan, P., Brown, P. D., Giannini, C., . . . James, C. D. (2006). Use of an orthotopic xenograft model for assessing the effect of epidermal growth factor receptor amplification on glioblastoma radiation response. *Clinical Cancer Research : An Official Journal of the American Association for Cancer Research, 12*(7 Pt 1), 2264-2271. doi:12/7/2264 [pii]

Schinkel, A. H., & Jonker, J. W. (2003). Mammalian drug efflux transporters of the ATP binding cassette (ABC) family: An overview. *Advanced Drug Delivery Reviews, 55*(1), 3-29.

Schwartzbaum, J. A., Fisher, J. L., Aldape, K. D., & Wrensch, M. (2006). Epidemiology and molecular pathology of glioma. *Nature Clinical Practice Neurology, 2*(9), 494-503.

Seligman, A. M., Shear, M., & Alexander, L. (1939). Studies in carcinogenesis: VIII. experimental production of brain tumors in mice with methylcholanthrene. *The American Journal of Cancer, 37*(3), 364-395.

Shanmugam, R., Kusumanchi, P., Cheng, L., Crooks, P., Neelakantan, S., Matthews, W., . . . Sweeney, C. J. (2010). A water-soluble parthenolide analogue suppresses in vivo prostate cancer growth by targeting NFκB and generating reactive oxygen species. *The Prostate, 70*(10), 1074-1086.

Shirahata, M., Iwao-Koizumi, K., Saito, S., Ueno, N., Oda, M., Hashimoto, N., . . . Kato, K. (2007). Gene expression-based molecular diagnostic system for malignant gliomas is superior to histological diagnosis. *Clinical Cancer Research : An Official Journal of the American Association for Cancer Research, 13*(24), 7341-7356. doi:13/24/7341 [pii]

Silbergeld, D. L., & Chicoine, M. R. (1997). Isolation and characterization of human malignant glioma cells from histologically normal brain. *Journal of Neurosurgery, 86*(3), 525-531.

Singh, S. K., Hawkins, C., Clarke, I. D., Squire, J. A., Bayani, J., Hide, T., . . . Dirks, P. B. (2004). Identification of human brain tumour initiating cells. *Nature, 432*(7015), 396-401.

Sottoriva, A., Spiteri, I., Piccirillo, S. G., Touloumis, A., Collins, V. P., Marioni, J. C., . . . Tavare, S. (2013). Intratumor heterogeneity in human glioblastoma reflects cancer evolutionary dynamics. *Proceedings of the National Academy of Sciences of the United States of America, 110*(10), 4009-4014. doi:10.1073/pnas.1219747110 [doi]

Stein, W. D., Figg, W. D., Dahut, W., Stein, A. D., Hoshen, M. B., Price, D., . . . Fojo, T. (2008). Tumor growth rates derived from data for patients in a clinical trial correlate strongly with patient survival: A novel strategy for evaluation of clinical trial data. *The Oncologist, 13*(10), 1046-1054. doi:10.1634/theoncologist.2008-0075 [doi]

Stein, W. D., Yang, J., Bates, S. E., & Fojo, T. (2008). Bevacizumab reduces the growth rate constants of renal carcinomas: A novel algorithm suggests early discontinuation of bevacizumab resulted in a lack of survival advantage. *The Oncologist, 13*(10), 1055-1062. doi:10.1634/theoncologist.2008-0016 [doi]

Stüer, C., Vilz, B., Majores, M., Becker, A., Schramm, J., & Simon, M. (2007). Frequent recurrence and progression in pilocytic astrocytoma in adults. *Cancer, 110*(12), 2799-2808.

Stupp, R., Mason, W. P., Van Den Bent, Martin J, Weller, M., Fisher, B., Taphoorn, M. J., . . . Bogdahn, U. (2005). Radiotherapy plus concomitant and adjuvant temozolomide for glioblastoma. *New England Journal of Medicine, 352*(10), 987-996.

Stylli, S. S., Luwor, R. B., Ware, T. M., Tan, F., & Kaye, A. H. (2015). Mouse models of glioma. *Journal of Clinical Neuroscience : Official Journal of the Neurosurgical Society of Australasia, 22*(4), 619-626. doi:10.1016/j.jocn.2014.10.013 [doi]

Swaminathan, S. K., Olin, M. R., Forster, C. L., Santa Cruz, K. S., Panyam, J., & Ohlfest, J. R. (2010). Identification of a novel monoclonal antibody recognizing CD133. *Journal of Immunological Methods, 361*(1), 110-115.

Szatmari, T., Lumniczky, K., Desaknai, S., Trajcevski, S., Hidvegi, E. J., Hamada, H., & Safrany, G. (2006). Detailed characterization of the mouse glioma 261 tumor model for experimental glioblastoma therapy. *Cancer Science, 97*(6), 546-553. doi:CAS [pii]

Tamaki, A., Ierano, C., Szakacs, G., Robey, R. W., & Bates, S. E. (2011). The controversial role of ABC transporters in clinical oncology. *Essays in Biochemistry, 50*(1), 209-232.

Tan, B. T., Park, C. Y., Ailles, L. E., & Weissman, I. L. (2006). The cancer stem cell hypothesis: A work in progress. *Laboratory Investigation, 86*(12), 1203-1207.

Thompson, E. M., Frenkel, E. P., & Neuwelt, E. A. (2011). The paradoxical effect of bevacizumab in the therapy of malignant gliomas. *Neurology, 76*(1), 87-93. doi:10.1212/WNL.0b013e318204a3af [doi]

Upadhyay, R. K. (2014). Drug delivery systems, CNS protection, and the blood brain barrier. *BioMed Research International, 2014*

Verhaak, R. G., Hoadley, K. A., Purdom, E., Wang, V., Qi, Y., Wilkerson, M. D., . . . Mesirov, J. P. (2010). Integrated genomic analysis identifies clinically

relevant subtypes of glioblastoma characterized by abnormalities in PDGFRA, IDH1, EGFR, and NF1. *Cancer Cell, 17*(1), 98-110.

Vigneswaran, K., Neill, S., & Hadjipanayis, C. G. (2015). Beyond the world health organization grading of infiltrating gliomas: Advances in the molecular genetics of glioma classification. *Annals of Translational Medicine, 3*(7)

Walker, M. D., Strike, T. A., & Sheline, G. E. (1979). An analysis of dose-effect relationship in the radiotherapy of malignant gliomas. *International Journal of Radiation Oncology* Biology* Physics, 5*(10), 1725-1731.

Wang, H., Han, H., Mousses, S., & Von Hoff, D. D. (2006). Targeting loss-of-function mutations in tumor-suppressor genes as a strategy for development of cancer therapeutic agents. Paper presented at the *Seminars in Oncology, , 33*(4) 513-520.

Weis, S. M., & Cheresh, D. A. (2005). Pathophysiological consequences of VEGF-induced vascular permeability. *Nature, 437*(7058), 497-504.

Wen, B., Hexum, J. K., Widen, J. C., Harki, D. A., & Brummond, K. M. (2013). A redox economical synthesis of bioactive 6, 12-guaianolides. *Organic Letters, 15*(11), 2644-2647.

Wen, P. Y., & Kesari, S. (2008). Malignant gliomas in adults. *New England Journal of Medicine, 359*(5), 492-507.

Wen, P. Y., Macdonald, D. R., Reardon, D. A., Cloughesy, T. F., Sorensen, A. G., Galanis, E., . . . Chang, S. M. (2010). Updated response assessment criteria for high-grade gliomas: Response assessment in neuro-oncology working group. *Journal of Clinical Oncology : Official Journal of the American Society of Clinical Oncology, 28*(11), 1963-1972. doi:10.1200/JCO.2009.26.3541 [doi]

Wiesner, S. M., Decker, S. A., Larson, J. D., Ericson, K., Forster, C., Gallardo, J. L., . . . Ohlfest, J. R. (2009). De novo induction of genetically engineered brain tumors in mice using plasmid DNA. *Cancer Research, 69*(2), 431-439. doi:10.1158/0008-5472.CAN-08-1800 [doi]

Wilson, T. A., Karajannis, M. A., & Harter, D. H. (2014). Glioblastoma multiforme: State of the art and future therapeutics. *Surgical Neurology International, 5*, 64-7806.132138. eCollection 2014. doi:10.4103/2152-7806.132138 [doi]

Wu, A., Oh, S., Ericson, K., Demorest, Z. L., Vengco, I., Gharagozlou, S., . . . Ohlfest, J. R. (2007). Transposon-based interferon gamma gene transfer overcomes limitations of episomal plasmid for immunogene therapy of glioblastoma. *Cancer Gene Therapy, 14*(6), 550-560. doi:7701045 [pii]

Wu, A., Oh, S., Gharagozlou, S., Vedi, R. N., Ericson, K., Low, W. C., . . . Ohlfest, J. R. (2007). In vivo vaccination with tumor cell lysate plus CpG oligodeoxynucleotides eradicates murine glioblastoma. *Journal of*

Immunotherapy (Hagerstown, Md.: 1997), 30(8), 789-797. doi:10.1097/CJI.0b013e318155a0f6 [doi]

Xu, L. W., Chow, K. K., Lim, M., & Li, G. (2014). Current vaccine trials in glioblastoma: A review. *Journal of Immunology Research, 2014*

Yip, S., Miao, J., Cahill, D. P., Iafrate, A. J., Aldape, K., Nutt, C. L., & Louis, D. N. (2009). MSH6 mutations arise in glioblastomas during temozolomide therapy and mediate temozolomide resistance. *Clinical Cancer Research : An Official Journal of the American Association for Cancer Research, 15*(14), 4622-4629. doi:10.1158/1078-0432.CCR-08-3012 [doi]

Yost, S. E., Pastorino, S., Rozenzhak, S., Smith, E. N., Chao, Y. S., Jiang, P., . . . Harismendy, O. (2013). High-resolution mutational profiling suggests the genetic validity of glioblastoma patient-derived pre-clinical models. *PloS One, 8*(2), e56185. doi:10.1371/journal.pone.0056185 [doi]

Yu, L., Wu, X., Cheng, Z., Lee, C. V., LeCouter, J., Campa, C., . . . Ferrara, N. (2008). Interaction between bevacizumab and murine VEGF-A: A reassessment. *Investigative Ophthalmology & Visual Science, 49*(2), 522-527.

Yuan, X., Curtin, J., Xiong, Y., Liu, G., Waschsmann-Hogiu, S., Farkas, D. L., . . . John, S. Y. (2004). Isolation of cancer stem cells from adult glioblastoma multiforme. *Oncogene, 23*(58), 9392-9400.

Zuniga, R., Torcuator, R., Jain, R., Anderson, J., Doyle, T., Ellika, S., . . . Mikkelsen, T. (2009). Efficacy, safety and patterns of response and recurrence in patients with recurrent high-grade gliomas treated with bevacizumab plus irinotecan. *Journal of Neuro-Oncology, 91*(3), 329-336.